UNIVERSITY OF VERONA

DEPARTMENT OF MEDICINE

PhD SCHOOL OF LIFE AND HEALTH SCIENCES

PhD IN INFLAMMATION, IMMUNITY AND CANCER

PhD CYCLE XXXIV/2018

Inhibition of NETs-associated ARG1 enhances the efficacy of anti-cancer immunotherapeutic approaches

MED/04

Coordinator: Prof. Gabriella Constantin

Tutor: Prof. Vincenzo Bronte

PhD candidate: Roza Maria Barouni

UNIVERSITY OF VERONA

DEPARTMENT OF MEDICINE

PhD SCHOOL OF LIFE AND HEALTH SCIENCES

PhD IN INFLAMMATION, IMMUNITY AND CANCER

PhD CYCLE XXXIV/2018

Inhibition of NETs-associated ARG1 enhances the efficacy of anti-cancer immunotherapeutic approaches

MED/04

Coordinator: Prof. Gabriella Constantin

Signature_____

Tutor: Prof. Vincenzo Bronte

Signature _____

PhD candidate: Roza Maria Barouni

Index

Abbreviations' List

Abbreviations	Definition
TME	Tumor microenvironment
ECM	Extracellular matrix
CAFs	Cancer associated Fibroblasts
Tregs	T regulatory cells
TAMs	Tumor associated macrophages
Foxp3	Forkhead box P3
IL-10	Interleukin-10
TGF	Tumor growth factor
ARG1/2	Arginase 1/2
BM	Bone Marrow
M-MDSCs	Monocytic-Myeloid derived suppressor cells
PMN-MDSCs	Polymorphonuclear-Myeloid derived suppressor cells
ROS	Reactive oxygen species
RNS	Reactive nitrogen species
PD-1	Programmed cell death protein 1
PD-L1	Programmed cell death protein ligand 1
CTLA4	Cytotoxic T-lymphocyte-associated protein 4
FasL	Fas ligand
iNOS	Inducible nitrix oxide synthase
IDO	Indoleamine-pyrrole 2,3-dioxygenase
ER	Endoplasmic reticulum
CTSS/CTSG	Cathepsin S/G
CLIP	Class II invariant chain peptide
RT-2	RIP1-Tag2 (RT2) transgenic mouse model
ODC	Ornithine decarboxylase
OAT	Ornithine aminotransferase
OTC	Ornithine transcarbamylase
CPS-1	Carbomoylphodphate synthase-1
TNFα	Tumor necrosis factor α
IFN-α,β,γ	Interferon α, β, γ
NSCLC	Non-small cell lung cancer
(nor-)NOHA	(nor-)Nω-hydroxyl-L-arginine
BEC	S-(2-boronoethyl)-L-cysteine
ABH	2(S)-amino-6-borobohexanoic acid
NETs	Neutrophil extracellular traps

HSCs	Hematopoietic stem cells
CLP	Common lymphoid progenitors
CMP	Common myeloid progenitors
GMPs	Granulocyte-monocyte progenitors
STAT3	Signal transducer and activator of transcription 3
C/EBP	CCAAT-enhancer-binding proteins
AP-1	Activator protein 1
preNEU	Pre-neutrophils
NeP	Neutrophils progenitor
MPO	Myeloperoxidase
PR3	Proteinase 3
NE	Neutrophil elastase
NSP4	Neutrophil serine protease 4
BPI	Bactericidal/permeability-increasing protein
NGAL	Neutrophil gelatinase-associated lipocalin
OLFM-4	Olfactomedin-4
SRPα	Sgnal-regulatory protein alpha
CR1	Complement receptor 1
VVN2	Vanin-2
LFA1	Lymphocyte function-associated antigen 1
MAC-1	Macrophage 1 antigen
CXCRs	C-X-C chemokine receptors
NDNs	Normal density neutrophils
LDNs	Low density neutrophils
PBMCs	Perpheral blood mononuclear cells
TANs	Tumor associated neutrophils
PDAC	Pancreatic ductal adenocarcinoma
LOX-1	Lectin-type oxidized LDL receptor 1
NLR	Neutrophils to lymphocytes ratio
OS	Overall survival
IRS-1	Insulin receptor substrate 1
PI3K	Phosphatidylinositol 3-kinase
PDGFR	Platelet-derived growth factor receptor
VEGF	Vascular endothelial factor
NF-κB	Nuclear factor kappa-light-chain-enhancer of activated B cells
FATP2	Fatty acid transport protein 2
CTCs	Circulating tumor cells
APCs	Antigen presenting cells
CTLs	Cytotoxic tumor lymphocytes

ADCC	Antibody-dependent cellular cytotoxicity
PMA	Phorbol-12-myristrate-13-acetate
PAD4	Peptidyl arginine deiminase 4
LPS	Liposacchiride
PKC	Protein kinase C
NADPH	Nicotinamide adenine dinucleotide phosphate
mTOR	Mammalian target of rapamycin
Akt	Protein kinase B
NOX	NADPH oxidase
KO	Knock out
mtDNA	Mitochondrial DNA
CEACAM1	Carcinoembryonic Ag cell adhesion molecule
MMPS	Matrix metalloproteinases
CCDC25	Coiled-coil domain containing 25
H3Cit	Citrullinated Histone 3
DDR	DNA famage repair
PRSS1	Cationic trypsinogen or Trypsin 1
TP53	Tumor protein 53
INK4A	Inhibitorr of cyclin-dependent kinase 4 (CDK4)
BRCA2	Breast cancer 2
LKB1	Liver kinase B1
KRAS	Kirsten rat sarcoma virus
SMAD4	Mothers against decapentaplegic homolog 4
CDKN2A	Cyclin-dependent kinase inhibitor 2A
KDM6A	Lysine-specific demethylase 6A or ubiquitously transcribed tetratricopeptide repeat, X chromosome (UTX
BCORL1	B-cell lymphoma 6 protein Corepressor Like 1
RBM10	RNA-binding motif 10
MLL3	Mixed-lineage leukemia protein 3
ADEX	Aberrantly differentiated endocrine exocrine
ICI	Immune checkpoint inhibitors
5-FU	5-fluorouracil
FOLFIRONOX	Folinic acid-fluorouracil-irinotecan-oxaliplatim
DCs	Dendritic cells
CAR T cells	Chimeric antigen receptor T cells
TCR	T cells receptor
CEA	Carcinoembryonic antigen
MUC-1	Mucin-1
MHC	Major histocompatibillity complex

CSF	Colony-stimulating factor
GM-CSF	Granulocyte-macrophage-CSF
M-CSF	Macrophage-CSF
CCLs	Chemokine (C-C motif) ligands
CCR	(C-C motif) chemokine receptor 2
HMGB1	High mobility group box 1
HIR	Humanized-immune reconstituted
Rag	Recombinant activating genes
HLA	Human leukocyte antigen
BAC	Bacterial artificial chromosome
CDX	Cell-derived xenografts
PDX	Patient-derived xenografts
HD	Healthy donor
RBCs	Red blood cells
PFA	Paraformaldehyde
DAPI	4′,6-diamidino-2-phenylindole
AAV9	Adeno-associated virus serotype 9
hTERT	Human telomerase reverse transcriptase
ACT	Adoptive cell therapy
MALDI-TOF	Matrix-assisted laser desorption ionization time of flight
rh	Recombinant human
LC-MS/MS	Liquid chromatography-Mass spectrometry/Mass spectrometry
FDR	False discovery rate
ITC	Isothermal calorimetry
NMR	Nuclear magnetic resonance
DLS	Dynamic ligh scattering
MSC-2	Mouse-derived cell line
HGF	Hepatocyte growth factor

Sommario

Nonostante gli straordinari risultati ottenuti dall'immunoterapia nel trattamento dei tumori, la sua efficacia risulta limitata a pochi pazienti. Tra i meccanismi responsabili di questa parziale efficacia gioca un ruolo chiave il microambiente tumorale (TME). Con le sue caratteristiche immunosoppressive, il TME è oggi oggetto di un'intensa ricerca, volta a identificare, caratterizzare e colpire le funzioni che lo regolano. Tra i componenti chiave del TME, annoveriamo le cellule mieloidi che, corrotte dalle cellule tumorali, intervengono nello spegnimento della risposta anti-tumorale attraverso svariati meccanismi. Tra questi, la degradazione di L-arginina nell'ambiente extracellulare da parte dell'arginasi 1 (ARG1) rappresenta un noto meccanismo immunosoppressorio. Sebbene siano stati fatti enormi sforzi per lo sviluppo di inibitori chimici efficaci contro l'ARG1, le differenze nella biologia di ARG1 tra uomo e modelli murini limita, ad oggi, l'efficacia della sua inibizione nella pratica clinica.

Nel nostro studio, dimostriamo che ARG1 è presente nei neutrophil extracellular traps (NETs) rilasciati dalle cellule polimorfonucleate (PMNs) stimolate. Nei NETs ARG1 viene tagliata dalla catepsina S (CTSS), originando frammenti di diverso peso molecolare con attività enzimatica. Come conseguenza, il risultato netto della funzione di ARG1 risulta aumentato a pH fisiologico. In pazienti con tumore pancreatico abbiamo evidenziato che tale meccanismo è presente in cellule mieloidi periferiche ed infiltranti il tumore. Abbiamo altresì dimostrato che l'attività di ARG1 può essere neutralizzata, *in vitro*, da un nuovo anticorpo monoclonale specifico per ARG1 umana, mentre classici inibitori risultano inefficaci. L'efficacia dell'anticorpo anti-ARG1 è stata inoltre valutata *in vivo* su omogenati di tumore pancreatico umano e in modelli murini. In tal senso, l'anticorpo si è dimostrato in grado di aumentare l'efficacia di terapie basate su checkpoint inhibitors e trasferimento adottivo di cellule T anti-tumorali.

Abstract

Despite the progress in the field of the cancer immunotherapy, the immunosuppressive tumor microenvironment (TME) remains a huge problem-to-be-solved nowadays. Among other key components, infiltrated myeloid cells in the TME can suppress anti-tumor immunity exploiting various mechanisms. L-arginine degradation from the extracellular milieu by arginase 1 (ARG1) is a notorious immunosuppressive mechanism. Although, huge effort has been made for the development of effective chemical inhibitors against ARG1, differences in ARG1 biology among species could restrain the successful translation of experimental model results in the clinical practice.

In our study, we have demonstrated that ARG1 is present in neutrophil extracellular traps (NETs) released by stimulated polymorphonuclear cells (PMNs), where it is cleaved by the cysteine protease cathepsin S (CTSS). This cleavage generated two truncated forms of lower molecular weight and unleashed ARG1 enzymatic activity at physiological pH. Subsequently, ARG1 enhanced activity resulted in the arrest of T lymphocytes proliferation. We have developed a neutralizing monoclonal antibody against ARG1, which efficiently blocked ARG1 activity, while the commercially available ARG1 inhibitors were unable to restore T cells proliferation when the cleaved forms were present.

In patients with pancreatic ductal adenocarcinoma (PDAC), neutrophils and $CD14^{+}ARG1^{+}$ cells released NETs-related ARG1 endowed with increased activity, due to CTSS cleavage, and administration of the ARG1 neutralizing antibody blocked its inhibitory function.

ARG1 blockade in combination with immune checkpoint inhibitors (ICI) in *ex vivo* PDAC tumors enhanced the efficacy of immunotherapy through increased activation of T lymphocytes, while combinatory treatment of tumor-bearing humanized mice with adoptive cell therapy (ACT) and ARG1 neutralizing antibody increased T cells infiltration in the tumor tissues and attenuated tumor growth.

Introduction

Chapter 1: Tumor Microenvironment

Despite the development of checkpoint blockade therapy in the last years and its proven anti-tumor efficiency, tumor cells still retain the ability to escape and more than 50% of the patients fail to respond [1]. Specifically, tumors create a highly immunosuppressive environment that promotes their growth and metastatic spread, while at the same time holds a protective role against the various anti-tumor therapeutic approaches [2]. In the last years, it has emerged that the tumor microenvironment (TME) is a key player of the tumor progression, thus understanding the mechanisms governing its regulation is a priority [3]. TME is the environment surrounding the tumor cells, which contains also immune and stromal cells, non-cellular components of the extracellular matrix (ECM) and signaling molecules [4]. Accumulating evidence shows that cellular and acellular components in TME can reprogram tumor initiation, growth, invasion, metastasis, and response to therapies [5], [6]. Consequently, targeting and manipulating the cells and factors of the TME during cancer treatment can help controlling malignancies and achieve positive patient's outcome.

1.1 Cellular components of the TME

Tumor cells communicate with the surrounding cells, altering their normal function and corrupting them to their advance. Cancer-associated fibroblasts (CAFs) are key component of the TME with diverse functions, including matrix deposition and remodeling, extensive signaling interactions with cancer cells and crosstalk with infiltrating leukocytes [7]. In addition, CAFs, through IL-6, promote immunosuppression via systemic effects on metabolism and support the metabolism of TME-infiltrating cells providing necessary metabolites[8]. Lastly, CAFs regulate survival signaling and promote angiogenesis, proliferation of the infiltrated cells [9], drug access and therapy

responses. CAFs secretome influences a range of leukocytes, including $CD8^+$ T cells, regulatory T (Treg) cells and macrophages, with both immunosuppressive and immunopromoting consequences [10]. However, the consensus is that the predominant effect of CAFs is immunosuppressive with IL-6, CXC-chemokine ligand (CXCL) 9 and TGFβ having well-established roles in reducing T cell responses [11]. More recently, antigen cross presentation by CAFs has been observed [12], and this may lead to $CD4^+$ T cell activation and suppression of $CD8^+$ T cells [13]. Clinical analysis further supports an inverse association between CAFs and $CD8^+$ T cells [14]. In fact, interference with the action of CXCL12 produced by CAFs was shown to promote T cell-mediated tumor control [15]. The exchange of metabolites and amino acids between cancer cells and CAFs is an additional avenue by which stromal fibroblasts interact with tumor cells [16; 17]. In this line, autophagy in stromal fibroblasts can generate alanine, which is subsequently used by pancreatic ductal adenocarcinoma (PDAC) cells to fuel the tricarboxylic acid (TCA) cycle [18; 19]. Furthermore, metabolic dysregulation of CAFs may also be coupled to altered immunoregulation, possibly through IL-6 production or depletion of immunomodulating amino acids [20].

On the other hand, TME is also infiltrated by immune cells with suppressive functions. T_{regs} represent one of these components, together with tumor-associated macrophages (TAMs) and myeloid-derived suppressor cells (MDSCs).

T_{regs} are a subset of T cells characterized by the expression of the transcription factor forkhead box P3 (FOXP3). T_{regs} consist in a suppressive population whose physiological role is to prevent pathological self-reactivity, maintain peripheral tolerance and stop immune responses to resolve inflammation. Different subsets of Tregs have been so far identified, depending on the expression and intensity of CD45RA, CD25, FOXP3 and CD4, and defined as nTregs, eTregs, non-Tregs [21]. nTreg possess weak immunosuppressive activity. Upon T cell receptor (TCR) stimulation, nTreg cells proliferate rapidly and differentiate into highly immunosuppressive eTreg cells. By contrast, $FOXP3^+$ non-Treg cells are not immunosuppressive but rather are immunostimulatory, producing inflammatory cytokines, such as IFNγ and IL-17 [22].

Tregs exert their immunosuppressive activity through various cellular and humoral mechanisms: competition for and consumption of IL-2, thereby limiting the amount available to T cells [23]; cytotoxic T-lymphocyte-associated protein 4 (CTLA-4) - mediated suppression of antigen presentin cells (APC) function, which inhibits the priming and/or activation of T cells [24]; production of immunosuppressive cytokines such as IL-10, IL-35 and TGFβ) [25; 26; 27]; conversion of ATP into adenosine [28], an immunomodulatory metabolite that can prevent optimal T cell activation; and secretion of granzyme and/or perforin to destroy effector cells [29]. Tumor cells exploit T_{regs} physiological function to control immune responses by triggering their recruitment at the tumor sites through cytokines, where T_{regs} exert their suppressive function on effector T cells thus promoting tumor development and progression.[30]. The TME generally contains an abundance of eTreg cells that overexpress immunosuppressive molecules, such as CTLA-4 and T cell immunoreceptor with Ig and ITIM domains (e.g. TIGIT), with low numbers of nTreg cells. A transcriptome analysis of human cancer specimens has also revealed that tumour-infiltrating Treg cells express high levels of various markers of Treg cell activation, such as lymphocyte-activation gene 3 protein (LAG3), T cell immunoglobulin mucin receptor 3 (TIM3), inducible T cell co-stimulator (ICOS), OX40 and glucocorticoid-induced TNFR-related protein (GITR) [31], a phenotype that is distinct from that of Treg cells in peripheral tissues, supporting the notion that Treg cells in the TME are activated and have a strong immunosuppressive capacity. Interestingly, evidence indicates that apoptotic Treg cells in the TME have greater immunosuppressive effects than non-apoptotic Treg cells. Apoptosis in Treg cells has been attributed to the weak nuclear factor erythroid 2-related factor 2 (NRF2)-associated antioxidant system and thus high vulnerability to reactive oxygen species (ROS) generated in the TME [32]. Apoptotic Treg cells in the TME have been shown convert large amounts of ATP to adenosine via CD39 and CD73, thereby suppressing the activity of local immune cells through the adenosine A2A receptor pathway [33].

Macrophages described as innate cells of the mononuclear phagocyte immune system exert crucial roles against infections. Macrophages engulf microorganisms and

stimulate adaptive immune cells when necessary. Through the secretion of cytokines, chemokines but also hypoxia and inflammation, tumor cells recruit circulating monocytes in the TME, which become TAMs [34]. Immunosuppressive TAMs are characterized by a secretory profile consisting of low levels of inflammatory cytokines, such as IL-18, IL-12, TNFα and IFNγ, and high levels of anti-inflammatory cytokines, such as IL-10 and TGF-β [35]. TAM and tumor cell–derived cytokines, like TGF-β, IL-10 and PGE2, are known to downregulate major histocompatibility complex (MHC) class-II molecules in TAMs. This results in dcreased Th1 differentiation, leading to a reduced anti-tumor response and expansion of Treg cells. TAMs also promote immune suppression through the recruitment of Th2 and Treg cells by the production of chemokines, such as CCL17 and CCL22, [36] and through the recruitment of eosinophils and naive T cells by the secretion of CXCL13, CCL16, and CCL18 [37]. TAMs express also immune checkpoint ligands, such as (programmed death-ligand) PD-L1, PD-L2, CD80 and CD86, which directly inhibit cytotoxic T cell functions, further dampening anti-tumor response [38]. T cell cytotoxicity can also directly be inhibited by macrophage-mediated depletion of L-arginine and tryptophan by arginase (ARG1) 1 and indoleamine 2,3-dioxygenase 1 (IDO1) [39; 40]. TAMs are also associated with tumor progression and facilitation of metastasis [41]. In fact, in metastatic sites, classical monocytes differentiate into a distinct, transient myeloid cell population (metastasis-associated macrophage precursors (MAMPs) that expresses mature macrophage markers (F4/80) and suppress the cytotoxic activity of $CD8^+$ T cells by a ROS–mediated mechanism [42]. Recent lineage tracing experiments showed that the MAMPs differentiate into metastasis-ass0ciated macrophages (MAMs) endowed with the ability to suppress $CD8^+$ T cell killing, instead with a mechanism dependent on the expression of CTLA-4 ligands, such CD80 and CD86 [42].

MDSCs are a heterogeneous group of cells belonging to the myeloid lineage that expand during pathological conditions, such as cancer, chronic inflammation or autoimmunity. In tumors, MDSCs are detected in the TME. MDSCs are pathologically-deviated cells that leave the bone marrow (BM) as immature precursors before reaching

their final maturation status in different tissues and TME [43]. MDSCs consist of two different subpopulations: the monocytic-MDSCs (M-MDSCs) and the polymorphonuclear-MDSCs (PMN-MDSCs). M-MDSCs have morphologic and phenotypic characteristics similar to monocytes, while PMN-MDSCs are similar to neutrophils [44]. In humans, M-MDSCs are characterized as $CD14^{+}HLA\text{-}DR^{-/lo}$ and PMN-MDSCs as $CD11b^{+}CD15^{+}CD14^{-}CD33^{+/lo}CD66b^{+}$ [45]. MDSC major function is to suppress anti-tumor immune responses, mainly through inhibition of T cell proliferation and activation through various established mechanisms. For example, MDSCs produce ROS and reactive nitrogen species (RNS), block T cells function and induce apoptosis through PD-L1, CTLA-4 and Fas ligand (FASL) [46]. Moreover, MDSCs support the suppressive functions of T_{regs} and TAMs in the TME [47]. In addition, MDSCs are able to orchestrate immune responses by controlling essential amino acids metabolism. More specifically, MDSCs metabolize L-arginine through ARG1 and inducible nitric oxide synthase (iNOS) and L-tryptophan through IDO1, provoking arrest of T cells proliferation [48].

1.2 Non-cellular components of the TME

Apart from the different cellular populations infiltrated in the TME, there are various non-cellular components with extreme importance for the tumor progression. Non-cellular components of the TME include cytokines, growth and soluble factors, metabolites, ligands and enzymes, nucleic acid and exosomes [49]. In addition, non-cellular components of the ECM, like proteins, glycoproteins and proteoglycans, contribute to tumor growth [50]. The various molecules facilitate communication between the cells in the TME while at the same time contribute in tumorigenesis, metastasis and angiogenesis. Similarly, these components play a role in the general immunosuppression that is present in the TME, by modulating immune cell function [4].

One of the most important families of enzymes are the cysteine cathepsins, which demonstrate increased levels and activity in tumor patients and are correlated with poor prognosis [51]. Cysteine cathepsins are lysosomal proteases that belong to the C1 papain

family and count 11 members, also called sulfhydryl or thiol proteinases, as they contain a cysteine residue in their active sites [52]. Cathepsins are produced as inactive pre-pro-enzymes or zymogens, since the propeptide sequence is necessary for cathepsins regulation and their entrance in the endoplasmic reticulum (ER) [53]. Proteins of this family are localized in the endo-lysosomal lumen, where they exert different proteolytic functions related to protein degradation, but they are also taking part in cell-cycle regulation, cell death and inflammation signaling and, under specific circumstances, cathepsins can be secreted in the extracellular environment [54]. Nevertheless, in cancer cathepsins acquire new functions and help tumor progression. For instance, cathepsins are implicated in the tumor angiogenesis, facilitate tumor invasion and extravasation by degrading ECM [52]. One member of this family that is intensively investigated for its role in cancer is cathepsin S (CTSS). CTSS is the only member of the cysteine cathepsins family that retains its enzymatic activity in neutral pH compared to the optimal acidic pH that supports the activity of the other members of this family [55]. CTSS is ubiquitously present in the lysosomes, but has a tissue specific distribution, as it is mainly found in spleen, lymph nodes and immune cells such as antigen-presenting cells, monocytes, macrophages and in the Ficolin-1 granules of neutrophils [56]. Its specific tissue distribution is explained by CTSS crucial role in immune responses and specifically in antigen presentation [57]. CTSS present in thymic DCs is the main protease that cleaves and generates autoantigens during T cell selection process [58]. Moreover, CTSS is one of the enzymes involved in the cleavage of the type II glycoprotein of invariant chain (li, CD74) in order to produce the class II invariant chain peptide (CLIP) and allow the antigen loading in MHCII in DCs, B cells and macrophages [59]. CTSS expression is upregulated in breast, pancreatic, liver, gastric, colorectal, liver cancers as also in Non-Hodgkin lymphoma [60]. Both tumor and tumor infiltrating cells, such as TAMs, are responsible for the observed high levels in the tumor microenvironment [61, 62]. High levels of CTSS correlate with poor prognosis in various tumor types. In pancreatic tumor models, expressing high levels of CTSS, it was shown that CTSS is necessary for tumor formation, invasion and angiogenesis, while in RIP1-Tag2 (RT2) transgenic mouse lacking CTSS expression tumor growth

was completely absent, suggesting the role of this protease in favoring tumor aggressiveness [63, 64]. In addition, in a pancreatic mouse model IL-4 stimulates CTSS expression by TAMs, which enhanced tumor growth [65]. Studies about CTSS activity blockade demonstrated positive results and many CTSS inhibitors have been developed and tested in last decades against various cancers [55], based on its tertiary structure. The main problem regarding the development of CTSS specific inhibitors is due to the high percentage of homology among the members of the cysteine cathepsin family, rendering the inhibitors non-selective [66] (Fig. 1).

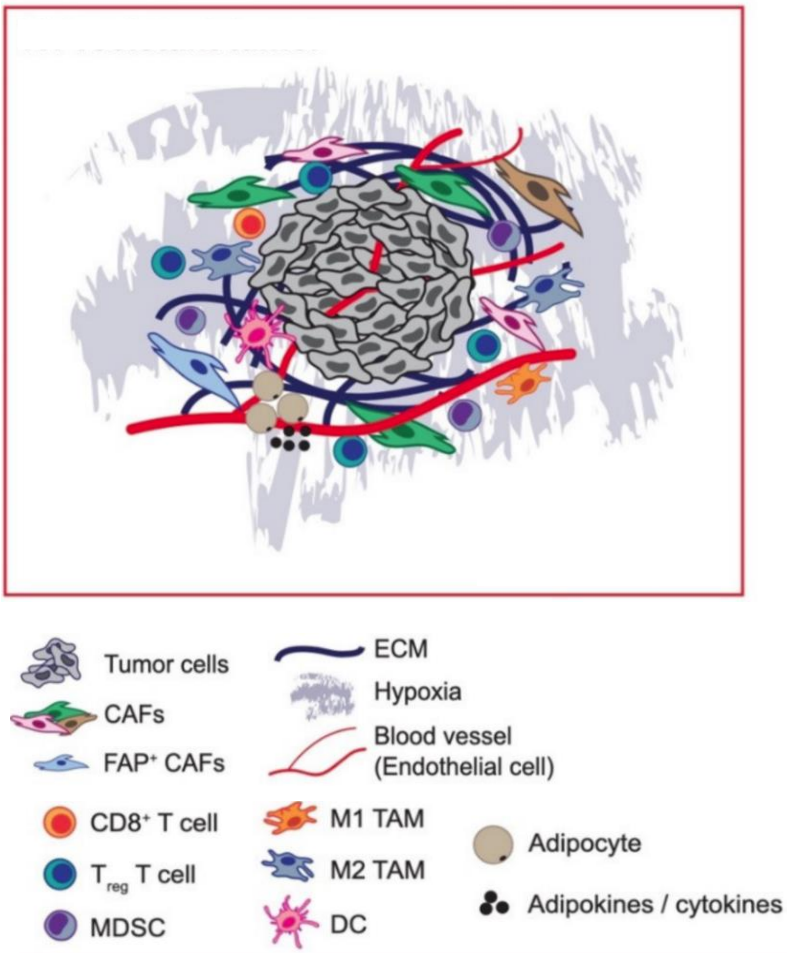

Figure 1. **Components of the TME.**

Pro-tumoral and anti-tumoral populations are detected in the complex TME of solid tumors and shape the anti-tumor immune responses and the outcome of the therapeutic treatments. Furthermore, complex ECM, acidic pH correlated with hypoxia and non-physiological angiogenesis characterize TME. Soluble factors, such as cytokines, chemokines and enzymes are also detected in the TME. Adapted from Krisnawan et al, October 2020, Cancers.

1.3 Metabolism

The catabolism of essential metabolites is central in the TME and represents an important alteration for cancer cell survival and suppression of anti-tumor immune responses. Tumor cells have an increased requirement for nutrients in order to sustain their excessive energy needs and exhibit an extreme metabolic plasticity, as they are able to adjust their metabolism based on their location and the availability of nutrients

in the extracellular milieu [67]. For example, tumor cells consume rapidly glucose, leading to accumulation of lactate which attenuates anti-tumor effector T and NK cells and stimulates T helper 17 (T_h17) cells to exert pro-tumoral functions [68]. Similarly, tumor cells and activated immune cells compete for amino acids in the TME. Amino acids deprivation results in dysfunctional T cells with low capacity to orchestrate anti-tumor responses. For instance, depletion of tryptophan by IDO1 leads to suppression of cytotoxic functions and induction of T_{regs} differentiation, while hydrolysis of glutamine by glutaminase results in the production of glutamate that induces T_{regs} expansion [69, 70]. Similarly, arginine is a semi-essential amino acid with critical role in the tumor immunology that is catabolized in the immune cells by ARG1, ARG2 and iNOS [71] (Fig 2). Catabolism of arginine by ARG is one of the main immunoregulatory mechanisms exploited by different cells to inhibit T cell-mediated responses. Arginine/ARG axis and its role in tumor progression will be described analytically in the following chapter.

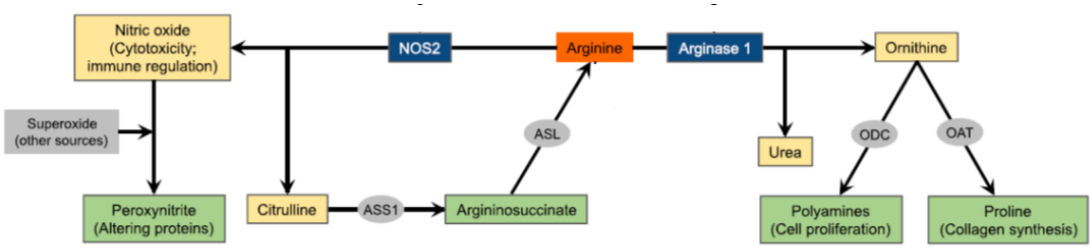

Figure 2. **Scheme of arginine metabolism.**

ARG1 and NOS2 (iNOS) are the responsible enzymes for arginine catabolism in immune responses. ASS1, argininosuccinate synthase 1; ASL, argininosuccinate lyase. Modified from Rodriguez et al, February 2017, Frontiers in Immunology.

1.3.1 Arginase 1

ARG is a manganese metalloenzyme that catalyses the last step of the urea cycle, being responsible for the conversion of L-arginine to urea and L-ornithine. This catalysis results in the organism's detoxification from ammonia because of the urea synthesis

but also in the production of prolines and polyamines through the further catalysis of L-ornithine by ornithine decarboxylase (ODC) or ornithine aminotransferase (OAT), respectively [72]. Additionally, L-ornithine can be converted to L-citrulline by ornithine transcarbamylase (OTC) and carbomoylphosphate synthase-1 (CPS-1).

ARG is a highly conserved enzyme and in vertebrates is present in two different isoforms: ARG1 and ARG2. Although the two enzymes are encoded by genes located in different chromosomes, they share more than 50% homology in their amino acid sequence and 100% homology in their catalytic sites [73]. Furthermore, their hydrolysis produces the same metabolites. In humans, ARG1 gene locus is located on the chromosome 6q23 and produces a 322 amino acid protein, while ARG2 gene is on the chromosome 14q24, generating a protein of 354 amino acids [74, 75].

The two isoforms are located in different subcellular compartments; ARG1 is located in the cytosol of hepatic tissues, although it is found in lower levels also in other cells, while ARG2 is a mitochondrial enzyme expressed in non-hepatic tissues [76]. A valid explanation of this phenomenon is that ARG2 derives from the ancestral enzyme, since it is expressed in all organisms (from bacteria to vertebrates), while ARG1 is expressed in the recently evolved species because of their necessity to metabolize higher levels of nitrogen [77]. Nevertheless, ARG2 is found in the cytosol of human endothelial or tumor cells, contributing to L-arginine degradation [78]. Arginase can also be detected in extracellular fluids, indicating that it is released from cells and can hydrolyze L-arginine in the extracellular environment [79].

Apart from the different intracellular location, the two isoforms are also expressed by different cell populations. In details, ARG1 is generally present in hepatocytes and myeloid cells (known also as liver arginase) and ARG2 is expressed ubiquitously in all mitochondria-containing extrahepatic cells, and among them in higher levels in the kidney, prostate, brain, blood and immune cells [80]. In extrahepatic cells, L-ornithine, the product of the enzymatic catalysis of L-arginine by ARG, is used for cell growth and proliferation. In humans, three different isoenzymes of ARG1 have been detected; the isoform 1 of 322 amino acids in the liver, the isoform 2 of 330 amino acids in PMNs

and erythrocytes, and finally the 236 amino acid long isoform 3 that has still unknown function and tissue distribution. Compared to isoform 1, isoform 2 contains 8 additional amino acids, starting from the amino acid position 43 [81].

Recent studies indicated that immune cell populations express ARG1 and ARG2, but the relative enzyme distribution varies among different organisms within the immune populations. Specifically, in mice ARG1 is expressed in monocytes and macrophages, while in humans ARG1 is stored in the tertiary granules of neutrophils and under physiological conditions is not detectable in monocytes [82]. In human neutrophil granules, ARG1 is inactive at physiological pH, and becomes active only upon its release in the extracellular environment [83]. In experiments performed by Rotondo et al, ARG1 activation was mediated by components of primary granules. Moreover, even though ARG1 exocytosis was induced by both tumor necrosis factor α (TNFα) and ionomycin, only the latter resulted in the release of both granule types and the activation of extracellular ARG1 at physiological pH [83].

Regarding ARG structure, initial studies on rat liver ARG1 revealed that the enzyme has a 105 kDa homotrimeric quaternary structure and each monomer has an a/b fold of a central parallel 8-stranded β-sheet with several α-helices on both sides [84] (Fig. 3). Human ARG1 and ARG2 share the tertiary structures with rat ARG1 [85, 86]. Moreover, each monomer contains a spin-coupled Mn^{2+} - Mn^{2+}, necessary for the proteolytic function of the enzyme, as it coordinates with the amino acid side chain, found on the border of the central β-sheet [76]. In particular, manganese ions create hydrogen bonds with the histidine and aspartate amino acids, resulting in the stability and the activity of the protein [87]. This knowledge led to the design of different chemical inhibitors targeting ARG1 enzymatic core.

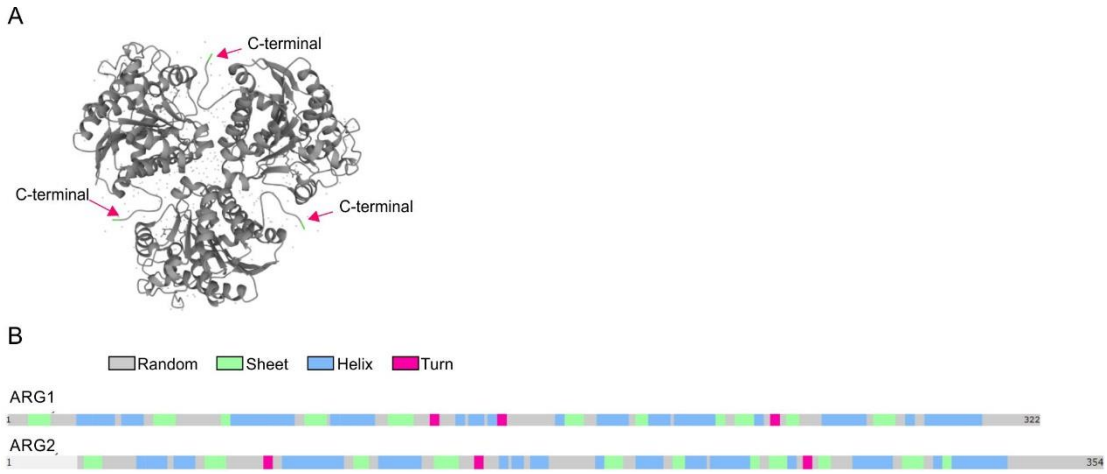

Figure 3. ARG1 and ARG2 structures.

A. ARG1 and ARG2 quaternary trimeric structures are shown. In each monomer the C-terminals are indicated with fuchsia arrows. B. Schematic representation of ARG1 and ARG2 secondary structures. Random sequences are indicated with grey color, β-sheets with light green, α-helixes with light blue and turns with fuchsia. The above figure is adapted by uniprot.org (https://www.uniprot.org/uniprot/P05089, https://www.uniprot.org/uniprot/P78540)

1.3.1.1 ARG1 function in cancer

In the recent years, numerous studies have shown that amino acid metabolism has a direct impact on immune cells function, either under physiological or pathological conditions. Specifically, ARG1 has a crucial role in the immune system's responses against tumor cells. In other words, ARG1 is a key enzyme in the generation of an immunosuppressive environment by tumors and pro-tumoral immune cells resulting in the suppression of anti-tumor immune responses mediated [48].

To begin with, L-arginine catabolism by ARG1 results in impairment of T cells function and response against tumors [88]. Moreover, tumor-induced inflammation stimulates L-arginine consumption by innate immune cells, through interferon (IFN)-α, -β and -γ signalling, leading to downregulation of CD3ζ chain that subsequently blocks T cells responses [89]. Amino-acid loss and accumulation of urea have been shown to modify the translation of several mRNAs, through the involvement of general control non-depressible 2 (GCN2) and mammalian target of rapamycin (mTOR). The level of tRNA that is uncharged increases in cells as a consequence of the amino-acid

loss, and this subsequently activates GCN2 ([90, 91, 92]). GCN2 binds uncharged tRNA and therefore signals amino-acid starvation and reacts by phosphorylating the serine residue at position 51 of the α-subunit of eukaryotic translation initiation factor 2 (EIF2α). Phosphorylation of EIF2α turns-off protein synthesis by halting the initiation of translation. Experiments performed by Rodriguez et al. showed that GCN2-deficient T cells were able to proliferate even in the absence of L-arginine, indicating the crucial role of arginine in the cell cycle of T cells [93]. However, Van de Velde et al. challenged these results showing that $CD8^+$ T cells lacking GCN2 could not proliferate after antigen stimulation in the absence of amino acids, like arginine, tryptophan etc., but $CD4^+$ T cells proliferation was not affected [94]. On the other hand, T helper cells can sense the absence of amino acids from the extracellular milieu through mTOR pathway. In details, $CD4^+$ T cells lacking Rictor, the main subunit of the mTORC2 protein complex, were engaged to proliferation in limiting concentrations of arginine and leucine [95].

The crucial role of L-arginine in T cells is further highlighted by the observation that increased concentration of intracellular L-arginine in T cells provokes a shift in their metabolism from glycolysis to oxidative phosphorylation, which supports T cell activation and function and promotes the differentiation towards central memory phenotype [96]. In addition, high level of ARG activity detected in pancreatic cancer patients limit L-arginine concentration and block the function of other enzymes, like NOS for the production of NO [71]; furthermore, decreased L-arginine levels stimulate T regulatory cells generation that further supports the tumor growth [97]. L-arginine availability is strictly associated with the functional performance of T cells; thus, many researches have focused on the cell populations that express ARG1 with the purpose to consume L-arginine and support tumor growth. For example, tumor-associated myeloid cells can uptake L-arginine from the extracellular environment by CAT-2B transporter and impair T cells responses [98]. It is also well established that M-MDSCs and macrophages can catabolize L-arginine, enhancing further the immunosuppression in the tumor tissues [91]. In non-tumor conditions, ARG1 expressing macrophages are

able to regulate T cells function and block bacterial or cytokine-driven inflammation, indicating that independently of the tumor effect, ARG1 is able to control T cells proliferation [99, 100].

In humans, Munder et al demonstrated that ARG1 released from PMNs, upon activation with ionomycin or PMA, downregulates CD3ζ chain expression, impairs TCR signalling and blocks T cell proliferation [83, 101]. IL-8, produced by non-small cell lung cancer (NSCLC) cells is also able to stimulate PMNs and induce ARG1 exocytosis that eventually suppresses T cells proliferation [102].

1.3.1.2 Targeting ARG1

Due to the role of ARG1 in cancer and other pathological conditions, ARG1 inhibition has been the focus of many studies resulting in the development of inhibitors during the past years [103].

ARG1 inhibitors can be clustered in two different groups [104]. The first group contains L-arginine analogues, like compounds with 2-aminoimidazole moieties that are stabilized through the hydroxide that connects ARG with the manganese cluster, mimic ARG interaction with L-arginine, and blocks the hydrolysis of the amino acid [105]. Conversely, the second group includes transition state analogues (boronic acid, hydroxyarginines and sulphonamides), which interact and bind to the manganese ions. For example, one of the most known potent inhibitors of ARG1 is Nω-hydroxyl-L-arginine (NOHA), an intermediate molecule in the NO synthesis that displaces the metal-bridging hydoxyde with N-hydroxyl [106]. Its derivative nor-NOHA exhibits the same inhibiting potency but with longer half-life and it is not a substrate of NOS [107]. Both of them are specific to ARG1, demonstrating no effect on NOS function. Two other examples of transition state analogues are boronic acid analog of L-arginine, S-(2-boronoethyl)-L-cysteine (BEC) or (ABH), were designed to bind to the manganese cluster and block the enzymatic activity of ARG1 [85]. The crystal structure of arginase lead to the design of the strongest α,α-disubstituted derivatives of ABH.

One of the most recently described chemical inhibitors is the small-molecule CB-1158, which was able to reverse myeloid cells-mediated suppression of T cell proliferation resulting in decrease tumor growth [108]. Currently, this inhibitor is tested in a Phase I clinical trial for its safety, pharmacokinetics and response against different solid tumors (NCT02903914, https://clinicaltrials.gov/ct2/show/NCT02903914?term=NCT02903914&draw=2&rank=1). In addition, based on ABH structure and using structural-based drug design Lu et al have designed a novel ARG1 inhibitor that took in advantage the empty space left from ABH-ARG1 interaction. This inhibitor features a proline core and exhibits good overall characteristics (potency, selectivity and oral bioavailability), although it has not been tested as an anticancer agent [109]. ABH structure was also the basis for the design of another boronic-acid compound that possessed a bicyclic ring system, increasing the stability of the complex ABH-ARG1 and demonstrating promising pharmacodynamic characteristics in tumor-bearing mice [110].

Due to ARG1 active site structure the therapeutic approach of neutralizing antibodies was not evaluated until recently, but ARG1 specific characteristic render the enzyme a good candidate. In details, ARG1 presence in the extracellular environment, where antibodies can target it and the broad available surface of ARG1 trimer for antibody binding indicate that targeting ARG1 with neutralizing antibodies in the extracellular milieu, without affecting its intracellular function, could be a successful therapeutic approach. Indeed, Palte R.L. et al. based on cryo-electron microscopy designed five full-length ARG1 monoclonal antibodies that were able to neutralize the enzymatic activity. Four out of the five generated antibodies inhibit ARG1 by steric occlusion of its active site due to the insertion of an amino acid side chain, while the fifth antibody prevents the formation of the complex between ARG1 and its substrate and product [111].

Overall, none of the commercially available inhibitors is isoform specific, targeting both ARG1 and ARG2, as all the inhibitors share similar structures [103]. Moreover, the available compounds demonstrated poor pharmacokinetic profiles and many side effects have been reported due to the high dosage. In addition, the chemical inhibitors

have been developed based on ARG1 crystal structure, without taking into consideration possible post-translational modifications or changes that could occur due to the expression in different populations between rodents and humans. Although the generation of neutralizing antibodies paves the way for their use as a therapeutic approach to target enzymes, it remains to be addressed whether these antibodies can function in preclinical and clinical models. Therefore, the development of novel or the amelioration of pre-existing therapeutic strategies to block ARG1 function specifically is necessary and is still an active sector of research.

Chapter 2: Neutrophils

Neutrophils, or otherwise known as PMNs, belong to the innate immunity system and constitute the most abundant immune population in humans, representing approximately 50 to 70 % of total leukocytes [112]. They are produced in higher numbers than any other population in BM (10^{11} each day) [113]. PMNs are released in the circulation as terminally differentiated cells having no capacity of renewal which leads to the necessity of constant replenishment [114]. Neutrophils lifespan is shorter than any other population in mammals, extending from 12 to 24 hours [115] but under non-physiological conditions, it can be prolonged. They are characterized by their multilobulated nucleus, the presence of diverse granules with defined content and the expression of a wide range marker in their extracellular membrane [116].

Neutrophils, exploiting a large arsenal of protective mechanisms, are the first line of defense against microbial infections. In details, there are three main mechanisms deployed by neutrophils in order to accomplish their function properly; phagocytosis, degranulation and formation of neutrophil extracellular traps (NETs) [117]. Particularly degranulation and NETosis will be discussed in the following paragraphs. An increasing number of studies coming out in the last decades reveals the numerous ways that neutrophils function is extended beyond their antimicrobial role in various diseases, including cancer, autoimmune and infectious diseases and sepsis [118].

2.1 Neutrophils ontogeny

Neutrophils ontogeny is a highly regulated complex process that takes place in the BM. To begin with, mature neutrophils are generated from committed myeloid progenitors that originate initially from hematopoietic stem cells (HSCs) resided in the BM. In details, based on the classical or hierarchical model, HSCs generate two different types of common progenitors, the lymphoid (CLP) and the myeloid one (CMP) [115]. CMPs, characterized as $Lin^{-}CD34^{+}CD38^{+}IL3R^{+}CD45RA^{-}$, give rise to

granulocyte/macrophage progenitors (GMPs, $Lin^{-}CD34^{+}CD38^{+}IL3R^{+}CD45RA^{+}$), that in response to granulocyte colony stimulating factor (G-CSF) become unipotent and differentiate through various steps to neutrophils. Then, the most famous model describing the committed granulopoiesis was divided in two major phases, the proliferative and the non-proliferative that follows chronically the former one. In the proliferative phase, GMPs differentiate to myeloblasts, promyelocytes and myelocytes, while in the non-proliferative phase myelocytes produce metamyelocytes, banded cells and mature neutrophils [119]. During this process, neutrophils change their nucleus shape and acquire their specific characteristics. This procedure is fine-tuned and regulated by specific transcription factors. Specifically, the most important ones are Signal transducer and activator of transcription (STAT) 3 and CCAAT/enhancer-binding protein (C/EBP) alpha that are present from the early developmental stages (GMPs and myeloblast, respectively), while others, such as C/EBPε, C/EBPδ, PU.1, C/EBPβ, C/EBPζ and activator protein 1 (AP1), regulate the steps of the non-proliferative phase [120].

The above mentioned classification is based on histological staining and electron microscopy that depend on neutrophil size, nucleus shape and cytosol specific granules. New studies, though have shed more light in the neutrophils ontogeny and demonstrated that in mice GMPs produce proliferative neutrophil-committed cells that are know now as pre-neutrophils (preNeu) [121]. PreNeus have the ability to give rise to immature and mature neutrophils, and moreover in inflammatory conditions these committed progenitors expand even more. PreNeus co-exist in the BM pools with common monocyte progenitors. Another elegant study identified the earliest neutrophil progenitor (NeP) downstream of GMPs in humans and confirmed also the presence of preNeu in humans, demonstrating that human preNeu represents an intermediate population between NeP and terminally differentiated neutrophils [122]. As it is clear now, new technologies can help us to identify and answer questions regarding neutrophils ontogeny forming a better picture of the actual situation in the BM.

2.2 Granulopoiesis

Another important aspect of neutrophils differentiation and maturation is the stepwise formation of granules and secretory vesicles, a procedure named granulopoiesis [123]. It starts with the appearance of the primary granules (once termed azurophilic) in the myeloblast and promyelocyte stage. At this stage the nucleus is still large and round. Then, at the myelocyte and metamyelocyte stages secondary granules (once termed specific) appear and the nucleus is shaped in the form of a kidney. Tertiary granules (or gelatinase granules) start appearing during the transition to band cells, named in this way because of the band form of the nucleus. Finally, ficolin-1 granules and secretory vesicles appear in the mature (segmented) neutrophils. By the end of granulopoiesis process fully mature PMNs emerge [124].

Each type of granules contains a specific collection of proteins produced at the corresponding differentiation stage. Primary granules are defined by the presence of myeloid peroxidase (MPO), that contain in high levels. Apart from MPO, primary granules contain serine proteases with proteolytic activity including proteinase 3 (PR3), cathepsin G (CTSG), neutrophil elastase (NE), and neutrophil serine protease 4 (NSP4) [125]. Additionally, membrane proteins, such as CD63, CD68, presenilin 1, stomatin and vacuolar-type H-ATPase and other antimicrobial peptides (defensin, azurocidin, and bactericidal/permeability-increasing protein (BPI)) are also included in primary granules. Secondary granules contain antibiotic molecules, like lactoferrin, neutrophil gelatinase-associated lipocalin (NGAL), resistin, olfactomedin-4 (OLFM-4) and signal-regulatory protein alpha (SIRPα) [115]. Tertiary granules contain enzymes (gelatinases) that degrade matrix when neutrophils get in contact with the endothelium and membrane receptors (CD11b/CD18, CD67, CD177, etc) [126]. The most important enzyme of tertiary granules is ARG1, known for its pleiotropic roles in various situations [124]. Ficolin-1 granules and secretory vesicles are similar in terms of protein content and role. Ficolin-1 granules contain human serum albumin, complement receptor 1 (CR1), vanin-2 (VVN2), lymphocyte function-associated antigen 1 (LFA-1), actin, and cytoskeleton-binding proteins and CTSS. Secretory vesicles contain

membrane receptors (CD10, CD11b/CD18, CD15, CD16, LFA-1, macrophage 1 antigen (MAC-1) etc) and proteins necessary for the immediate inflammatory response of neutrophils. In general, both ficolin-1 granules and secretory vesicles are easily exocytosed, as a response to neutrophils' activation [56, 127].

Granules exocytosis or otherwise known as degranulation follows a contrariwise linear order in comparison to their production [128]. In details, as we mentioned above activation of neutrophils from minimal stimulation results in the exocytosis of secretory vesicles and ficolin-1 granules. Increasing potency of the stimulation causes then the release of tertiary, secondary and in the end primary granules [129]. We must stress here that the exocytosis of primary granules is particular since they require a really strong stimulus and subsequently the majority of them releases their content in the phagosomes and they do not exocytose directly in the extracellular environment [130].

2.3 Heterogeneity of neutrophils in health and cancer

Another emerging important aspect of neutrophils biology is their heterogeneity. Specifically, studies are identifying neutrophils populations, both mature and immature, with specific characteristics in healthy and pathological conditions [131]. Neutrophils plasticity and heterogeneity begin early in the maturation procedure in bone marrow, continue in the blood where circulating neutrophils exhibit numerous phenotypes, acquire more complexity when tissue-specific neutrophils are examined and finally depend also on the health status [132].

It is known that neutrophils have limited time-frame in the blood and this has established the idea that circulating neutrophils have the same characteristics and phenotype. However, this is not the case [133]. Even in healthy conditions, neutrophils in the blood show different characteristics that are correlated with a phenomenon known as neutrophil ageing. When neutrophils remain more than 6 hours in the circulation they start decreasing CD62L (L-selectin) expression and upregulate CD11b and CXC chemokine receptors (CXCR) type 4 (CXCR4) levels [134]. Moreover, neutrophils from

healthy volunteers appear to undergo diurnal oscillations for phagocytosis and ROS production, which are under the control of circadian clock genes [135, 136].

In different tissues, neutrophils are influenced by their surrounding environment and modify their lifetime duration, as their phenotypic and functional properties [137]. In addition, in acute inflammation in mouse model neutrophils have active chromatin remodeling when neutrophils leave the bone marrow to enter the circulation and when abandon the circulation to enter in the tissues [138]. In human spleens, $CD15^{low}CD16^{low}$ neutrophils support and stimulate B cells through the expression of cytokines and chemokines [139, 140].

Neutrophils phenotypic and functional complexity passes on another level when we must study their heterogeneity in pathological conditions, like cancer [141]. Actually, the confusion in this case is growing even more due to complex nomenclature. To begin with, systemic inflammation activates mature circulating neutrophils, but at the same time stimulates a process called emergency granulopoiesis. In cancer, mature and immature neutrophils with anti-tumor and pro-tumor function are detected in the circulation [131]. Specifically, in the peripheral blood of cancer patients there have been identified three populations of neutrophils: normal density neutrophils (NDNs), that received their name because they are isolated from the granulocyte fraction upon density-gradient centrifugation; low density neutrophils (LDNs) and PMN-MDSCs, isolated from the peripheral blood mononuclear cell (PBMCs) fraction. Moreover, tumor tissues are infiltrated by neutrophils that called tumor-associated neutrophils (TANs) [142]. Below we will discuss analytically the differences and the common points of these populations detected in cancer and we will also refer to the missing points of their biology.

2.3.1 NDNs

The NDN term refers to the neutrophil population with mature phenotype that is isolated from cancer patients [142]. NDNs display in some cancers immunosuppressive

phenotype, exerted mainly through the release of ROS, ARG1 and several other proteases. Studies have also demonstrated that NDNs are able to suppress T cells response through cell-to-cell contact and Mac-1 [143], [144]. NDNs have the common phenotypic markers of neutrophils (CD66b, CD11b, CD15, CD16) [145] and can be distinguished from the LDN population only with density centrifugation, rendering difficult to isolate, specifically characterize and study these populations.

2.3.2 LDNs

As we mentioned before, LDNs constitute a heterogeneous population of immature and mature neutrophils found in the sediment of PBMCs in pathological conditions, like cancer. LDNs have been detected in different types of cancer such as NSCLC, hepatocellular carcinoma, PDAC, colorectal etc, and they are correlated with poor prognosis [146]. LDNs display neutrophil-morphology, express CD66b and demonstrate a heterogeneity regarding their phenotype, maturation and activation. In details, LDNs population exhibits different maturation stages, going from mature $CD11b^{+}CD16^{+}$ neutrophils to immature $CD11b^{low/-}CD16^{low/-}$ neutrophils of the band and/or metamyelocyte stage [147]. It is not clear yet the origin of LDNs but since it is such a heterogeneous population with cells in different maturation states there are two possible explanations. LDNs are immature cells from bone marrow that have entered the circulation prior to reach the mature differentiation stage or mature neutrophils that have been activated, degranulated and therefore, losing their physiological cellular density, reside in PBMCs ring [148].

2.3.3 PMN-MDSCs

PMN-MDSCs consist the immunosuppressive part of LDNs detected in cancer patients. As in LDNs, also in PMN-MDSCs have been detected mature and immature neutrophils which as a main functional characteristic exhibit pro-tumor functions and increased capacity to suppress anti-tumor immune responses exerted by T cells [44]. In

humans, PMN-MDSCs heterogeneity lies on the different levels of activation markers, like CD62L, CD54, CD274 and others, the expression of functional molecules, like ARG1 and ROS or receptors CXCR2 and CXCR4 and on maturation specific markers, like CD16 and CD124 [45]. It is really important to stress at this point that PMN-MDSCs exhibiting the above described phenotype, show suppressive activity and specific biochemical and molecular molecules associated with their function. Otherwise, this population must be called MDSC-like [44]. A great effort has been made by the scientific community in order to distinguish PMN-MDSCs from NDNs, since up to recently there were no specific phenotypic markers that could separate these populations, leaving gradient centrifugation as the only choice. Condamine et al published an elegant study demonstrating that NDNs and PMN-MDSCs isolated from the same cancer patients have completely different gene profiles. Specifically, the lectin-type oxidized LDL receptor 1 (LOX-1) was highly upregulated in PMN-MDSCs compared to the neutrophil population that showed limited expression. This study suggested that LOX-1 could be a possible marker to separate neutrophils from PMN-MDSCs, and maybe LDNs [149].

2.3.4 TANs

Neutrophils detected in tissues belong to the group of TANs. Up to now there are no evidence regarding the origin of TANs in the tumor tissues. In other words, we do not know whether different neutrophil populations infiltrate tumor tissues or if they acquire different characteristics once they enter [150]. In mice, TANs display plasticity and based on this observation, Fridlender et al proposed the N1 and N2 dichotomy (following the M1 and M2 phenotype characterization of macrophages). They showed that upon environmental signaling TANs can be polarized in anti-tumor N1 and pro-tumor N2 neutrophils. Notably, this observation has been limited in mice, while in humans it is believed that N2 neutrophils are similar to PMN-MDSCs [151]. In humans, studies regarding TANs are really difficult to be performed but TANs infiltration has been associated with poor prognosis. Two studies that have successfully isolated TANs from

tumor tissues reported opposite observations [142]. In details, TANs isolated from CRC patients were suppressing T cell responses, while TANs isolated from early-stage lung cancer patients supported T cell proliferation and activation and for this reason they have been characterized as APC-like "hybrid neutrophils" [152, 153]. Overall, TANs characteristics and functions are not firm, but change based on the signals and stimuli received by the tumor microenvironment [154].

2.4 Neutrophils role in cancer

Only lately, has been recognized by the scientific community that tumor associated neutrophils are heterogeneous, are characterized by plasticity and play a role in the progression of cancer [155]. Now, their implication in cancer is beyond any doubt, but their role depends on factors, cancer type and timing. Neutrophils can exert both pro-tumoral and anti-tumoral functions based on the signals that receive from their environment and cancer cells [113]. For instance, anti-tumor functions of neutrophils have mainly been observed in the early stages of tumor progression, while in the later stages neutrophils support tumor growth, metastasis formation and suppress anti-tumor immune responses [114]. Moreover, in many cancers (breast, melanoma, colorectal carcinoma, non-small-cell lung, pancreatic and other type of cancers) neutrophils-to-lymphocytes ratio (NLR) is used as prognostic marker for the response to therapy prediction or overall survival (OS) [156, 157, 158, 159, 160]. In addition, TANs infiltration in tumor tissue biopsies is correlated with poor prognosis in aggressive pancreatic and other cancers [161, 162].

Generally, various studies in mice support the pro-tumoral activity of neutrophils in tumor progression, but the role of neutrophils should be evaluated more in human cancer subjects, since the two organisms have profound differences not only regarding tumor evolution but also in neutrophils biology [163].

2.4.1 Pro-tumoral role

Various studies have demonstrated that neutrophils exert tumor-promoting roles through various mechanisms and pathways. For example, NE, released by neutrophils, once entered in the endosomal compartment, degrades insulin receptor substrate 1 (IRS-1) and simultaneously activated phosphatidylinositol 3-kinase (PI3K) and mitogen platelet-derived growth factor receptor (PDGFR), promoting the proliferation of lung cancer cells both in mice and humans [164]. In the early stages of tumor generation, MMP-9 expressing neutrophils support angiogenesis inside the tumor lesions due to vascular endothelial growth factor (VEGF) activation [165]. Moreover, lung cancer has proven to be resistant to bortezomib, an inhibitor of NF-kB, through a mechanism that involves neutrophils. In details, nuclear factor kappa-light-chain-enhancer of activated B cells (NF-κB) blocking in myeloid cells results in increased cleavage of pro-IL-1β from CTSG, leading subsequently to increased production of active IL-1β that stimulates epithelial cell proliferation [166].

Furthermore, neutrophils with distinguished characteristic have been directly linked with pro-tumoral activities. A specific subtype of neutrophils, called SiglecF^{high} neutrophils, regulated by osteoblasts, supports lung cancer growth [167]. In addition, PMN-MDSCs, both from humans and mice, overexpress fatty acid transport protein 2 (FATP2) upon GM-CSF mediated activation of STAT5, which is involved in their immunosuppressive activity through uptake of arachidonic acid for prostaglandin E2 synthesis. Simultaneous inhibition of FATP2 and immune checkpoint molecules resulted in arrest of tumor progression in mice [168]. In mice with early stage tumor, neutrophils with a distinct metabolic signature escaped bone marrow and migrated, although they did not have any immunosuppressive activity, while bone marrow neutrophils of later stages exhibited a strong immunosuppressive capacity. This population shared the same characteristics with neutrophils and PMN-MDSCs observed in cancer patients [169] (Fig. 3).

2.4.2 Metastasis

Neutrophils have, beyond any doubt, a crucial role in the metastasis formation. For example, neutrophil-like MDSCs, stimulated by IL-17 expressed from γδ T cells, suppress CD8-mediated anti-tumor immune responses and support metastasis formation [170]. Several chemokines and their receptors activate signaling axis in neutrophils that enhance their metastatic role [171], while neutrophils, through leukotrienes support the initiation of lung metastasis in breast tumor mice [172]. In particular, CXCR2 signaling in the neutrophils is required for pancreatic cancer metastasis [173]. Lung inflammation recruits neutrophils from bone marrow and leads to the proteases release from primary granules. These proteases degrade thrombospondi-1 and allow the formation of metastasis [174]. In addition, neutrophils support Snail expression in lung tumors, facilitating in this way cancer progression, maintaining their recruitment and establishing a suppressive tumor microenvironment [175]. Circulating tumor cells (CTCs) have been found to associate in the bloodstream with neutrophils, which support their cycle progression and their metastatic potential [176]. Finally, in breast cancer, lung mesenchymal cells promote neutrophils to accumulate lipids that are then transferred to metastatic tumor cells via a macropinocutosis-lysosome pathway and support their survival [177] (Fig. 3).

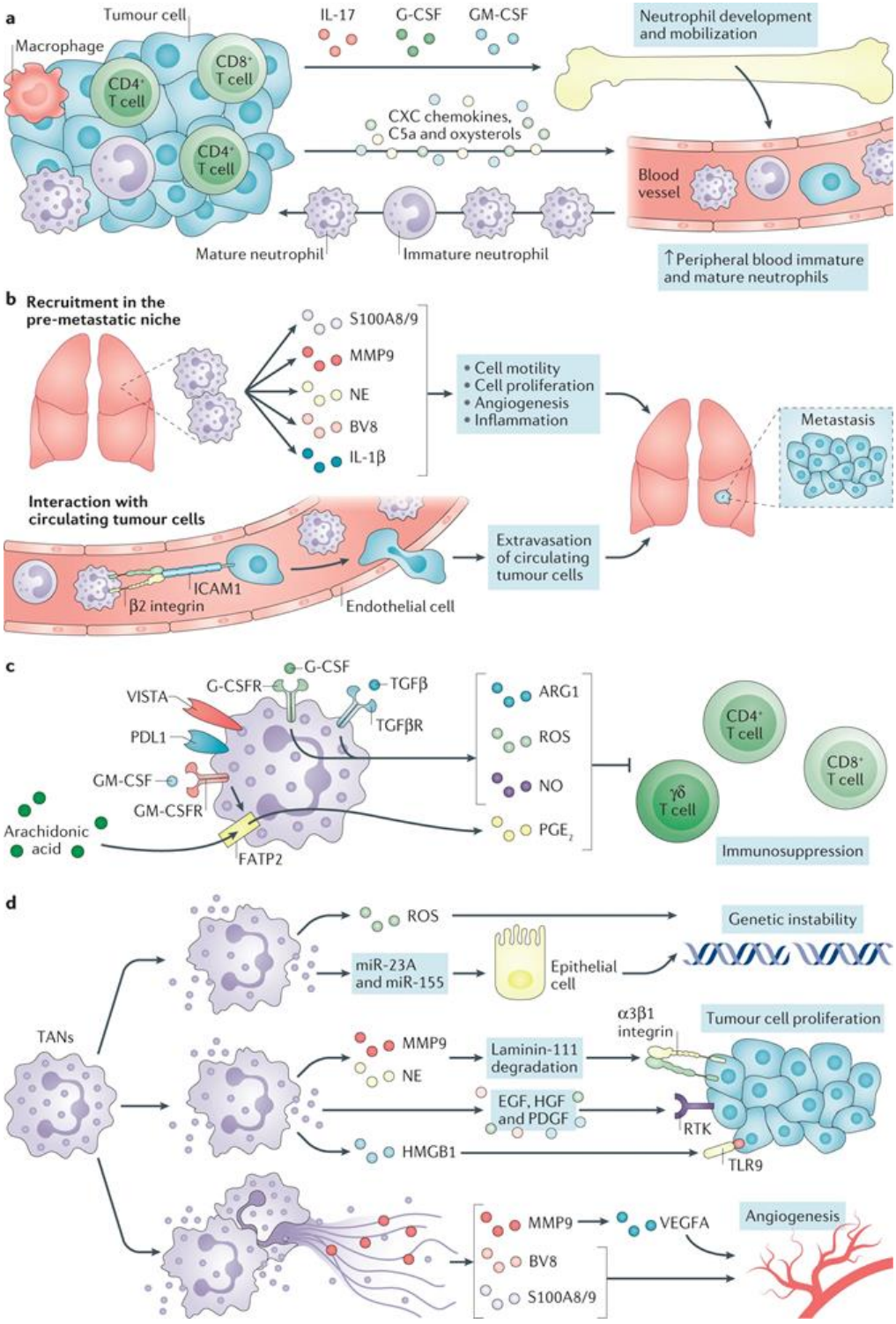

Figure 4. **Protumoral roles of neutrophils.**

Neutrophils can sustain tumor growth via different mechanisms. A) Neutrophils generation, recruitment and survival are driven by various soluble factors produced by tumor and immune cells of the TME. B)

Neutrophils, mobilized by chemokines contribute to the foundation of the pre-metastatic niche by guiding or escorting metastatic tumor cells. C) | Neutrophils upon stimulation by cytokines (G-CSF, TGF-β) secrete molecules, such as ARG1, iNOs etc that inhibit the activation of T cells proliferation, activation and function. D) Neutrophils induce genetic instability, mediated by ROS production and microparticles containing microRNAs. Moreover, neutrophils support tumor proliferation via the production of growth factors, degranulation of molecules and the release of NETs. Neutrophils sustain tumor angiogenesis through the release of the pro-angiogenic factors. G-CSFR, G-CSF receptor; GM-CSFR, GM-CSF receptor; ICAM1, intercellular adhesion molecule 1; RTK, receptor tyrosine kinase; TAN, tumor-associated neutrophil; TGFβR, TGFβ receptor. Adapted by Jaillon S., July 2020, Nature Reviews Cancer.

2.4.3 Anti-tumoral role

Although, the majority of the studies demonstrate that neutrophils support tumor progression, there are some that highlight neutrophils anti-tumor properties. For instance, in breast cancer mouse models neutrophils colonize lungs, before the metastatic cells and impede tumors from creating the metastatic niche in a hydrogen peroxide dependent mechanism [178]. Moreover, IFNγ produced by monocytes recruited in the lungs, stimulated neutrophils to kill tumor cells and prevent metastasis formation [179]. TANs stimulate T cell proliferation, activation and anti-tumor responses in the early stages of lung cancers [180], while a specific subset of neutrophils has APCs properties and is able to promote anti-tumor T cell responses in human lung cancers [152]. NE expressed by TANs infiltrating breast cancer tissues was uptaken as an antigen by cancer cells and NE resulted in activation of Cytotoxic T lymphocytes (CTLs) and lysis of tumor cells [181]. In colon cancer, neutrophils support CD8 T cells activation and memory phenotype, and $CD66b^+$ infiltration is associated with a good prognosis and survival [182]. Neutrophils, activated through antibody-dependent cellular cytotoxicity (ADCC), kill cancer cells by trogocytosis [183]. Human, and not murine, neutrophils release active NE, which cleaves the CD95 death domain that interacts with histone 1 to kill tumor cells without affecting the non-immune cells [184]. Neutrophils also block early stage development of uterine cancer by detaching tumor cells from the basement membrane [185]. MET proto-oncogene is essential for the anti-tumor activity of neutrophils, and when targeted in cancer patients results in the presence of neutrophils with a pro-tumoral phenotype [186].

Chapter 3: NETs formation

As we mentioned above, one of the three mechanisms exploited by neutrophils to kill pathogens is the formation of NETs, through a process that is named NETosis. Upon activation, neutrophils release NETs, that are described as extracellular DNA web-like structures, generated by the decodensation of chromatin, which carry nuclear, cytoplasmic and granule proteins. NETs function is to trap and kill invading pathogens, but as we will discuss below, they have also an important role in other disorders, like cancer and autoimmune diseases [187].

NETs were first characterized in 1996, when Takei et al. were investigating how phorbol-12-myristrate-13-acetate (PMA) can induce neutrophils death. During their experiments, they discovered that PMA induces neutrophils death through a distinct unknown death pathway [188]. Eight years after, Zychlinsky's group defined NETs' role and named this process NETosis [189]. Nowadays, the term NETosis is not true, since numerous studies have demonstrated that the formation of NETs is not necessarily accompanied by neutrophil's death. In other words, NETosis can occur without neutrophils lysis when are activated by Staphylococcus aureus [190, 191]. For this reason, we can distinguish two different types of NETosis, the classical or suicidal and the vital one [192] (Fig.4).

Briefly, NETs formation starts when neutrophils are activated by pathogens, such as bacterial cell components, fungi, viruses and as well as immune components, such as antibodies, cytokines, chemokines and component. *In vitro* NETs can be induced by calcium and potassium ionophores and phorbol esters. For example, ionomycin and A23187 are two known calcium inducers, while PMA belongs to the phorbol esters group [193]. These molecules activate extracellular receptors and provoke alterations in neutrophils' intracellular calcium concentration, which leads to the activation of specific kinases and the production of ROS [194]. In turn, ROS stimulates MPO that triggers NE translocation from primary granules to the nucleus. There MPO and NE start to degrade histones resulting in chromatin's decodensation, characterized by the

loss in heterochromatin and DNA spreading [195]. Subsequently, neutrophils undergo structural changes starting from depolarization and deconstruction of the nucleus and release of chromatin in the cytoplasm where interacts with cellular and granular proteins [196]. Then, the plasma membrane is disrupted and NETs are released in the extracellular environment up to 8 hours after the initial stimulation [187]. Below, we will describe analytically the complex mechanisms associated with NETs formation (Fig.4).

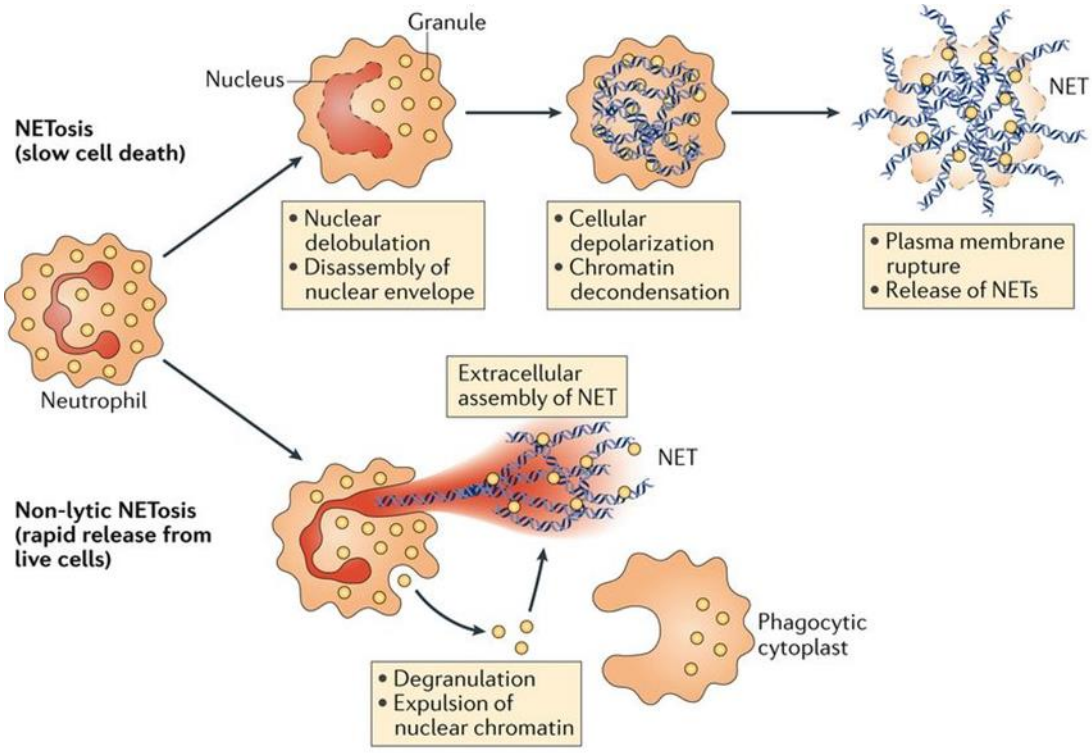

Figure 5. **The pathways of NETosis.**

Lytic NETosis is a slow cell death pathway, which starts with nuclear delobulation and the disassembly of the nuclear envelope, while results in cellular depolarization, chromatin decondensation and plasma membrane rupture. The second form of NETosis is a non-lytic one, characterized by rapid release of NETs from live cells, occurring independently of cell death and involves the secreted expulsion of nuclear chromatin accompanied by degranulation. These components assemble extracellularly and leave behind active anucleated cytoplasts that continue to ingest microorganisms. Adapted from V. Papayannopoulos, October 2017, Nature Reviews Immunology.

3.1 Mechanisms of NETs formation

To begin with, neutrophils activation through binding of stimulatory molecules to receptors of the plasma membrane, such as Fcγ receptors, Toll-like receptors and complement receptors, results in the opening of calcium channels of the membrane [187]. Furthermore, ER releases the stored calcium upon stimulation with liposacchride (LPS), IL-8, PMA and ionomycin. The increase in the intracellular calcium concentration activates the peptidyl arginine deiminase 4 (PAD4) protein, that has been shown to play a critical role in NETs formation. Following, calcium increase stimulates kinases and regulators of the cell cycle [197]. For example, PMA, ionomycin and IL-8 induce protein kinase C (PKC). In addition, PMA stimulation triggers the activation of cyclin-dependent kinase 6 and Raf-MEK-ERK-MAP kinase pathway. Both calcium source and activated signaling pathway depend on the stimuli [198]. In turn, activation of PCK and Raf-MEK-ERK-MAP pathway leads to activation of nicotinamide adenine dinucleotide phosphate (NADPH) oxidase, which is responsible for the generation of ROS [198]. Other signaling pathways, such as PI3K- mTOR- protein kinase B (Akt) pathway, have been also linked to the initiation of NETosis [199]. Increased ROS production generated by NADPH oxidase or by mitochondria function is stimulated by PMA and A23187. On the other hand, ionomycin and potassium ionophore do not induce generation of ROS by NADPH but are still able to induce NETs formation. Based on the above clarification, NETosis can be distinguished mechanistically to NADPH oxidase (NOX) dependent and independent [200]. NADPH oxidase converts oxygen to superoxide, which is subsequently converted to hydrogen peroxide. Then, hydrogen peroxide stimulates azzurosome dissociation and MPO-mediated release of NE, that in turn binds to actin filaments, degrades them and enters in the nucleus [196]. Once MPO and NE enter in the nucleus, they proteolytically cleave histones, initiating the loss of chromatin's structure [201].

As we mentioned, increase calcium concentration and hydrogen peroxide presence activate PAD4, which contributes to chromatin's decodensation, by modifying post translationally histones [202]. Specifically, PAD4 converts arginine to citrulline, changing

arginine's positive charge and resulting in a decrease in the affinity between histones and the negatively charged DNA. PAD4 citrullinates multiple arginine residues of histones, as arginines 2, 8, 17 and 26 at histone 3, arginine 3 at histone 4 and histone 2A and arginine 54 at histone 1 [203]. Subsequently, histones dissociate from DNA, chromatin loses its compacted form and decodenses as linker DNA and histones are not able to form their compacted structure. Studies have demonstrated that ionomycin, PMA and TNFα induce NETosis through PAD4 activation, and neutrophils from PAD4 knock out (KO) mice do not form NETs [204]. Moreover, calpain, a serine protease that can be activated by calcium, contributes in chromatin decodensation when PAD4 is present [205]. In contrast, other studies have shown that NETosis can occur without histone citrullination from PAD4 and other factors can also contribute to histones decodensation, confirming anew the importance of the initials stimulus [206]. Indeed, chromatin decodensation is also regulated by proteases. NE and PR3 are able to cleave histones in vitro when PMA is used as stimuli [207].

Following nucleus loss of structure, DNA is released from the nucleus to the cytosol through a mechanism involving laminin remodeling and nuclear membrane permeabilization [208]. Specifically, PMA and ionomycin stimulate disruptions in laminin networks probably due to PKCα phoshorylation or PAD4 mediated degradation respectively, that allow the release of DNA [209]. Immediately afterwards, occurs the rupture of the nuclear envelope as a result of gasdermin D activation. Gasdermin D is a protein that forms pores and is activated by caspases that release its N-terminal domain [210]. Then, this domain oligomerizes and forms pores on the membranes. Studies have demonstrated that LPS induces gasdermin D cleavage by caspase 11, while PMA results in gasdermin D cleavage by NE during NETosis [210, 211, 212]. When gasdermin D is knocked out nuclear envelope rupture is impossible to happen and DNA cannot be released in the cytosol upon LPS or PMA stimulation.

In the final steps of NETosis, prior though to the release of NETs in the extracellular environment, decodensed chromatin must surpass the network of cytoskeleton and organelles. Indeed, in cytoskeleton and organelles occur drastic conformational

changes in suicidal NETosis [213]. Actin cytoskeleton, microtubules and vimentin intermediate filaments disassemble, while endoplasmic reticulum vesiculates, granules disintegrate and mitochondria release their DNA [208]. In details, PMA, ionomycin and LPS induce filament depolarization and lead to actin disassemble. In addition, microtubules are also disassembled probably directly by calcium ions while vimentin intermediate filaments remodeling could be mediated by PAD4 that citrullinates vimentin [214, 215]. Organelles, such as ER and mitochondria undergo alterations during NETosis. For example, LPS and ionomycin provoke ER's vesiculation, while proteins released from granules are found on NETs [208]. Mitochondrial DNA (mtDNA) is released extracellularly and is also found on NETs [216]. Finally, release of DNA in the extracellular environment requires the rupture of plasma membrane, which is a complex but still an under investigation process. Plasma membrane permeabilization to molecules happens progressively during NETosis, since there are no evidence showing rapid bursting or swelling of the membrane [208]. Gasdermin D can be again a pore mediator, as also biophysical mechanisms due to increased pressure to the membrane can also play a role [217].

3.2 NETs role in cancer

It is known now that NETs, apart from their physiological in immune response against pathogens, play also an important role in cancer progression and metastasis. In a model of breast cancer, but also in samples from triple negative breast cancer patients, cancer cells induce NETs formation that support and surround metastatic cancer cells in the lungs [218], while in colon carcinoma, NETs-associated protein carcinoembryonic Ag cell adhesion molecule 1 (CEACAM1) traps cancer cells and facilitates cancer metastasis [219]. Agonists of CXCR1 and CXCR2 released by tumors, promote the formation of NETs which shield tumor cells and protect them from $CD8^+$ T cells and NK mediated cytotoxicity, allowing them to successfully metastasize [220]. In addition, NETs associated NE and matrix mettaloproteinase (MMP) 9 proteases were able to induce dormant cancer cells proliferation, when lung inflammation induced the release of

NETs [221]. Circulating NETs in breast and colon cancer patients are recognized by cancer cells through the transmembrane protein coiled-coil domain containing 25 (CCDC25) and this interaction mobilizes cancer cells to form metastasis in distant sites [222]. Finally, NETs have been also associated with thrombosis in cancer patients. Specifically, elevated levels of circulating citrullinated histone 3 (H3Cit), that is known as a key protein in NETs, have been associated to increased risk of thrombosis in cancer patients [223].

Chapter 4: Pancreatic Ductal Adenocarcinoma

PDAC is the most frequent type of pancreatic cancers, constituting 90% of the total cases [224]. Based on statistics of the American Cancer's Society (https://www.cancer.org/cancer/pancreatic-cancer/about/key-statistics.html), PDAC is the fourth more lethal type of cancer in the western world and is predicted to climb up to the second place as leading cause of cancer-related deaths until 2030, since the chance to develop PDAC during the life period is currently 1 to 64 for each individual [225]. The survival rate of PDAC patients is dramatically low; less than 8% of the cases survive up to 5 years, while less than 20% of the patients surpasses the 1-year survival [226].

PDAC development is associated with various risk factors, such as smoking, age, diabetes and also familial predisposition [227]. Regarding the inheritance, germline mutations in the tumor suppressor genes (INK4A, BRCA2, LKB1), the DNA mismatch repair genes and the cationic trypsinogen gene (PRSS1) increase the risk of PDAC development. As far as the non-familial cases are concerned, mutations in four genes have key roles in PDAC development and they have been detected in more than 50% of the cases. These genes include KRAS, TP53, SMAD4 and CDKN2A [228, 229]. Moreover, other genes (KDM6A, BCORL1, RBM10, MLL3 etc) carry mutations in 5-10% of PDAC cases [230, 231]. In other cases, structural rearrangements of DNA have been found and patients can be categorized in four different groups based on the stability of their genome [230]. Another portion of PDAC patients shows DNA damage repair (DDR) deficiency, while recently it has been demonstrated that a great percentage of PDAC tumors is caused not in a stepwise manner, but is rather the result of a chromothripsis [232, 233].

Whole genome sequencing and deep-exome sequencing of 456 pancreatic cancers revealed that patients with pancreatic cancers can divided in four subgroups with different histopathological properties and mechanisms of evolution [234]. The four subtypes are the squamous, the pancreatic progenitor, the immunogenic and the

aberrantly differentiated endocrine exocrine (ADEX). The squamous subtype is associated with poor prognosis and is characterized by upregulation of genes involved in inflammation, hypoxia response, TGF-β signaling, metabolic reprogramming and MYC pathway. Tumors of this group carry mutations in TP53 and KDM6A, which in combination with mutation on TP53 regulate different pathways related to tumor progression, while hypermethylation of pancreatic endodermal cell-fate determining genes results in complete loss of their cellular identity. Pancreatic progenitor subtype shows modifications mainly in transcription factor genes linked to the early stage of tumor development. These genes regulate various pathways like fatty acid oxidation, steroid hormone biosynthesis and drug metabolism. Immunogenic pancreatic adenocarcinoma is similar to the pancreatic progenitor subtype but shows increased immune cell infiltration. In details, genes associated with different immune cell types, mostly linked to B and T cell infiltration and function, are upregulated. In addition, upregulation of CTLA-4, programmed cell death 1 (PD-1) and their related immune checkpoint pathways, suggest that patients belonging to this category could be treated with immune checkpoint inhibitors (ICI). Finally, ADEX tumor profile is defined by the expression of genes associated with the later stages of pancreatic development in both endocrine and exocrine lineages [234].

In general, numerous genomic studies have shed light in pancreatic cancers heterogeneity and led to the description of the phylotranscriptomic tree of pancreatic cancer, which categorizes patients based on their characteristic to the appropriate group. This categorization of patients in subgroups aims to find the best therapeutic approach for each patient and develop specific therapeutic agents for each subtype [224].

4.1 Therapeutic approaches in PDAC

The low rate survival, that we have previously mentioned, is the result of complex and various parameters that lead to PDAC development and progression. In other words, the lack of specific and early symptoms, the presence of a highly immunosuppressive

TME, the intermediate mutational burden and the desmoplastic stroma surrounding the tumor are associated with tumor progression, invasion and treatment resistance [235].

The majority of the patients with PDAC cancer bear non operable tumors (approximately 80%) either due to the advanced stage of the tumor or to the position of the tumor in the pancreas [236]. Patients having non-operable, advanced and/or metastatic tumors can be treated with chemotherapy alone or in combination with radiotherapy. These treatments are accompanied though with high toxicity and various side effects, without offering striking benefits [237]. On the other hand, following operation, patients undergo specific chemotherapeutic treatments with 5-fluorouracil (5-FU), gemcitabine or a combination of them [225]. Patients that received gemcitabine or 5-FU based chemoradiotherapy upon tumor removal have prolonged survival and disease-free survival compared to the group that was under observation, although the survival period is not extended for many months [238], [239]. Moreover, in metastatic disease, treatment with gemcitabine did not have any impact on overall survival, while treatment with multidrug regimen folinic acid-fluorouracil-irinotecan-oxaliplatim (FOLFIRINOX) prolonged survival for 5 more months [225]. There are also many ongoing trials that use 5-FU, gemcitabine and cisplatin in combination with other inhibitory drugs [240]. These therapeutic approaches used for PDAC tumors are far less than sufficient and have only moderate effects in prolonging overall survival, disease-free survival and patients' quality of life for few months [236]. Thus, there is a pivotal necessity to discover and develop novel approaches and strategies to target PDAC.

4.1.1 Immunotherapeutic approaches in PDAC

In the last years, immunotherapy has received a great amount of attention mainly because of striking effects on the treatment of patients with advanced stage cancers. Therefore, immunotherapeutic approaches are now under intense investigation for PDAC, showing that patients receiving immunotherapy have improvement of survival, even though the OS was not prolonged. A possible explanation of this phenomenon is the presence of the highly immunosuppressive TME, that could block the effect of the

treatments, indicating that combinatorial treatment could enhance the therapeutic efficacy [241]. The different immunotherapies on PDAC can be categorized into the following groups: neoantigens and cancer vaccines, adoptive cell therapy, immune checkpoint inhibitors, monoclonal antibodies and administration of cytokines. Below, we will mention the most important ones (Fig.5).

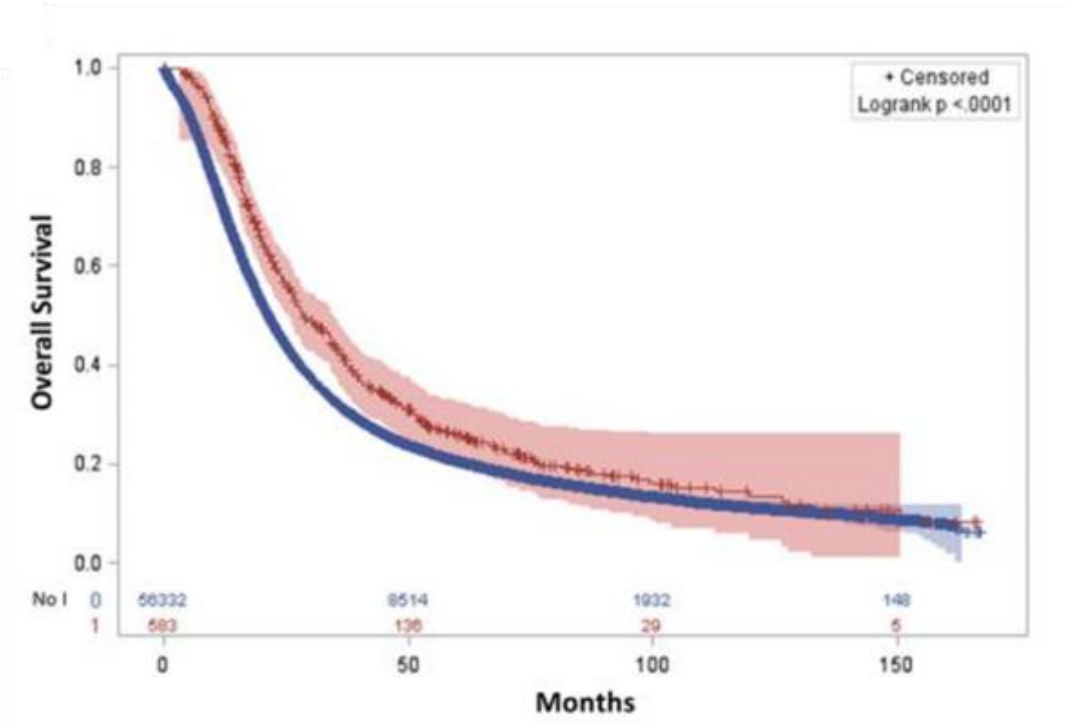

Figure 6. **OS with or without immunotherapy.**

Overall survival with (red) or without (blue) immunotherapy in a cohort of 63154 patients. Among those patients, 636 (1.01%) received immunotherapy. In the multivariable analysis, patients who received immunotherapy had a significant improvement of the survival, compared to the ones who did not. Nevertheless, the OS remains poor. Adapted from Amin S. et al, September 2020, Clin Transl Radiat Oncol.

4.1.2 Neoantigens

Even though PDAC mutational burden is intermediate compared to other tumors, a series of neoantigens have been discovered through the years. Neoantigens, defined as tumor-specific peptides produced by mutated somatic genes, can be used as targets for tumor treatment [242]. In PDAC genome, although approximately 30,000 mutations have been detected on DNA sequences, only 10% of the variants are transcribed, and among them few have been shown to be immunogenic and able to activate an anti-tumor immune response [243]. In PDAC long term survivors' neoantigens quality is proved to be superior than the quantity regarding the immunogenicity and neoantigen-mediated immunity could be correlated with prolonged survival and less cases of relapse [244]. Nevertheless, neoantigen-based immunotherapy is still obstructed by the complex TME present in PDAC, poor antigenicity, and high heterogeneity of pancreatic cells. Therefore, few clinical trials of Phase I are ongoing with peptide vaccines and just one with dendritic cells (DCs) stimulated with PDAC neoantigen (DC vaccine) [245].

4.1.3 CAR T cells

Adoptive T cell therapy is a promising treatment for many solid tumors, as it takes advantage of T cells feasibility to recognize tumor antigens and kill tumor cells. Specifically, chimeric antigen receptor (CAR) T cells are T cells isolated from the peripheral blood of patients and manipulated in the laboratory in order to express CARs that mimic TCRs activity. The final goal of this process is to create CAR T cells that recognize tumor antigens specifically expressed in each patient, expand them and infused them back to the patients to initiate antigen-mediated anti-tumor T cell responses [246]. The efficacy of CAR T cells in preclinical models of PDAC, such as transplantable human tumors or syngeneic tumors, patient-derived xenografts etc., has been demonstrated, while in humans, there are ongoing early phase clinical trials with CAR T cells targeting mesothelin, carcinoembryonic antigen (CEA) or (mucin-1) MUC-1 that are proteins expressed in high levels in pancreatic tumors [246, 247, 248]. For sure, though, overcoming the extremely immunosuppressive tumor microenvironment

and surpassing of the desmoplastic stroma, immunosuppressive cells and secreted inhibitory cytokines, will be a challenge to address in order to achieve maximal performance and survival of CAR T cells [249].

4.1.4 Immune checkpoint inhibitors (ICI)

The engagement of major histocompatibility complex (MHC) presenting antigens to the TCR results in T cells activation with a simultaneous activation of stimulatory and inhibitory signals, known as immune checkpoints. These molecules are responsible for the fine-tuning of T cell responses, while they maintain the balance between self-tolerance and the response to the non-self-antigens. Even so, cancer cells exploit this function of immune checkpoint molecules and use it for their own benefit, abolishing co-activatory signals and increasing co-inhibitory signals in order to evade anti-tumor immune responses [250]. The two most known co-inhibitory immune checkpoint axis used by tumors are the PD-1/PD-L1 and the CTLA4/ CD80 or CD86. In details, activated T cells upregulate PD-1 on their surface that binds to its ligand expressed in other immune cells, resulting in the shutting down of the T cells response. CTLA-4, also upregulated in T cells, interacts with CD80 or CD86 and inhibits immune responses [251].

Against those two pivotal molecules have been generated monoclonal antibodies with a great success in clinical trials. Ipilimumab, targeting CTLA4, was approved in 2011 while pembrolizumab and nivolumab, targeting PD-1, were approved in 2014 [252, 253, 254]. Although, these immune checkpoint inhibitors are a breakthrough in the treatment of many solid cancers, their results in PDAC remain poor. One of the reasons is the low infiltration of the pancreatic tumor tissues by effector T cells, while T_{regs} are the main infiltrating T cell population [255]. As in the previously described treatments, the strong stroma presence, the intermediate mutational burden and the highly immunosuppressive TME consist three more causes of ICI failure in PDAC [256].

Overall, although the immunothepareutic approaches sound promising, there is an urgent need to understand the suppressive mechanisms present in the TME of PDAC tissues, with view to target them and render TME more accessible to immunotherapy. Only in this way, immunotherapy could have a strong beneficial role on the treatment of PDAC.

4.2 The tumor microenvironment in PDAC

The complex TME of PDAC is responsible for tumor's rapid progression and immune evasion and the failure or inefficiency of the different therapeutic [257]. In details, PDAC surrounding microenvironment is consisted by a strong desmoplastic stroma of CAFs and ECM, which provide an unapproachable mechanical barrier to effector immune cells [258]. Specifically, pancreatic stellate cells, upon activation by cancer cells, generate a fibrotic environment that protects tumor cells from therapeutic agents, while simultaneously impedes normal vascularization and infiltration by tumor cells [259], [260]. This is further supported by the surrounding ECM where MMPs expression is upregulated in pancreatic tumor cells to assist tumor invasion [261]. Additionally, many ECM components are produced by CAFs, that also exert tumor-supporting functions, like angiogenesis, immune system suppression and metastasis [262]. Proline-derived ECMs are consumed by tumor cells to support mitochondrial respiration of tumor cells, generate energy and enhance tumor survival and proliferation [263]. Ultimately, nutrients availability in the tumor tissues shapes the behavior of each cell population, by modulating its function and this is another hallmark of PDAC. The reprogramming of infiltrated cells metabolism is mainly altered due to L-arginine and glutamine deprivation from the extracellular milieu. For example, L-arginine regulates pancreatic tumor progression, invasion and migration through various pathways (activation of mTORC1, NF-κB etc.) [264].

Moreover, PDAC tumors are characterized as 'cold' tumors, meaning that they are not infiltrated by effector T cells, but rather by immune cells with suppressive function that

further orchestrate and maintain the hostile, immunosuppressive TME of PDAC. Immunosuppressive populations that have been implicated in PDAC progression are the T_{regs}, TAMs, MDSCs and TANs [257]. In addition, cytokines, chemokines and other molecules, produced by the suppressive populations, play a fundamental role in the creation of this complex TME.

In this direction, PDAC tumors have been classified based on the representation of immunological cell populations in three subsets [265]. Firstly, the immune escape subset was characterized by low presence of effector T and B cells but high presence of T_{regs}. The OS of PDAC patients belonging to this group is 10 months and 54% of the PDAC cases are categorized in this group. Secondly, the immune rich subset, found in 35% of PDAC cases, has the exact opposite characteristics compared to the immune escape subset regarding cell infiltration. In other words, it is characterized by higher infiltration of effector T and B cells and lower presence of T_{regs}. Subsequently, patients show a longer OS (19 months) and they are appropriate subjects for immunotherapeutic approaches. The last and rarest immune exhausted subset, found in 11% of PDAC patients and having 10 months of OS, is subdivided in patients that exhibit high PD-L1 expression and $CD8^+/T_{reg}$ ratio and in patients with loss of DNA repair genes, microsatellite instability and highest $CD8^+/T_{reg}$ ratio [266].

Regarding T_{regs} role in PDAC, in early PanIN, T_{regs} are present in increased levels both in murine models and in human specimens, while their presence is also correlated with poor prognosis [267]. Moreover, TAMs, having the polarized M2 phenotype, are major orchestrators of immune suppression in the tumor sites. Specifically, PDAC pancreatic cells, expressing mutant KRAS, create local inflammation that leads to TAMs recruitment which in turn support pancreatic carcinogenesis and acinar-to-ductal metaplasia through the secretion of cytokines and components of ECM [268, 269]. TAMs promote cancer invasion, stimulate angiogenesis and inhibit anti-tumor immune responses by NK and T cells [270]. MDSCs are recruited in the tumor site or even in premalignant lesions and inhibit anti-tumor immune responses in murine models with $Kras^{G12D}$-dependent increase of granulocyte-macrophage colony-stimulating factor

(GM-CSF) or Tp53 mutation-dependent upregulation of TGFα, [271, 272]. Finally, PDAC cells recruit MDSCs in the tumor sites though the chemokine (C-C motif) ligand 2 and (C-C motif) chemokine receptor 2 (CCL2/CCR2) axis [273].

4.3 Neutrophils role in PDAC

More and more studies are now demonstrating the pro-tumoral role of recruited neutrophils from the periphery to the PDAC tissues [274]. Most importantly, TAN-high infiltrated PDAC tumors were found to have the poorest prognosis compared to TAN-low tumors [275].

To begin with, pancreatic tumor cells secrete chemokines that recruit neutrophils from the circulation. For instance, CXCR2 expressing neutrophils are recruited from tumor cells expressing CXCL1-3. When CXCR2 is knocked down specifically in the myeloid compartment of tumor bearing mice, less MPO^+ neutrophils and $CD11b^+Ly6G^+$ MDSCs infiltrated the tumor tissues [276]. Moreover, increased expression of CXCL-1, CXCL-2 and CXCLl-5 was positively correlated with increased infiltration of MPO^+ neutrophils in a KPC mouse model [173]. In humans, upregulation of CXCL-5 in PDAC patients is associated with higher infiltration of PDAC tissues from $CD15^+$ neutrophils and NE^+ granulocytes [277].

Another important issue regarding neutrophils' relationship with PDAC tumor relies on the secretion of cytokines from tumor cells that support neutrophils recruitment and survival. For example, PMN-MDSCs and neutrophils activity is supported by GM-CSF, G-CSF, and monocyte colony-stimulating factor (M-CSF) secreted by PDAC cells [278]. IL-1β, CD200 and ubiquitin-specific protease 22 (USP22) are also supporting neutrophils and PMN-MDSCs infiltration in PDAC tissues [279, 280, 281].

In KPC mice depletion of neutrophils delayed tumor progression, abolished metastasis and increased tumor cell apoptosis [274]. Neutrophils isolated from PDAC patients enhanced the migration of tumor cells in *in vitro* assays [282].

Neutrophils retain the ability to influence T cell responses. Neutrophils can interact with T_{regs} enhancing their proliferation, while they suppress $CD8^+$ T cells proliferation, leading them to apoptosis [278, 283]. In a pancreatic tumor model, blockade of IL-17 axis resulted in the decreased recruitment of neutrophils which were not able to form NETs and at the same time this was accompanied by increased levels of activated $CD8^+$ T cells [284].

Several studies have demonstrated that NETs produced by neutrophils have also pro-tumoral activity in PDAC. Serum collected from PDAC patients induced NETs formation, that support also pancreatic cells proliferation [282, 284]. NETs can also detain pancreatic tumor cells and induce epithelial-mesenchymal transition through the high mobility group box 1 (HMGB1) protein that is present in the NETs [285]. Inhibition of NETs formation resulted in inhibition of tumor growth [286].

Chapter 5: Humanized mouse model

Despite the impressive progress in the field of tumor immunology in the last decades, major questions remain unaddressed due to issues regarding the biological differences among humans and animal models. In other words, preclinical findings cannot be easily translated to clinical applications because often the model organisms cannot recapitulate the complexity and functionality of the human biological system. Thus, it has emerged the need for the development of a pre-clinical model closer to the human complexity but at the same time feasible for large scale experiments. This necessity led to the development of the humanized-immune reconstituted (HIR) mouse model [287]. HIR mice are generated with xenotransplantation of human derived cells of the human hematopoietic system or human tissues in deficient mouse recipients [288]. In details, HIR mice generation is based on three milestones: human cells source, deficient mouse strains and the presence of human soluble factors that will support the survival of human cells.

To begin with, different sources of human cells can be used for the reconstitution of the human biological system even though the engraftments of $CD34^+$ HSCs or PBMCs are the most successful approaches for the generation of HIR mice. $CD34^+$ HSCs derive from human fetal liver, cord blood, adult BM and peripheral blood after specific mobilization of the donor with G-SCF [289]. Fetal or neonatal derived cells display a more efficient engraftment than adult-derived cells. Before the injection of human cells, mice are conditioned by sublethal γ-radiation or chemical deletion of all endogenous HSCs [290]. Thus, the engraftment of human cells is facilitated

Recipient mice are the second crucial part for the successful reconstitution of the human immune system in HIR. In normal mice, other species derived-cells would be immediately rejected. Therefore, it is necessary the use of mice recipients with genetic deficiencies in cell populations responsible for the human cells rejection. Specifically, three mouse models are the most commonly used: NSG (NOD.Cg-Prkdc^{scid}Il2rg^{tm1wjl}), NOG (NODShi.Cg-Prkdc^{scid}Il2rg^{tm1Sug}) and BRG (C;129S4-Rag2^{tm1Flv}Il2rg^{tm1Flv}) mice

strains [291]. These strains contain specific mutations in enzymes involved in V(D)J recombination, resulting in the absence of mature B and T cells. Severe combined immunodeficiency (scid) or otherwise Prkdc^{scid} mutation results in a defective protein kinase involved in DNA repair, while mutations in the recombinant activating genes (*Rag)* impede DNA recombination [292, 293, 294]. In addition, mutated IL-2 receptor (IL-2R) γ-chain locus results in the defective NK, B and T cells, since the signaling pathways starting from this receptor are impeded [295]. A work in progress is the expression of human leukocyte antigen (HLA)-molecules in combination with murine H2 expression reduction in order to impede host innate immune functions and better performance by the human cells of the adaptive immunity [287].

As a third important part of a successful reconstitution of HIR mice, we can name the signaling soluble molecules (cytokines, chemokines and adhesion molecules) of the human system. In the absence of human factors, the human hematolymphoid system cannot be fully functional or exhibit long period survival in the murine recipients. To resolve this problem, recombinant cytokines are injected in the mice based on the desired model [296]. Another approach is the injection of vectors, such as plasmids, lentiviruses and adenoviruses, that encode for the human proteins [297]. Last but not least, genetic engineering of human cytokines genes in the recipient mice either by insertion of the human gene in the mouse locus or by using the bacterial artificial chromosome (BAC) transgenesis, are two other successful methods [291]. Based on the scientific questions, specific human cytokines are introduced in the mice recipients. For example, expression of human IL-3, GM-CSF and stem cell factor (SCF) in HIR mice leads to the increased presence of myeloid cells in the BM [298], while M-CSF expression results in increased percentages of monocytes and macrophages in HIR mice [299].

5.1 HIR mice in immune-oncology research

Regarding cancer research, despite the huge progression made in the last years, clinical translation of findings observed in rodents remains poor, as most of the studies

performed with mouse models fail to simulate efficiently the complex characteristics of human cancers [300].

In cancer research, immunodeficient mice can be engrafted with either cell-derived xenografts (CDX) or patient-derived xenografts (PDX). CDX model is based on the injection of human cancer cells, preferentially of early passages in order to maintain patient derived heterogeneity. On the other hand, PDX engrafted mice retain higher levels of the primary tumor malignancy and are considered a more potent model for the evaluation of anti-cancer drug screening in the pre-clinical studies, but their limitation consists in the fact that a complete human immune system is not present and therefore it is impossible to study the complex interaction that take play in the TME [301]. Obviously, both of the models lack the oncologic transformation of normal cells to malignant cells, as it happens in humans. Studies, though, demonstrated that transplantation of human healthy cells with mutations in tumor-suppressing genes or overexpression of oncogenes in immunenodeficient mice established progressively human tumors [300, 302]. In general, to overcome these obstacles, it is necessary to engraft mice with human-derived HSCs that will generate the human immune system, which subsequently will interact with the human tumors.

Although the optimization of the HIR model in cancer research is still active, many studies have demonstrated interesting results using it. Overall, HIR model can reveal the complex interplay among the different players (cancer cells, T cells, myeloid cells, stroma etc) of the reconstituted human TME [290]. Additionally, HIR mouse model shows great potential for the identification of biomarkers, the time-window analysis of the human cancer pathology and the evaluation of the therapeutic potential of anti-cancer therapies (like ICI). Most importantly, HIR mouse model can bridge the gap between preclinical murine model's and human's biology.

Aim of the Study

Although immunotherapeutic approaches have gained a lot of attention in the last years because of their impressive beneficial effect in many malignancies, their efficiency in several solid tumors remains extremely poor. The highly immunosuppressive microenvironment is pointed as one of the main culprit for such a failure, thus rendering urgent to investigate and understand the molecular mechanisms driving a tumor-promoting TME.

Tumor infiltrating myeloid cells alter anti-tumor T cells responses by consuming essential metabolic components. Particularly, the consumption of L-arginine by ARG1 has long been investigated and ARG1 role in immune suppression is notorious in tumor immunology; L-arginine consumption by ARG1 blocks T cells activation and proliferation.

Recent data in tumor-bearing mice indicate that myeloid ARG1 can impair the function of tumor-specific T lymphocytes; however, the evidence that the human ARG1 can act in the same way is still missing. While in mice, ARG1 is a cytosolic enzyme activated in monocytes/macrophages, in humans ARG1 is stored in PMN granules whose exocytosis is induced by different pro-inflammatory stimuli. Furthermore, secreted ARG1 is active as a full-length protein at alkaline pH, while it is inactive at physiological pH unless cleaved by PMN proteases. These differences among species restrain the clinical translation of results achieved in conventional mouse models.

We plan to investigate the immune regulatory activity of the cleaved, extracellular form of human ARG1 and exploit newly generated anti-human (h)ARG1 monoclonal antibodies to reprogram the immunosuppressive environment in human immune reconstituted mice engrafted with human tumors. We will then verify the ability of this hARG1-targeting strategy to increase the therapeutic effectiveness of adoptive cell transfer of telomerase-specific T cell receptor engineered T cells and immunotherapy based on checkpoint inhibitors. We expect to understand better the role of hARG1 in

cancer progression and confirm it as target for improving cancer immunotherapy of human tumors.

Material and Methods

Human samples

Peripheral blood samples, tumor tissues and serum were collected from patients with stages III and IV of PDAC, admitted at the Unit of General and Pancreatic Surgery of the Azienda Ospedaliera Universitaria Integrata of Verona before surgical resection or Healthy Donors (HD). Clinical-pathologic features of patients and HD are reported in Table 4. No subject had a prior history of cancer or was undergoing therapy at the time of sample collection. Informed consent was obtained from all participants and the study was approved by the Ethics Committee: for the use of PDAC and HD PBMCs, Prot. 25978, Prog. 2172 on 29/05/2012 P.I. Aldo Scarpa; for the use of PBMCs isolated from buffy coats (BC) or peripheral blood of healthy donors Prot. 24114 on 16/05/2017 P.I. Vincenzo Bronte.

Isolation of human PBMCs and PMNs

Peripheral blood from HDs or PDAC patients was collected in EDTA-coated tubes and layered on top of Ficoll-Paque™ Plus (17-1440-03, GE Healthcare) to obtain PBMC and RBC fractions. Upon stratification the cells were spun at 400g, 30 minutes, RT, brake turned off. The PBMC fraction was collected, washed three times with PBS and then cells were counted. The monocyte fraction ($CD14^+$) was further isolated, starting from the PBMC fraction, by CD14-microbeads (130-050-201, Miltenyi Biotec), following manufacturer's instructions. From the $CD14^-$ fraction LDNs were isolated by the sequential addition of CD66b-FITC antibody (555724, BD Biosciences, NJ, USA) and microbeads anti-FITC (130-048-701, Miltenyi Biotec), following manufacturer's instructions.

PMNs were isolated from the red blood cells (RBC) layer by dextran density gradient (Sigma-Aldrich) after 20 minutes incubation at 25 °C and collection of the upper layer. The cells were spun at 200g, 5 minutes, 25 °C, then the remaining contaminant RBCs were lysed with 4 mL of 0.2 % NaCl solution (30 seconds, 25 °C) and the reaction was

blocked by adding 9 mL of 1.2 % of NaCl solution. PMNs from healthy donors were plated and stimulated with ionomycin calcium salt (5 μM, 10634-5MG, Sigma-Aldrich) for 30 minutes or 2 hours. At the end of the stimulation, supernatant-containing NETs and cells were collected and used for downstream assays. NDNs were isolated by CD66b-antibody as LDNs. Samples with purity, evaluated by FACS analysis; greater than 95 % were assessed in the functional assay.

In some experiments, isolated PMNs either stimulated or left untreated, were evaluated for cell size by ImageJ software upon being plated on cover glasses and imaged by SP5 Leica confocal microscope.

Cell size determination in activated HD-derived neutrophils

In some experiments, HD-derived $CD66b^+$ NDNs either stimulated with ionomycin calcium salt (5 μM, 10634-5MG, Sigma-Aldrich) for 30 minutes or 2 hours or left untreated, were evaluated for cell size by ImageJ software. Briefly, cells were plated (1 $x10^6$/ml) and let to adhere for 30 minutes to cover glasses, then stimulated for 30 minutes and 2 hours, at 37 °C. At the end cells were fixed in 4 % paraformaldehyde (PFA), washed twice with PBS, stained with 4′,6-Diamidino-2-phenylindole dihydrochloride (DAPI) and anti-histone H3 citrulline on arginine residues R2, R8 and R17, 1 μg/ml (ab 5103, Abcam) then mounted in microscope slides and imaged with SP5 Leica. Intensity of the signal of both DAPI and H3citr helps to define the changes in size, as described in [213, 303].

NETs formation and quantification

PMNs isolated from peripheral blood or buffy coats of HD, were plated (1 $x10^6$/ml) and stimulated with ionomycin calcium salt (5 μM, 10634-5MG, Sigma-Aldrich) for 30 minutes and 2 hours, at 37 °C. At the end of the stimulation, supernatants, containing NETs, were collected and spun at 600g, 10 minutes, 25 °C to remove cellular debris. The NET-enriched supernatants were evaluated for DNA content, using NanoDrop

ONE (13400518, Thermo Scientific). NETs were then assessed for their suppressive capacity in proliferation assay. Simultaneously, the plated cells were detached using PBS-EDTA 2 mM, and were also spun down and stored at -80 ˚C.

NET quantification by DNA-MPO- complex ELISA

In serums from PDAC patients and HD and NET-containing supernatants collected from PDAC patients we evaluated the presence of NETs, following the protocol published by Veras et al. [304]. Briefly, NUNC flat 96-well plates were coated with the anti-MPO antibody (Thermo Scientific; cat. PA5-16672) overnight at 4 °C and then blocked with 1% BSA. Samples were incubated for 2 hours at 25 °C with gentle shaking (320 rpm) and then the plate was washed thrice with PBS. The complex of DNA-MPO was quantified with the Quant-iT PicoGreen kit (Thermo Scientific; cat. P11496) according to the manufacturer's instructions.

Cell lines

SK-MEL-5 cell line (human metastatic melanoma) was acquired by American Type Culture Collection (ATCC) (HTB-70™). Cells were cultured in RPMI 1640 medium (Lonza Biowhittaker) supplemented with 10% Fetal Bovine Serum (FBS) Superior (Merck), 2 mM L-glutamine, 0.1 mM sodium pyruvate, 0.1 mM HEPES and 100 U/ml penicillin and streptomycin (all from Euroclone), according to ATCC recommendations. Cell cultures were kept in incubators of 37 °C and 5 % CO_2. Cell lines were thawed from primary stocks maintained under liquid nitrogen and cultured for a maximum of 1 month, during which time all experiments were performed. Cell lines were tested by PCR for mycoplasma before the experiments using MycoAlert LookOut® Mycoplasma PCR Detection Kit (Sigma-Aldrich). T2 human T leukemia (HLA-A 02^+) cell line was obtained from ATCC (CRL-1992™), and was maintained in RPMI 1640 medium (Lonza Biowhittaker). Medium was supplemented with 10 %

FBS (Gibco), 2 mM L-Glutamine, 10 mM HEPES, 100 U/ml Penicillin, and 100 U/ml Streptomycin, and cells were maintained at 37 °C in a 5 % CO_2 atmosphere.

Mice

NOG mice were purchased from Taconic Biosciences. All mice were maintained under specific pathogen-free conditions in the animal facility of the University of Verona. Animal experiments were performed according to national (protocol number 12722 approved by the Ministerial Decree Number 14/2012-B of January 18, 2012 and protocol number BR15/08 approved by the Ministerial Decree Number 925/2015-PR of August 28, 2015) and Europeans laws and regulations. All animal experiments were approved by Verona University Ethical Committee (http://www.medicina.univr.it/fol/main?ent=bibliocr&id=85) and conducted according to the guidelines of Federation of European Laboratory Animal Science Association (FELASA). In each animal experiment, mice were randomly assigned to each group.

Humanization of mice

NOG mice were γ-irradiated (1.2 Gy) and after six hours engrafted with 10^5 hHLA $A2^+$-$CD34^+$ cord blood cells via tail vein injection (i.v.), as previously reported [305]. To favor the expansion of myeloid compartment, 108 MOI of recombinant adeno-associated virus serotype 9 (AAV9) vectors coding for human CSF3, IL-3, IL-8 and hepatocyte growth factor (HGF) were administered intramuscularly (i.m.) at week 4 after engraftment. In brief, cDNAs were purchased from GeneScript and AAV9 vectors were produced by Prof. M. Giacca's laboratory by co-transfection of HEK293T cells, as described [306]. Human hematopoietic engraftment was considered adequate when 10-25 % of hCD45-expressing cells were detectable in peripheral blood of mice by flow cytometry, according to the formula: frequency of $hCD45^+$ cells / (frequency of $hCD45^{+\ +}$ frequency of $mCD45^+$ cells) x 100.

Systemic treatment of humanized mice

Ten weeks after AAV9 transfer, humanized (HIR) mice were inoculated subcutaneously with 10^6 SK-MEL-5 cell line. When the tumor reached 200 mm^3 the treatments started (V (mm^3)=(d2 x D)/2, where d (mm) and D (mm) are the smallest and largest perpendicular tumor diameters, respectively, as assessed by caliper measurement). 2.5 x 10^6 human telomerase reverse transcriptase $(hTERT)_{865-873}$-TCR-engineered T cells were injected every 5 days for the first two injections, then once a week for the last two injections. The antibody clone 1.10 αARG1 followed the same scheme of injection of hTERT CD3 T cells except that it was administered two days in advance. At the same time of adoptive T cell transfer, IL-2 was injected i.p. 20 IU/mL (Novartis), then IL-2 was given every other day. The day before hTERT-specific T cell injection, the mice received i.p. 20 mg/kg of αARG1 clone 1.10 or IgG1 isotype control. Two days after the last hTERT-specific T cell injection, the mice were sacrificed, organs (spleen, lymph nodes, tumor and bone marrow) were collected and analyzed by flow cytometry and IF. Some mice received hTERT-specific T cells only or in combination with αARG1 clone 1.10 or IgG1 isotype control. Some mice were left untreated.

Systemic treatment of humanized mice with checkpoint inhibitors

HIR mice were inoculated (s.c.), at week 14 from $CD34^+$ engraftment, with 106 SK-MEL-5 melanoma cells. When the tumor reached 200 mm^3, some mice received a combination of Nivolumab (Opdivo, Bristol Mayers Squibb) 10 mg/kg (i.p.) and Ipilimumab (Yervoy, Bristol Mayers Squibb) 5 mg/kg (i.p.), every 5 days (doses and schedule were adapted from [306]. Some mice received αARG1 clone 1.10 (20 mg/kg) i.p. alone or in combination with Nivolumab and Ipilimumab.

Humanized mouse analysis of organs and blood

Analysis of leukocytes populations was performed on tumors, spleens, bone marrow and peripheral blood of tumor bearing HIR treated with adoptive cell therapy (ACT). Upon the sacrifice of the animals, the organs were collected reduced to single cell suspension. Peripheral blood was collected, once every two weeks, to test the humanization levels of the mice. Red blood cells were lysed and samples were stained according to the protocol. Tumors were cleaned from irrelevant tissues, minced and digested using an enzymatic mix containing 1 mg/ml collagenase IV, 1 mg/ml hyaluronidase and 4.5 mg/ml DNase (Sigma-Aldrich). After a 45 minutes-1 hour incubation at 37 °C, samples were filtered through a 70 µm pore size filter, and centrifuged at 300g, 5 minutes at 4 °C. When necessary, red blood cells (RBCs) were lysed with ACK buffer (10-548E, Lonza BioWhittaker). Tumor cells were counted and used for flow cytometry staining, according to the protocol described below. Spleens were mechanically digested and filtered through a 70 µm pore size filter, and centrifuged at 300g, 5 minutes at 4 °C. RBCs were lysed by adding 5 mL of ACK lysis buffer for 10 minutes at 25 °C. Reaction was blocked with the addition of 5 mL 10 % FBS-RPMI. Samples were centrifuged as before and cells were counted and stained. Bone marrow was isolated from bones of the limbs by flashing it out and processed as described above.

Flow cytometry analysis of HIR mice peripheral blood

For HIR-derived samples, the staining was performed using 10^5 cells. Samples were washed once with PBS 1X and non-specific binding sites were blocked by adding 2 µl of human FcR Blocking reagent (130-059-901, Miltenyi Biotec) and 2 µl of purified anti-mouse CD16/32 (clone: 93, 101302, Biolegend) reagent for 10 minutes at 4 °C. Without any wash, we added the following antibodies, diluted in 2 % FBS-PBS: human anti-CD45 PerCP-Cy5.5 (clone: 2D1, 368504, Biolegend), mouse anti-CD45 APC eFluor™ 780 (clone: A20, 47-0453-82, Thermo Scientific), human anti-CD19 FITC

(555412, BD Biosciences), human anti-CD3 APC (551378, BD Biosciences), human anti-CD15 V450 (642917, BD Biosciences), human anti-CD14 PE (clone: M5E2, Biolegend), anti-mouse Vβ3 TCR (clone: KJ25, 553208, BD Biosciences), human anti-CD34 BV421 (clone: 581, 562577, BD Biosciences) anti-CD3 PE/Cy7 (UCHT1, Thermo Scientific). Samples were incubated for 30 minutes at 4 °C, washed with 2 % FBS in PBS 1X and centrifuged in the same conditions as before. Then, samples were lysed by adding 2 % FBS in PBS 1X and Cal-Lyse lysing solution (GAS010, Thermo Scienfitic) at a ratio 1:1, incubated for 10 minutes at 25 °C protected from the light, followed by addition of 1 mL of milliQ water and a 10 minutes incubation, as before. In the end of the second incubation, samples were washed with 2 % FBS in PBS 1X and read in BD FACS Canto II (BD Bioscience). In some samples we evaluated the expression of CD69 (clone L78, PE Mouse Anti-Human CD69, BD Biosciences, 3 µg/ml), CD25 (clone M-A251, BV510 Mouse Anti-Human CD25, BD Biosciences) and PD-1 (clone RMP1-30, BV421 Rat Anti-Mouse CD279, BD Biosciences). For the intracellular detection of Ki67 (clone B56, Alexa Fluor 488 Mouse anti-Ki-67, BD Biosciences) cells were first stained with the mix of antibody described above then the cells were fixed and permeabilized using eBioscience™ Foxp3/ Transcription Factor Staining Buffer Set according to the manufacturer's instructions (00-5523-00, Thermo Scientific). In some experiments, BD Horizon Brilliant Stain Buffer was used (563794/566349, BD Biosciences).

Flow cytometry analysis of human cells

To quantify the amount of monocytes and monocyte subsets (defined as classical, $CD14^{high}CD16^{low/dim}$; intermediate $CD14^{int}CD16^{+}$; non classical $CD14^{low/dim}CD16^{high}$), peripheral blood was incubated with FcR Blocking reagent (Miltenyi Biotec, Paris, FR) followed by the addition of: anti-human PE-conjugated CD56 (BD Bioscience, San Jose, CA, USA; clone NCAM16.2), FITC-conjugated-CD16 (Biolegend, San Diego, CA, USA; clone 3G8), PerCP-Cy5.5- conjugated CD3 (BD Bioscience, San Jose, CA, USA; clone UCHT1), PE.Cy7-conjugated HLADR (eBiosciences, Thermo Scientific,

Waltham, MA, USA; clone L243), APC.H7- conjugated CD14 (BD Bioscience, San Jose, CA, USA; clone MφP9), Brilliant Violet 421™- conjugated PD-L1 (BD Bioscience, San Jose, CA, USA; clone MIH1) antibodies and Aqua LIVE/DEAD dye (Thermo Scientific, Waltham, MA, USA). RBCs were lysed using Cal-Lyse™ Lysing Solution (GAS010, Thermo Scientific, Waltham, MA, USA). For the intracellular ARG1 and MPO detection, cells were first stained with the mix of antibody described above then the cells were fixed and permeabilized using eBioscience™ Foxp3/ Transcription Factor Staining Buffer Set according to the manufacturer's instructions (00-5523-00, Thermo Scientific). The monoclonal Alexa-Fluor647-conjugated anti-Arginase-1 (1mg/ml, clone 1.10, hybridoma described in this manuscript) was diluted 1:1000 and added for 1h. Anti-MPO (3 µg/ml, clone 5B8, BD Biosciences) antibody was added to the cells and incubated for the same time.

Proliferation assay

For samples derived from HD, 5 x 10^5 PMNs resuspended in L-arginine free complete RPMI 1640 (06-1100-07-1A, Biological Industries) were seeded in 24-well plates, and they were stimulated with ionomycin calcium salt (5 µM, 10634-5MG, Sigma-Aldrich) for 30 minutes or 2 hours and at the end of the stimulation, supernatants were collected. Alternatively, from PDAC-derived samples, 2 x 10^5 - 5 x 10^5 NDN $CD66b^+$ or LDN $CD66b^+$ PMNs resuspended in L-arginine free complete RPMI, were seeded in 24-well plates and after 12 hours, supernatants were collected. 4 x 10^4 - 8 x 10^4 CellTrace labelled PBMCs, were resuspended in the appropriate supernatants according to the experiment, and were stimulated with coated anti-CD3 (clone: OKT-3, 16-0037-81, Thermo Scientific) and soluble anti-CD28 (clone: CD28.2, 16-0289-81, Thermo Scientific). 150 µM of L-arginine (Sigma-Aldrich) were also added in the culture. According to each experiment, inhibitors or antibodies were added: αARG1 clone 1.10 and isotype IgG1 (10 ng/ml, 100 ng/ml, 500 ng/ml, 10 µg/ml , 50 µg/ml, 100 µg/ml, 150 µg/ml, 250 µg/ml), nor-NOHA (30 ng/ml, 399275, Calbiochem), BEC (10.5 ng/ml, 197900, Calbiochem). For the PDAC samples, the functional assay was performed by

adding 200 µl of serum, instead of L-arginine free complete RPMI. As positive control we used PMBC stimulated with only anti-CD3 and soluble anti-CD28. As negative control (resting) was used PBMCs in RPMI complete media, containing 150 µM L-arginine. At the end of the culture, cells were stained with anti-CD3-PE/Cy7 (clone: UCHT1, 25-0038-42, Thermo Scientific) and CellTrace signal of lymphocytes was analysed with FloJow software (Tree Star, Inc. Ashland).

CellTrace labelling of PBMCs

PBMCs collected from buffy coats or peripheral blood of healthy donors through the stratification of the blood on top of Ficoll-Paque™ Plus, as described above, were washed, counted and frozen in liquid nitrogen. Upon thawing, PBMCs were re-counted and stained with CellTrace Violet Kit (Thermo Scientific) according to the manufacturer's instructions. Briefly, 1 µL of 5 mM CellTrace dye was added to 10^7/mL PBMCs (final concentration, 5 µM). Cells were incubated for 5 minutes at 37 °C and the reaction was blocked by the addition of RPMI containing 10 % FBS. Cells were centrifuged at 1400 rpm, 5 minutes, 4 °C. The cells were resuspended in RPMI containing 10 % FBS and left to rest at least 2 hours prior to the functional assay setting.

Matrix-assisted laser desorption ionization time of flight (MALDI-TOF) mass spectrometry analyses

Recombinant human (rh) ARG1 was diluted in a TFA solution (50:50 acetonitrile: water, 0,1 % TFA). The sample solution was mixed with an internal standard (BSA) and then with a sinapinic acid (10 mg/ml in ACN:H20 1:1 with 0,1% TFA), and 1 µl of the resulting sample/matrix solution was spotted in triplicate onto a Ground steel MALDI target plate (Bruker Daltonics) and allowed to dry at room temperature. Maldi TOF MS analyses were performed on a Bruker UltrafleXtreme MALDI-TOF/TOF instrument (Bruker Daltonics). Mass spectra were collected from m/z 5000 to 50000 in positive linear mode. Instrument calibration was performed using a protein standard

mixture composed of bovine serum albumin, protein A and trypsinogen. An ARG1 standard solution was incubated with 2.5 µg of Cathepsin S or Cathepsin G for 2 hours and 12 hours at the end of incubation was added 2 mM PMSF. The digested peptides (in 0.1% TFA) were extracted by ZipTip (tipe size P10Millipore) C4 and C18 tips with a sandwich layer method on target plate. The analysis was performed in a mass range 1200-7000 m/z and 800-3000 m/z for C4 and C18 tips respectively. All mass spectra were acquired in reflector mode. Instrument calibration was performed using a peptide calibration standard from Bruker Daltonics.

Liquid chromatography- mass spectrometry (LC-MS/MS) for Analysis of Proteome

Peptides were separated on an EASY-nLC 1000 HPLC system (Thermo Scientific) coupled online to a Q Exactive mass spectrometer via a nanoelectrospray source (Thermo Scientific). Peptides were loaded in buffer A (0.5 % formic acid) on in house packed columns (75 µm inner diameter, 50 cm length, and 1.9 µm C18 particles). Peptides were eluted with a non-linear 270 min gradient of 5 %–60 % buffer B (80 % ACN, 0.5 % formic acid) at a flow rate of 250 nl/min and a column temperature of 50 °C. Operational parameters were real-time monitored by the SprayQC software. The Q Exactive was operated in a data dependent mode with a survey scan range of 300-1750 m/z and a resolution of 70’000 at m/z 200. Up to 5 most abundant isotope patterns with a charge ≥ 2 were isolated with a 2.2 Th wide isolation window and subjected to higher-energy C-trap dissociation (HCD) fragmentation at a normalized collision energy of 25. Fragmentation spectra were acquired with a resolution of 17,500 at m/z 200. Dynamic exclusion of sequenced peptides was set to 45 s to reduce the number of repeated sequences. Thresholds for the ion injection time and ion target values were set to 20 ms and 3E6 for the survey scans and 120 ms and 1E5 for the MS/MS scans, respectively. Data were acquired using the Xcalibur software (Thermo Scientific).

Analysis of Proteomics Data

MaxQuant software (version 1.3.10.18) was used to analyze MS raw files. MS/MS spectra were searched against the human Uniprot FASTA database and a common contaminants database by the Andromeda search engine. Cysteine carbamidomethylation was applied as fixed and N-terminal acetylation and methionine oxidation as variable modification. Enzyme specificity was set to trypsin with a maximum of 2 missed cleavages and a minimum peptide length of 7 amino acids. A false discovery rate (FDR) of 1 % was required for peptides and proteins. Peptide identification was performed with an allowed initial precursor mass deviation of up to 7 ppm and an allowed fragment mass deviation of 20 ppm. Nonlinear retention time alignment of all measured samples was performed in MaxQuant. Peptide identifications were matched across different replicates within a time window of 1 min of the aligned retention times. A library for 'match between runs' in MaxQuant was built from additional single shot analysis at various time points as well as from OFF gel fractionated peptides of PMNs. Protein identification required at least 1 razor peptide. A minimum ratio count of 1 was required for valid quantification events via MaxQuant's Label Free Quantification algorithm (MaxLFQ). Data were filtered for common contaminants and peptides only identified by side modification were excluded from further analysis. In addition, it was required to have a minimum of two valid quantifications values in at least one group of replicates. Copy numbers were estimated based on the protein mass of cells.

Isothermal titration calorimetry (ITC)

The interaction of rhARG1 with either the Ab clone 1.10 or rhCTSS were investigated by isothermal titration calorimetry using a MicroCal PEAQ-ITC instrument (Marven). Typically, 40 consecutive injections of 1 µL aliquots of the interacting (Ab clone 1.10 and rhCTSS) protein were added at a stirring speed of 750 rpm into the calorimeter cell filled with the binding protein (rhARG1). Injections were made at intervals of 3 minutes. Control experiments were recorded by injecting the same protein solutions into the buffer solution and the resulting heat changes were subtracted from the

measured heats of binding. The heat generated by the interactions upon each injection was measured by the system and plotted against the molar ratio in the reaction cell. The data were then fitted using the MicroCal analysis software to estimate the binding constants and thermodynamic parameters. For all proteins the buffer was exchange with PBS pH 7.2 using an Amicon Ultra concentrator (10 kDa filter, 0.5 mL). To evaluate the binding between Ab clone 1.10 and rhARG1, the antibody was present at a concentration of 45 µM while rhARG1 was used at a concentration of 3 µM. In the case of the binding of rhARG1 with rhCTSS, rhARG1 was at 22 µM, and rhCTSS at 4 µM.

Immunoblots

Pellets were lysed by incubation with PIERCE ™ RIPA buffer (89901, Thermo Scientific) containing 2 mM PMSF, 0.2 µM sodium ortovanadate and 1x proteases inhibitor cocktail tablets (11836145001, Roche), for 30 minutes on ice. Samples were centrifuged for 10 minutes at 4 °C and total protein was quantified by BCA assay with the Quantum Protein Bicinchoninic Protein Assay kit (EMP014250, Euroclone S.p.A.) using as a standard the Protein Standard (P0914-10AMP, Sigma-Aldrich). 40 µg of pellet derived lysates or 36 µl of PMNs derived supernatants, containing 2X Laemmli Sample Buffer (161-0737, Bio-Rad Laboratories) or 4X Laemmli Sample Buffer (161-0747, Bio-Rad Laboratories), were separated in NuPAGE™ 10 % Bis-Tris Midi Gels (WG1201BX10, Thermo Scientific) and then transferred to nitrocellulose membranes 0.45 µm (162-0115, Bio-Rad Laboratories). Blocking of the membranes was performed with 5 % non-fat milk diluted in 0.1 % TBS-Tween 20 (170-6531, Bio-Rad laboratories, Inc.) for 1 hour at 25 °C. Primary antibodies diluted in the appropriate buffers according to the data sheets were incubated overnight at 4 °C. Primary antibodies used were: arginase I (clones: 19.8, 1.10), Cathepsin S E-3 (SC-271619, Santa Cruz Biotechnologies), mouse β-actin-HRP conjugated (clone: 8H10D10, 12262S, Cell Signaling), rabbit GAPDH-HRP conjugated (clone: 14C10, 3683S, Cell Signaling). Membranes were washed with 0.1 % TBS-Tween-20 (3 times, 5 minutes

each, 25 °C). Secondary antibodies, diluted in 5 % non-fat milk in 0.1 % TBS-Tween-20, were added to the membranes for 1 hour at 25 °C. Secondary antibodies used were: ECL™ Anti-Rabbit, Horseradish Peroxidase linked whole antibody from donkey (NA934V, GE Healthcare), Anti-Mouse Horseradish Peroxidase Linked whole antibody from sheep (NXA931V, GE Healthcare). Membranes were washed with 0.1 % TBS-Tween-20 (3 times, 5 minutes each, 25 °C) and PBS 1X (1 time, 5 minutes, 25 °C). Membranes were developed using Super Signal ™ West Femto Maximum Sensitivity Substrate (34096) or Super Signal® West Pico Chemiluminescent Substrate (34080) by Thermo Scientific. Images were acquired with the Luminescent Image Analyzer ImageQuant 4000 by GE Healthcare.

Immunoprecipitation

5 x 10^7 PMNs from buffy coats, isolated as described above, were cultured with RPMI containing ionomycin calcium salt (5 μM, 10634-5MG, Sigma-Aldrich) for 30 minutes or 2 hours in petri dishes. Control conditions of this stimulation were the time point 0 minutes, from which pellets were collected and stored at -80 °C, and the time points 30 minutes and 2 hours untreated (media). Media of the cultures was collected, centrifuged (1400 rpm, 10 minutes, 4 °C) and supernatants were stored at -80 °C. Also, cells from the cultures were detached using PBS – 2 mM EDTA, centrifuged (1400 rpm, 10 minutes, 4 °C) and stored as pellets at -80 °C. Pellets from the different time points were lysed by a 30 minutes' incubation with PIERCE ™ IP Lysis buffer (87788, Thermo Scientific) containing 2 mM PMSF, 0.2 μM sodium ortovanadate, 1X proteases inhibitor cocktail tablets (11836145001, Roche) and 1X Halt™ phoshatase inhibitor cocktail (1862495, Thermo Scientific). Protein concentration was quantified by the BCA assay with the Quantum Protein Bicinchoninic Protein Assay kit (EMP014250, Euroclone S.p.A.) using as a standard the Protein Standard (P0914, Sigma-Aldrich). 150 μg of protein or 200 μl of supernatants were used for the immunoprecipitation experiment, which was performed with the Immunoprecipitation Kit-Dynabeads ™ Protein G (10007D, Thermo Scientific) according to the

manufacturer's instructions. Antibodies used were: ARG1 clone 1.10 (2 µg), mouse IgG (2 µg, stock: 1 mg/ml, I-2000, Vector Laboratories Inc.). 1 mM DTT was added to the samples. Samples were run, according to the Immunoblot protocol described above and proteins were detected by incubation with αARG1 clone 19.8 following the indication described above in the immunoblot section.

Immunofluorescence staining of NETs in cells

4 x 10^5 PMNs, isolated as described above, were seeded in coverslips for 2 hours in incubators of 37 °C, 5 % CO_2 and then were stimulated with ionomycin calcium salt (5 µM, 10634-5MG, Sigma-Aldrich), PMA(12 nM, P8139, Sigma-Aldrich, as control was used DMSO in the same dilution), and IL-8 (20 nM, 130-108-979, Miltenyi Biotec) for 30 minutes and 2 hours or left untreated (media). Cells were fixed with 4 % PFA (stock: formaldehyde solution 36,5-38 % diluted in H2O, F8775-4X25ML, Sigma-Aldrich) for 10 minutes and washed with 0.05 % PBS-Tween-20 (170-6531, Bio-Rad laboratories, Inc.) for 3 times, 5 minutes, 25 °C. Blocking of unspecific binding sites was performed with 20 % normal goat serum (S-1000, Vector laboratories, Inc.) in 0.1 % PBS-Triton® X-100, Sigma Ultra (T9284, Sigma Aldrich) for 2 hours at 25 °C. Primary antibodies were incubated overnight at 4 °C diluted accordingly in PBS and washed with 0.05 % PBS-Tween 20 (3 times, 5 minutes, 25 °C). Primary antibodies used were: ARG1-Alexa Fluor 647 conjugated (1:1000), mouse IgG1 k Isotype control APC (stock: 1 mg/ml, 1:3000, P3.6.2.8.1, 16-4714-82, Thermo Scientific), rabbit polyclonal anti-CTSS (H00001529-D01, Abnova), rabbit polyclonal anti-myeloperoxidase (ab9535, Abcam). Secondary antibodies, diluted in 20 % Normal goat serum in 0.1 % PBS-Triton X-100, were incubated for 1 hour at 25 °C and washed with 0.05 % PBS-Tween-20 (3 times, 5 minutes, 25 °C). Secondary antibodies used were: Alexa Fluor ® 488 goat anti-rabbit IgG (H^+L) (stock: 2 mg/ml, 1:1000, A11034, Thermo Scientific). DAPI (1:1000, D9542-10MG, Sigma-Aldrich) was used for the visualization of the nuclei and washed PBS 0.05 % Tween-20 (2 times, 5 minutes, 25 °C) and once with PBS 1 X (5 minutes, 25 °C Cover slips were mounted with ProLong

® Gold antifade reagent (P36930, Thermo Scientific) and visualized with Leica TCS SP5 AOBS inverted confocal live cell imaging system. Analysis of the images was performed with Leica Application Suite X (LAS X) or ImageJ software. NETs were quantified by the colocalization of (Pearson's correlation) extracellular DNA and MPO. On NETs, we then quantified the levels of ARG1, to define the amount of ARG1 associated to NETs.

IF quantification in HIR-derived tumor tissues

Images were acquired from mice tumor tissues using an SP5 tandem confocal scanning microscope at a magnification of 10X with a resolution of 1.024 × 1.024 pixels (1.240 × 1.240 μm area). Cells were counted in a blinded fashion in three sections for each tissue. Ten images were acquired randomly in a blinded fashion for each section with a median z-volume of 40 μm. The results were expressed as a mean value of the absolute number of cells per acquisition field or the total number of cells for each tissue.

NETs detection in tumor tissues by immunofluorescence

NETs were evaluated in tumor tissues of PDAC patients. Tumor tissues were fixed in 4 % PFA, embedded in paraffin and cut into 7 μm thick sections. Paraffin was removed and antigen retreaval with citrate buffer (pH 6.5) was performed before the tissue slides were incubated in blocking buffer for 2 hours at room temperature and then treated with the following primary antibodies: 5 μg/ml anti-myeloperoxidase (MPO, AF3667, R&D) overnight at 4 °C and anti-histone H3 citrulline $R2^{+}R8^{+}R17$, 1 μg/ml (ab 5103, Abcam). After washing with 0.05 % Tween-20 in PBS, we added a fluorophore-conjugated secondary antibody (Alexa Fluor 488, Alexa Fluor 680, Thermo Scientific) in blocking solution. Nuclei were stained with 1 μg/ml DAPI (Sigma-Aldrich) for 8 minutes in the dark. Finally, the sections were washed with PBS, transferred to glass slides and mounted with Dako medium. Glass slices were kept at 4 °C in the dark and analyzed using an SP5 confocal scanning microscope (Leica, Germany). NETs were

quantified by the colocalization of (Pearson's correlation) extracellular DNA and MPO or DNA and H3 citrullinated. On NETs, we then quantified the levels of ARG1 and CTSS to define the amount of ARG1 associated to NETs. IF analysis was performed using Image J software.

Quantification of proteins in serum

ELLA (R&D Systems) was used to evaluate the serum levels of IL-8, using the following chip (SPCKA-PS-003229, Protein Simple a Biotechne brand), according to the manufacturer's instructions.

Colorimetric determination of ARG1 activity assay

This assay was performed in supernatants collected from untreated or treated PMNs and in serum collected from PDAC patients, and the evaluation of ARG1 activity was based on the concentration of L-ornithine (µM) calculated based on defined standard curve. Standard curve was prepared by seven consecutive 1:2 dilutions of the 50 µM stock concentration of L-ornithine. Then, in 30 µL of each point of the standard curve, blank and samples, were added 25 µL of MnCl2 21.6 mM, followed by 20 minutes incubation at 55 °C (only the samples). 150 µL of 100 mM carbonate buffer pH 9.5 or 7.3 were added, as also 50 µL of 100 mM L-arginine. All the tubes were incubated for 2 hours at 37 °C. The reaction was blocked by adding 750 µL of glacial acetic acid and succeeded by the addition of 250 µL of ninidrine solution. Samples were incubated for 30 minutes at 100 °C, followed by an incubation of 10 minutes at 25 °C in the dark. Samples were transferred, diluted or undiluted, in 96-well plates and the plate was read at 492 nm.

Nuclear Magnetic Resonance (NMR) Spectroscopy

To evaluate the arginase activity, the enzyme was directly diluted in the NMR tubes containing 20 mM phosphate buffer (pH 7.4), 10 % of D2O and 1 mM of arginine as substrate, with or without the addition of the inhibiting molecules. NMR experiments were recorded on a Bruker Avance III spectrometer (Bruker, Germany), operating at 600.13 MHz 1H Larmor frequency, equipped with a triple resonance TCI cryogenic probe. One-dimensional 1H-NMR experiments were acquired at 25 °C, with a standard pulse sequence incorporating the excitation sculpting water suppression scheme. A total of 16 transients were acquired over a spectral width of 12019.23 Hz, using a recycle delay of 2 s. Arginine and ornithine signals were identified by comparison of related chemical shifts with data deposited in the Biological Magnetic Resonance Bank (http://www.bmrb.wisc.edu/). All spectra were manually phased, and the baseline corrected prior to the integration of the resonances. Relative integrated peak areas of arginine or ornithine Hd protons were used to quantify the substrate consumption and product formation, respectively [307].

ARG1 ELISA

For the measurement of ARG1 concentration in serum, we used the Human Arginase Liver Type Elisa kit (RD193028000R, BioVendor – Laboratorni Medicina a.s.) according to the manufacturer's instructions.

In vitro digestion assay

This assay was performed according to the protocol described by [308]. Briefly, human recombinant proteins rhARG1 (200 ng), rhCTSS (800 ng) and rhCTSG (800 ng), were diluted in digestion buffer containing 50 mM NaAc, 5 mM EDTA, and 0.1 % Triton X-100 pH 6.5 in a molar ratio 1 ARG1 to 4 CTSS or CTSG. CTSS was firstly pre-reduced in 2 mM DTT for 7 minutes. Proteins were incubated together or alone

(control) for 30 minutes, 2 hours or 12 hours at 37 °C. The assay was blocked by adding the appropriate amount of 4X Laemmli Sample Buffer (161-0747, Bio-Rad Laboratories). Following, samples were boiled at 95 °C for 5 minutes and run in the western blot system described above or used for functional assays.

CTSS activity assay

The CTSS activity was measured with the fluorimetric Cathepsin S activity assay kit (ab65307, Abcam), according to the protocol's instructions.

CTSS ELISA

Measurement of CTSS protein levels in serum and NET-containing supernatants collected from ionomycin-stimulated PMNs was performed using Human Cathepsin S ELISA Kit (ab155427, Abcam) according to the protocol's instructions.

Telomerase expression

Telomerase expression was assessed by western blotting. Cell lysates were subjected to 10 % sodium dodecyl sulfate polyacrylamide gel electrophoresis (BioRad) and transferred to PVDF membrane (Millipore). The membrane was blocked in 5 % fat-free milk (Sigma-Aldrich), followed by incubation with the primary antibody mouse anti-hTERT (clone: 2C4, stock: 1 mg/ml, NB100317, Novus Biologicals) diluted 1:1000 TBS $^{+}$ 5 % milk, overnight at 4 °C. Then, HRP-conjugated goat anti-rabbit IgG secondary antibody (12-384, 1 mg/ml, Sigma-Aldrich) diluted 1:2000 in TBS-5 % milk was added for two hours at 25 °C. The probed proteins were visualized using the SuperSignal West Pico (Thermo Scientific). The blotted membranes were stripped and re-probed with mouse β-actin-HRP conjugated (clone: 8H10D10, 12262S, Cell Signaling) to evaluate the equal loading control.

$hTERT_{865-873}$ transgenic TCR T cells generation and maintenance

For the generation and maintenance in culture of the hTERT-specifc TCR transgenic T cells we follow our previously published protocol [305].

IFN-γ ELISA

To evaluate IFN-γ production, human ELISA IFN-γ kit (EH249RB, Thermo Scientific) was used, according to manufacturer's instructions. Briefly, 10^5 engineered CTLs were co-cultured at 1:3 (effector:target) ratio with either human T2 (positive control), SK-MEL-5 cells, for 24 hours. To evaluate hTERT-specific transgenic T cells functional avidity, transgenic T cells were co-cultured with T2, SK-MEL-5 cells either pulsed with $hTERT_{865-873}$ peptide (10^{-9} M) or irrelevant $hHCV_{1406-1415}$ peptide (10^{-9} M).

Evaluation of IFN-γ and IL-2 in the supernatants of PDAC tumor-derived cells

To evaluate IFNγ and IL-2 production, human ELISA IFNγ kit (Abcam, ab46048) and human ELISA IL-2 kit (Abcam, ab46054) were used, according to manufacturer's instructions.

Ex vivo PDAC assay

PDAC tumors were dissociated, mechanically using gentleMACS Dissociator (Miltenyi), using the program m_heart_02. After debris removal, cells were analyzed for the expression of CD45, CD3, CD66b, CD8 and CD4. Then cells were enriched for $CD45^+$ cells by magnetic sorting (Miltenyi, 130-045-801) following manufacturer's instructions. Then 0.1 x 106 cells were seated in a 384 well plate (RPMI 1640 L-

arginine free supplemented with 10% human AB serum (Lonza), 1% Penicillin/Streptomycin, 1% L-glutamine and 1% of sodium pyruvate [all from Gibco-Invitrogen]) and 150µM L-arginine. Cells were treated with either isotype control (IgG1, 150 µg/ml), or Nivolumab (10 µg/ml) + Ipilimumab (10 µg/ml), or Nivolumab (10 µg/ml) + Ipilimumab (10 µg/ml) + αARG1 (150 µg/ml) monoclonal antibody, or antibody αARG1 (150 µg/ml), or left untreated. After 24 h of incubation with or without drugs cells were collected, membrane stained to discriminate between different lymphocyte subsets ($CD45^+$, $CD3^+CD4^+$, $CD3^+CD8^+$, $CD3^+CD4^+Foxp3^+$, $CD8^+PD\text{-}1^+$, $CD8^+CD25^+$). Intracellular staining for Foxp3 was then performed using Foxp3/Transcription factor Fixation/Permeabilization kit (eBiosciences).

rARG1-25 and rARG1-3, cloning, expression and purification

Cloning and expression of the truncated forms were performed by Proteogenix. Recombinant proteins of ARG1 cleaved forms were cloned in E.coli and purified in collaboration with the Proteogenix company. E. coli cell cultures containing the cloned gene were grown overnight at 37°C with shaking at 250 rpm in 5 mL of LB broth containing ampicillin (LB/Amp). The overnight cultures were centrifuged to obtain the cell pellets. Cells were harvested by centrifugation at 4500 × g. Cell pellets were re-suspended in Ni-NTA lysis buffer (50 mM K_2HPO4, 300 mM NaCl, pH 8.0) and subjected to sonication on ice with a Misonix Ultrasonic Liquid Processors on a 15 second burst cycle (power 10). The cell homogenate was treated with the protease inhibitors cocktail (Thermo Scientific), followed by centrifugation to clarify the cell lysate. Supernatants were tested for enzyme activity and the presence of expressed protein was further verified using SDS-PAGE. A stock solution of culture determined to have the highest expression of both ARG1-25 and ARG1-31 were prepared in 15% glycerol and stored at -80°C. The selected recombinant plasmids were sequenced (Proteogenix). For protein purification the bacterial stock solution of the recombinant plasmid was cultured overnight at 37°C in 5 mL of LB/Amp broth in a shaker incubator. The culture was divided into equal amounts between three flasks containing 1 L

LB/Amp broth and allowed to grow at 37°C to A600 = 0.9. The culture was induced with 0.5 mM isopropyl β-D-1-thiogalactopyranoside (IPTG) and growth was continued overnight at 25°C in a shaker incubator. The overnight culture was centrifuged at 4500 × g for 60 minutes to obtain a cell pellet, which was re-suspended in 30 mL of lysis buffer (pH 8.0). The re-suspended cells were lysed by sonication. The sonicated mixture was treated with protease inhibitor cocktail and centrifuged for 20 minutes to clarify the cell lysate. The supernatant was added to a Ni-NTA matrix and mixed gently at 4°C for an hour to allow binding of ARG1-25 or ARG1-31. The mixture was batch-cleaned using lysis buffer to remove unbound protein and added to a chromatography column. After the matrix was packed and cleaned with lysis buffer, protein was eluted using elution buffers 300 mM imidazole (ARG1-25) and 100 mM (ARG1-31) in lysis buffer (pH 8.0). One milliliter fractions were collected and tested in for L-ornithine production in the presence of different amount of L-arginine. Fractions containing the ARG1 activity were placed into a dialysis bag and dialyzed in 50 mM phosphate buffer (pH 8.0) to remove the imidazole. Dialysis was carried out against two one liter volumes of phosphate buffer at 4°C. SDS/PAGE was used to analyze the purity of ARG1-25 and ARG1-31 following the purification process.

Dynamic light scattering (DLS)

In order to probe whether the recombinant Arginase-I maintains the trimeric structure of mammalian arginases, DLS experiments were performed at 25 °C with a Zetasizer Nano- ZS (Malvern Instruments) operating at λ=633 nm and equipped with a back scattering detector (173°). The Arginase-I was dissolved at a concentration of ∼10 μM in in 20 mM phosphate buffer (pH 7.4) and the measurements for hydrodynamic diameter estimation were repeated three times and the data are reported as mean ± standard error.

Far-UV Circular Dichroism (CD) Spectroscopy

Circular dichroism (CD) was used to assess the secondary structure of proteins that have been obtained using recombinant techniques. Circular dichroism (CD) spectra were carried out using a Jasco J-1500 spectropolarimeter equipped with a Peltier control device. Far UV (260–190 nm) spectra of 10 μM Arginase-I were recorded at 25 °C in 20 mM phosphate buffer (pH 7.4) at a scan rate of 50 nm min−1, a bandwidth of 1 nm, and an integration time of 2 s, in 0.1 cm cuvettes. Spectra from three accumulations were averaged and the spectrum of the buffer was subtracted [309].

Epitope fine mapping

The approach was used for the identification of residues within the epitope of rhARG1 that is recognized by αARG1 clone 1.10 antibody. Amino acids on the peptides generated by Pepscan were mutated and the αARG1 antibody binding capacity was tested with Pepscan-based ELISA.

Statistical analyses

Student's t-test was applied for parametric groups and for comparison of two groups, one-way ANOVA test was used in case of multiple comparisons and Tukey test was used as post-hoc analysis. Growth curves were analyzed with Mann-Whitney test. Survival analysis was performed using the Kaplan-Meier survival analysis (Log-Rank) method. Values were considered significant at $p \leq 0.05$. Values are reported as mean ± standard error (SEM) or standard deviation (SD). Pearson's correlation coefficient was used to define the colocalization in IF experiments. All analyses were performed by using Prism 8 (GraphPad Software, San Diego, CA, USA).

Results

Ionomycin-stimulated PMNs release cleaved and active ARG1 in NETs

It has been proved that stimulated human PMNs release ARG1 extracellularly [102]. Activated PMNs can release NETs and depending on the type and strength of the stimuli, different forms of NETosis have been described up to date [310]; yet whether ARG1 is present and active in NETs is still unknown. Therefore, we performed IF staining of ARG1, MPO and DNA on PMNs isolated from peripheral blood (PB) of HD either stimulated with 5 µM iomonycin or left untreated (media) for 30 minutes and 2 hours (Fig. 7A). A time dependent increment in NETs was observed (Fig. 7B-D), with the early stage of NETosis (30 min) characterized by predominant, granule-restricted expression of ARG1; at later stage (2 hrs), cells exhibited large decondensed nuclei, increased size (Fig. 7E), and ARG1 co-expression together with MPO along the network of chromatin strands (Fig. 7F).

It is known that ARG1 is stored in PMN tertiary granules as inactive molecule [82], whereas the enzyme released upon PMN exocytosis efficiently catabolizes L-arginine [101]. Thus, we tested whether ARG1 functional activation might result from different molecular forms of the ARG1 protein in NETs. We isolated and characterized NETs (Fig. 7D) and observed a time-dependent increment in low molecular weight bands in NETs of activated PMNs (major forms at 31 and 25 kDa), which were only slightly present in NETs from control PMNs (media, 30 min and 2 h) and completely absent in cell pellet lysates from both activated and control PMNs (Fig. 7G, middle and right panels), freshly isolated PMNs and PBMCs (Fig. 7G, left panel) suggesting a protein cleavage. We then evaluated by colorimetric assay and NMR analysis, if ARG1 present in the NETs upon stimulation with ionomycin had higher enzymatic activity than the one of PMNs cell pellets. We tested two different pHs, 9.5 and 7.3. The former as the optimal pH for the ARG1 enzymatic activity and the latter because is the physiological pH of the extracellular environment. At pH 9.5, we observed a time-dependent increase in the enzymatic activity, with 2 hrs stimulation reaching an overall similar activity in

both NETs and cell lysate (Fig. 7H); conversely, ARG1 activity was detectable almost exclusively in NETs at pH 7.3 (Fig. 7I). These results hint that the cleaved forms of ARG1 are associated with the enzyme gain of function at physiological pH. ARG1 is known to downregulate CD3ζ and CD3ε in T cells [48], thus we investigated whether NETs containing ARG1 affect T cells function. NETs from stimulated PMNs, containing a significant amount of active ARG1 (Fig. 7J), were collected and physiological L-arginine concentration (150 µM) was restored, before adding this preparation to activated T cells. ARG1 from NETs suppressed T lymphocyte activation by anti-CD3/anti-CD28, as shown by the down modulation of CD3ε (Fig. 7K). We then evaluated the effect on T cell proliferation in the presence of newly generated monoclonal antibodies directed to hARG1 or isotype controls (IgG). Antibody clone 1.10 (IgG1) significantly restored T-cell proliferation (Fig. 7L) at a dose of 150 µg/ml, while commercially available ARG1 inhibitors were either slightly effective or ineffective nor-NOHA and BEC, respectively] (Fig. 7M). These results portray a novel scenario in which extracellularly released ARG1 is trapped in NETs where it is cleaved and acquires functional activity which negatively impacts T cell proliferation. Interestingly, newly generated monoclonal antibody restores T cell.

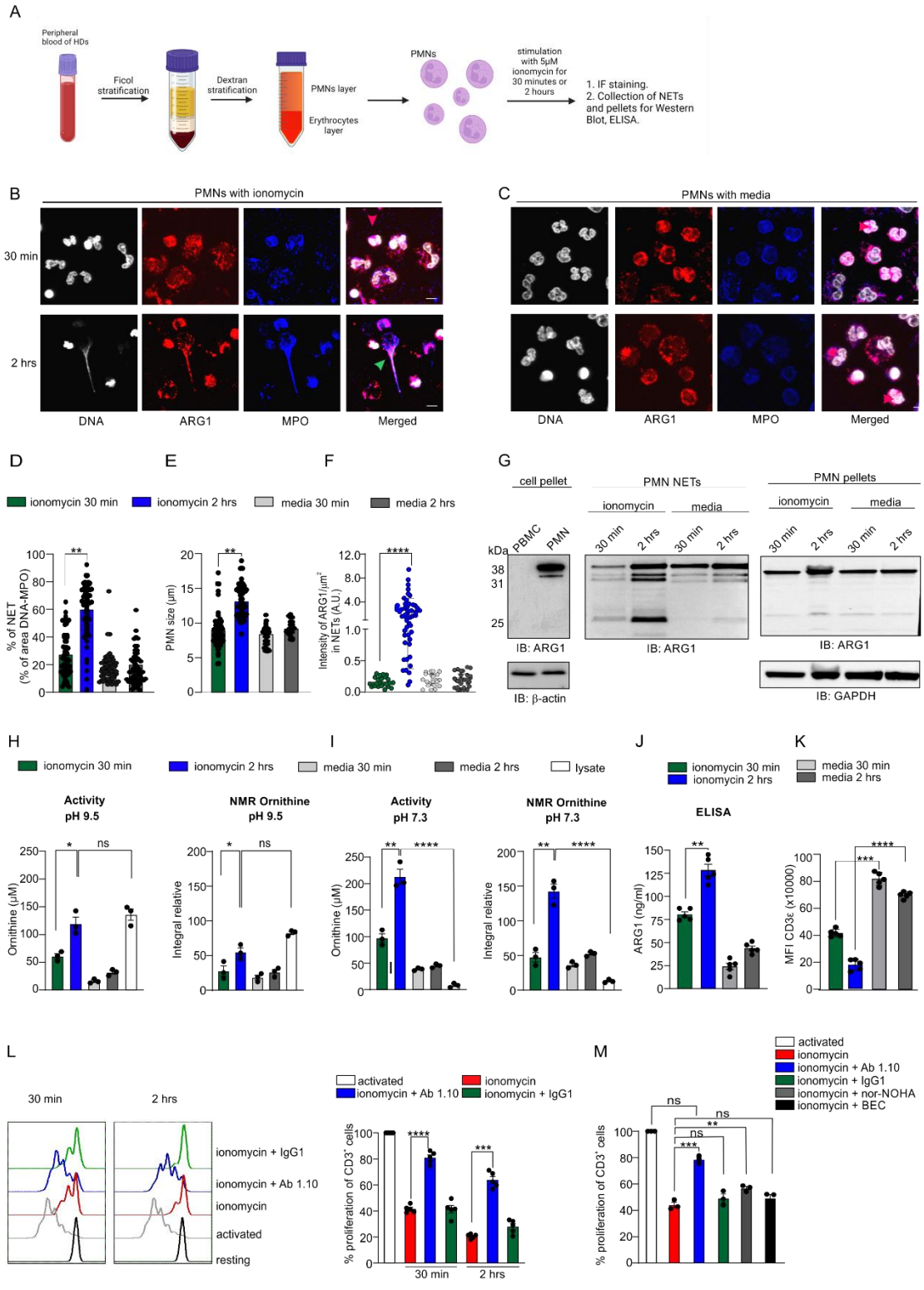

Figure 7. **Activated PMNs release in NETs the cleaved and enzymatically active ARG1.**

A. Experimental layout of PMNs in vitro stimulation. Briefly, PMNs were isolated from the PB of HDs upon density gradient stratification and stimulated with ionomycin for 30 minutes or 2 hours. As control, we used PMNs without stimuli (media control). Then, samples were stained for IF or NETs and pellets were collected and processed. B. Representative immunofluorescence images showing ARG1 (red), MPO (blue) and DNA (grey) of PMNs treated with 5 µM ionomycin for 30 minutes and 2 hours (n=3). The pink arrow indicates intact cells and the light blue arrow indicates PMN undergoing NETosis. Scale bars: 10 µm. C. Representative immunofluorescence images showing ARG1 (red), MPO (blue) and DNA (grey) of untreated PMNs (media) for 30 minutes and 2 hours(n=3). The pink arrows indicate intact PMNs. Scale bars: 10 µm. D. Quantification of NETs produced by PMNs treated with 5 µM ionomycin or left untreated (media) for 30 minutes and 2 hours (n=3). The data are presented as mean ± SEM of 60 counted cells. Paired Student's t-test; **p = 0.003. E. Quantification of the cell size changes (µm) occurring during NETosis of PMNs treated with 5 µM ionomycin or left untreated for 30 minutes and 2 hours (n=3). The data are presented as mean ± SEM of 60 counted cells. Paired Student's t-test; **p = 0.006. F. Quantification of NET-associated ARG1 intensity (from A) in PMNs treated with 5 µM ionomycin or left untreated for 30 minutes and 2 hours (n=3). The data are presented as mean ± SEM. Unpaired Student's t-test; ****p < 0.0001. G. Left panel: immunoblot showing ARG1 protein molecular weight profile obtained from PBMC and PMN whole cell lysates. Loading control: β–actin. Middle panel: immunoblot of ARG1 protein molecular weight profile derived from NETs produced by either treated (5 µM ionomycin, 30 minutes and 2 hours) or untreated (media, 30 minutes and 2 hours) PMNs. Right panel: Immunoblot of ARG1 protein molecular weight profile derived from whole cell lysates of treated (5 µM ionomycin, 30 minutes and 2 hours) or untreated (media, 30 minutes and 2 hours) PMNs. Loading control: GAPDH. H-I. Determination of ARG1 activity in NETs produced by PMNs treated with 5 µM ionomycin or left untreated (media) for 30 minutes or 2 hours. Ornithine levels are evaluated by colorimetric assay (left panel) and by NMR analysis (right panel). PMN whole cell lysate is shown as control. ARG1 activity was assessed at pH 9.5 (G) and 7.3 (H) (n=3). The data are presented as mean ± SEM. Paired Student's t-test; *p = 0.0452, **p = 0.0076, ***p = 0.003. ns, not significant. J. Quantification of ARG1 levels (ng/ml) by ELISA in NETs produced by PMNs treated with 5 µM ionomycin or left untreated (media) for 30 minutes and 2 hours (n=5). The data are presented as mean ± SEM. Paired Student's t-test; ** p = 0.00638. K. Mean fluorescence intensity (MFI) evaluation, by FACS analysis, of CD3ε in anti-CD3 and anti-CD28 activated T cells cultured with PMN-derived NETs (n=5). The data are presented as mean ± SEM. Paired Student's t-test; ***p = 0.00259, ****p < 0.0001. L. Proliferation assay showing the percentage of anti-CD3 and anti-CD28 activated, $CD3^+$ $CellTrace^+$ T cells cultured with NETs produced by PMNs treated with 5 µM ionomycin for 30 minutes and 2 hours in the presence of neutralizing antibody αARG1 clone 1.10 (150 µg/ml) or IgG1 isotype control. Activated T cells are set as 100 % proliferation and used as control. (n=5). Suppressive activity is represented as percentage of proliferation of $CD3^+$ $CellTrace^+$ cells. The data are presented as mean ± SEM. Paired Student's t-test; ***p = 0.00128, ****p < 0.0001. ns, not significant. M. Proliferation assay showing the percentage of anti-CD3 and anti-CD28, activated $CD3^+$ $CellTrace^+$ T cells cultured with NETs produced by PMNs treated with 50µM ionomycin for 30 minutes in the presence of neutralizing antibody αARG1 clone 1.10 (150 µg/ml), BEC (10.5 ng/ml), nor-NOHA (30 ng/ml) and IgG1 isotype control. Activated T cells are set as 100 % proliferation and used as control (n=3). Suppressive activity is represented as percentage of proliferation of $CD3^+$ $CellTrace^+$ T cells. The data are presented as mean ± SEM. One-way Anova, multiple comparisons; **p = 0.00785, ***p = 0.001310; ns, not significant.

ARG1 is enriched in NETs released by differentially activated PMNs

NETosis is induced by either NADPH-dependent or –independent mechanisms [187]. Ionomycin belongs to the NADPH-independent stimuli, while PMA is conventionally used to induce NETs in a NADPH-dependent manner. To understand whether ARG1 release in NETs was a unique of feature of NADPH-independent stimuli, we purified PMNs from HDs and activated with PMA (12 nM) for 30 minutes and 2 hours, as before. Representative IF images for ARG1, MPO and DNA revealed a significant amount of ARG1 in NETs already at 30 minutes of stimulation, compatible with a fast and sustained release (Fig. 8A-B). Ionomycin and PMA are not physiological stimuli, therefore we next investigated whether a physiological stimulus, such as IL-8, which is known to regulate both PMN degranulation and NETosis [311, 312], induces the release of ARG1 in NETs. PMNs from HDs were isolated and stimulated with IL-8, 20 nM, for 30 minutes and 2 hours (Fig. 8C). The results showed that IL-8 induced ARG1 release in NETs in a time-dependent manner, although to a less extent than ionomycin (Fig. 8C-D). Furthermore, taken together these data demonstrate that different stimuli have different potential and induce different kinetics of NETs release by activated PMNs.

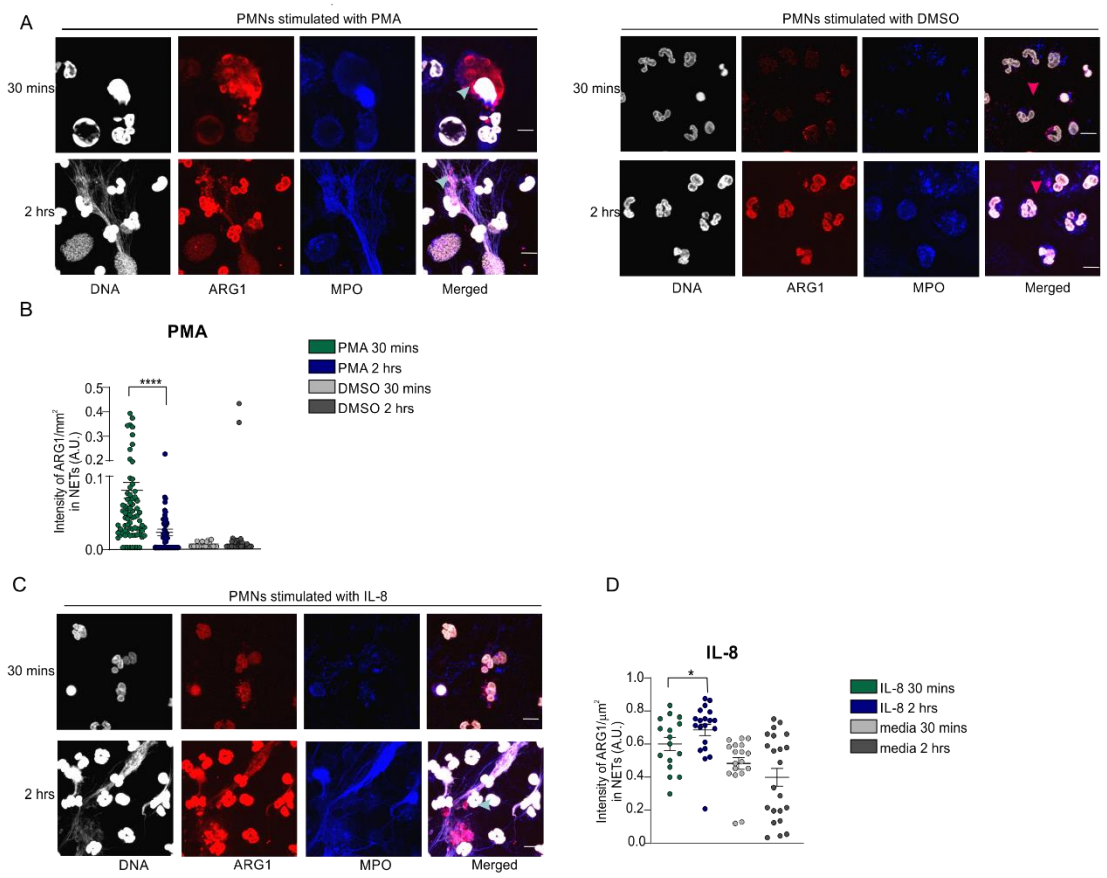

Figure 8. **PMNs activated by different stimuli release ARG1 that localizes in NETs.**

A. Representative immunofluorescence images showing ARG1 (red), MPO (blue) and DNA (grey) of 30 minutes and 2 hours, treated PMNs with PMA (12 nM) and DMSO (1:500 dilution, control). The pink arrows indicate intact cells and the light blue arrows indicate PMNs undergoing NETosis. Shown is the maximum projection. Scale bars: 10 µm. B. Quantification of NET-associated ARG1 intensity (from A) in PMNs treated with 12 nM PMA or DMSO (control) for 30 minutes and 2 hours (n=2). The data are presented as mean ± SEM. Unpaired Student's t-test. ****p< 0.00001. C. Representative immunofluorescence images showing ARG1 (red), MPO (blue) and DNA (grey) of 30 minutes and 2 hours, treated PMNs with IL-8 (20 nM). The pink arrows indicate intact cells and the light blue arrows indicate PMNs undergoing NETosis. Shown is the maximum projection. Scale bars: 10 µm. D. Quantification of NET-associated ARG1 intensity (from C) in PMNs treated with 20 nM IL-8 or left untreated for 30 minutes and 2 hours (n=2). The data are presented as mean ± SEM. Unpaired Student's t-test.*p<0.05 ns, not significant.

Generation and development of neutralizing monoclonal antibodies to hARG1

Since the identification of ARG1 as an immune regulator, development of inhibitors has attracted a lot of interest. The few inhibitors available today, suffer of *in vivo* toxicity and lack of specificity [313]. Therefore, we decided to approach ARG1 inhibition by developing isoform-specific human ARG1 antibodies, using the hybridoma technology. We immunized Balb/c mice with the last 19 aa of the C-terminal part of hARG1 (Fig. 9A-B). Among the various hybridoma clones that were obtained, we first validated their specificity (Fig. 9C), affinity (Fig. 9D) and reactivity (Fig. 9E). Among them, we selected clone 1.10 for its neutralizing ARG1 function. The clone demonstrated high specificity for hARG1, as it could not recognize mARG1 from the mouse-derived cell line (MSC-2) stimulated with IL-4 and hARG2 present in isolated PBMCs from PB (Fig. 9E).

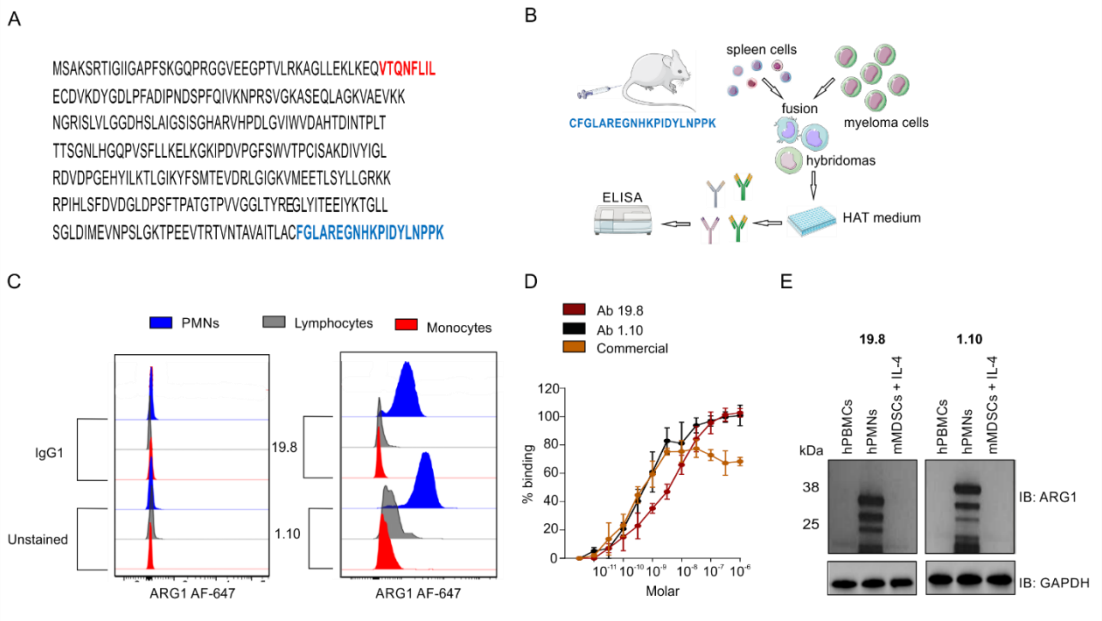

Figure 9. **Strategy employed to generate and develop monoclonal antibodies to hARG1.**

A. Amino acid sequence of the human ARG1 isoform 2. Highlighted in blue is the C-terminal sequence used for the immunization of mice and in red the sequence corresponding to the 8aa stretch typical of the isoform 2 of ARG1. B. Layout of hybridoma production employing the C-terminal peptide of hARG1. C. Flow cytometry histograms showing the ability of hybridoma–derived clones upon conjugation with the Alexa-Fluor 647 dye to recognize ARG1 protein in human PMNs (blue). As

controls, lymphocytes (grey) and monocytes (red) were used. D. Affinity of binding evaluated for each hybridoma clones. The binding was assessed against rhARG1 and comparison was made with a commercially produced antibody αARG1. E. Representative immunoblots showing the ability of the hybridoma–derived clones to recognize ARG1 present in whole lysates of PMNs. As controls were used PBMCs and the mouse-derived MDSC cell line (MSC2) treated with IL-4, known to express murine ARG1. Loading control: GAPDH.

Epitope mapping analysis and competition experiments revealed the minimal epitope recognized by αARG1 clone 1.10, located within the sequence the extreme C-terminal of hARG1 (Fig. 10A-B, Table 1). Single amino acid replacement analysis identified the sequence DYLNP as the core amino acids recognized by αARG1 clone 1.10. (Fig. 10C). To understand better the binding properties of the αARG1 clone 1.10 to rhARG1 we performed ITC, that revealed the thermodynamic parameters of the binding. ARG1 interaction with the αARG1 clone 1.10 was exothermic and a good data fitting was achieved using the three sequential binding sites model which yielded dissociation constants (Kd) of 3.27×10^{-11}, 1.37×10^{-10} and 8.08×10^{-3} M, respectively. The model revealed that three molecules of αARG1 clone 1.10 bound to one molecule of ARG1 and the binding affinity of the second and third site were influenced by the binding at the first site (Table 2). Although the first two binding sites interaction had high affinity, the third site showed a significantly lower affinity interaction, possibly due to steric hindrance. Despite being bivalent, the antibody bound to rhARG1 only with one Fab fragment, indicating a ratio of three Fabs per trimeric ARG1. The high enthalpy (ΔH) value could be ascribed to the formation of several Van der Waals, hydrogen bonds and electrostatic interactions, while the high entropy (ΔS) reflected the conformational rearrangement upon complex formation (Fig. 10D). The C-terminal part of ARG1 was necessary for the molecular interactions among the monomers to form a stable trimer, hence, we believe that αARG1 binding to this region destabilizes the quaternary structure of the enzyme and subsequently its function. Having described the properties of the αARG1 clone 1.10 we proceeded by testing its ability to neutralize both rhARG1, generated to have the exact same sequence as the one expressed by PMNs (erythroid isoform 2), and ARG1 in NETs. We performed a kinetic assay, measuring with NMR the consumption of L-arginine by rhARG1 and at the same time the production of L-

ornithine and urea over time. rhARG1 uses 50% of L-arginine in less than 30 minutes. When we added the commercially available ARG1 inhibitors, BEC and nor-NOHA, we observed a complete inhibition of the enzyme, while, the αARG1 clone 1.10 delayed the consumption of L-arginine when used in a ratio dependent manner (Fig. 10E).

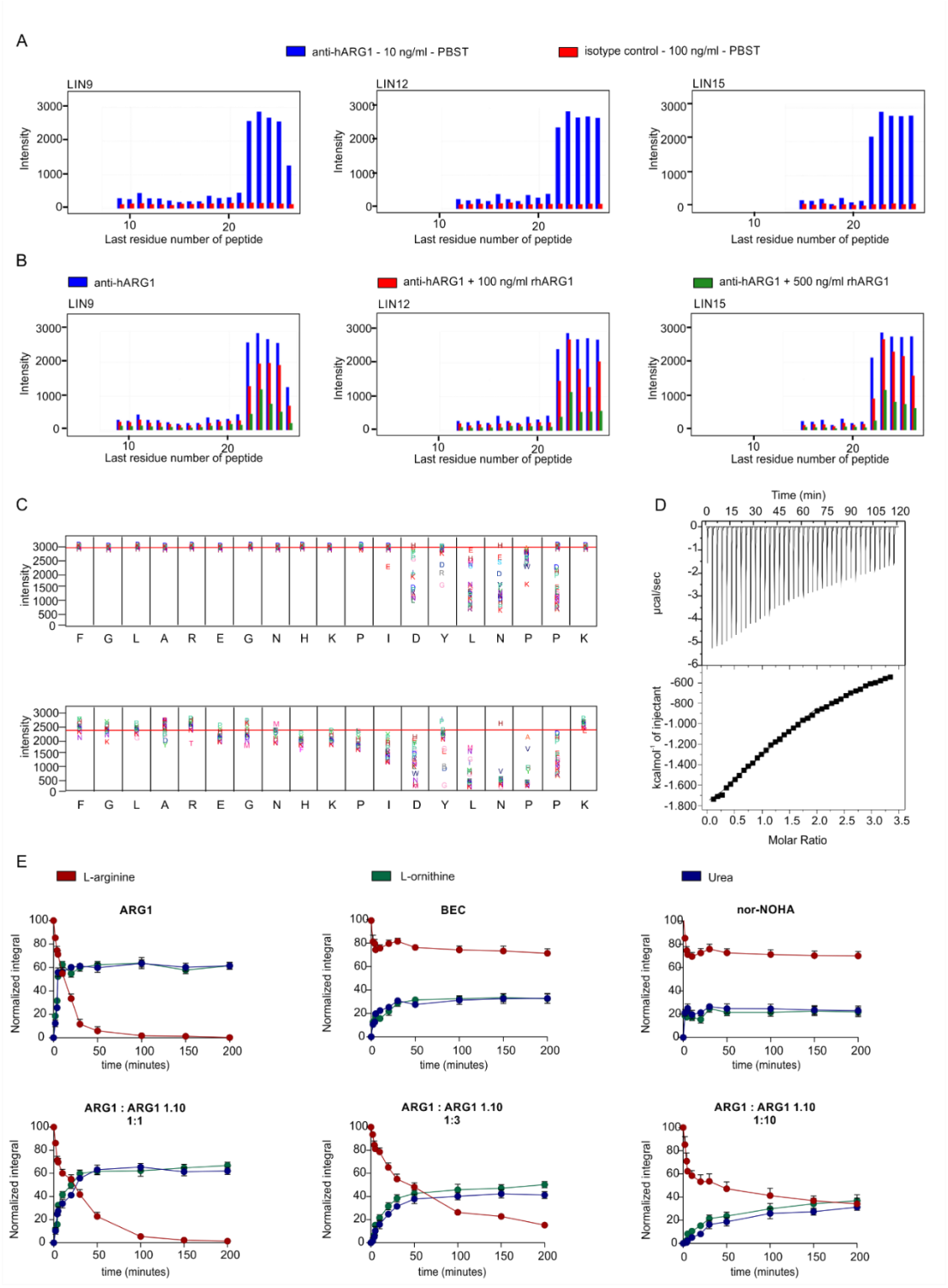

Figure 10. **Characterization of the monoclonal antibody to hARG1.**

A. Intensity profiles recorded for αARG1 on the linear peptide arrays. Bar plots show the peptide intensities for αARG1 (blue) and an isotype control (red) on the linear 9-mer, 12-mer, and 15-mer peptide

array. Signal intensities are plotted on the y axis and positions of the last residues of a peptide with respect to the target sequence is on the x axis. B. Intensity profiles recorded for competition experiments of αARG1 with recombinant ARG1 on the linear peptide arrays. Bar plots show the peptide intensities for αARG1 (blue), αARG1 with 100 ng/ml rhARG1 (red) or with 500 ng/ml rhARG1 (green) on the linear 9-mer (LIN9), 12-mer (LIN12), and 15-mer (LIN15) peptide array. Signal intensities are plotted on the y axis and positions of the last residues of a peptide with respect to the target sequence is on the x axis. C. Letter plot representation of replacement analysis data recorded for αARG1 on rhARG1 linear peptides. Linear peptides were generated bearing single amino acid substitutions at each position of the native lead peptide sequence, shown below the plot. Screenings were performed at 1 µg/ml and 10 ng/ml. Values obtained for replacements are indicated by the letter code for each replacement residue plotted at the height of the recorded value. Red line indicates median value. D. Isothermal titration calorimetry (ITC) of the binding interaction between antibody αARG1 clone 1.10 and rhARG1 in 50 mM HEPES (20 mM CaCl2) of pH 7.3, at 298.15 K. E. NMR evaluating the enzymatic rhARG1 activity alone or in combination with BEC, nor-NOHA and αARG1 clone 1.10 at a molar ratio of 1:1 , 1:3 and 1:10. Data are obtained from two independent experiments with each time point read in triplicates. The levels of L-arginine (red), L-ornithine (green) and urea (blue) either consumed or formed by the time (minutes) are indicated. The data are presented as mean ± SD.

CTSS interacts with ARG1 in NETs of stimulated PMNs

To investigate the complexity of ARG1 biology in NETs, we defined ARG1 interactome. We isolated NETs released from PMNs stimulated with ionomycin for 2 hours and we performed Co-IP of ARG1 using the αARG1 clone 1.10. Samples were loaded on SDS-PAGE and the region of interest of the gel was excised and subjected to LC-MS/MS, upon confirmation of ARG1 correctly pulled down (Fig. 11A). Several interacting proteins were identified, with CTSS receiving our attention because it is a protease active at physiological pH. We validated the proteomic data by Co-IP (Fig. 11B-C) and IF, which confirmed the exclusive interaction on NETs and the co-localization of ARG1 and CTSS on both NADPH-dependent (PMA-induced) and independent (ionomycin-induced) NETs, respectively (Fig. 11D-G). Therefore, these data highlight that ARG1 interacts with CTSS in NETs, independently of the NETosis-induced mechanism.

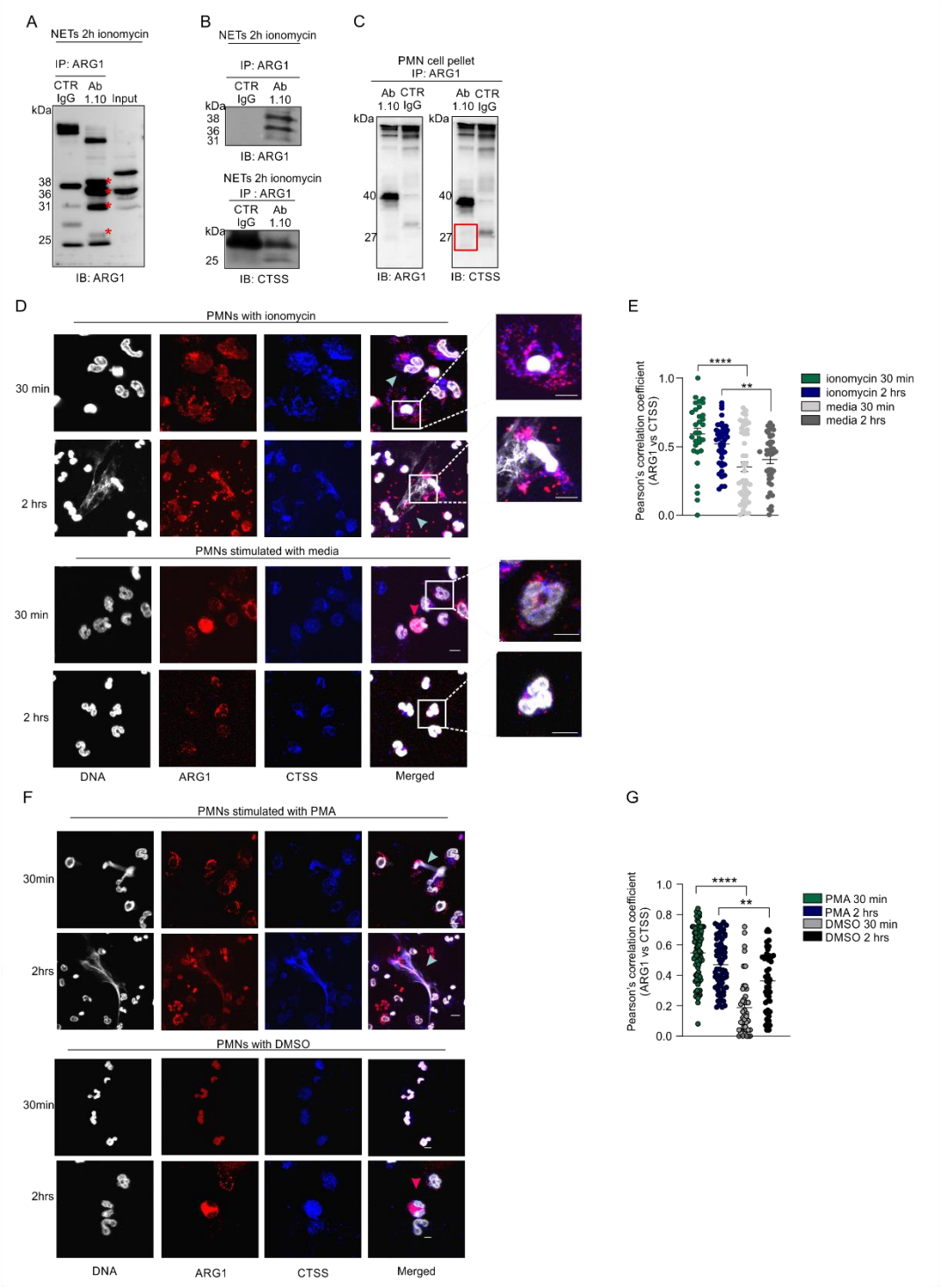

***Figure 11*. ARG1 interacts with CTSS in NETs of activated PMNs.**

A. Immunoblot showing ARG1 protein band pattern (38, 36, 31 and 25 kDa, red stars) of co-IP ARG1 from NETs of PMNs treated with ionomycin 5 µM for 30 minutes. Specific antibody to ARG1 (Ab 1.10) and isotype control IgG1 antibody are indicated. B. Immunoblot showing ARG1 (upper panel) and CTSS

(lower panel) co-expression obtained from co-IP of ARG1 (Ab 1.10, 2 µg, or IgG1 control) from NETs of PMNs treated with ionomycin 5 µM for 30 minutes. C. Immunoblots showing ARG1 and CTSS co-expression obtained from co-IP of ARG1 (Ab 1.10, 2 µg, or IgG control) from cell lysate of ionomycin-activated PMNs. D. Representative immunofluorescence images showing ARG1 (red), CTSS (blue) and DNA (grey) of PMNs treated with ionomycin 5 µM or left-untreated for 30 minutes and 2 hours. The light blue arrows indicate PMNs undergoing NETosis. Shown is the maximum projection. Scale bars: 10 µm. E. Quantification of ARG1 and CTSS co-localization within the NETs produced by 30 minutes and 2 hours, ionomycin–treated or untreated PMNs. Pearson's correlation coefficient analysis. The data are presented as mean ± SEM. **p = 0,0014 , ****p < 0.0001. F. Representative immunofluorescence images showing ARG1 (red), CTSS (blue) and DNA (grey) of 30 minutes and 2 hours, PMA (12 nM) or DMSO (control, 1:500)-treated PMNs. (n=2). The pink arrows indicate intact cells and the light blue arrows indicate PMNs undergoing NETosis. Shown is the maximum projection. Scale bars: 10 µm. G. Quantification of ARG1 and CTSS co-localization on the NETs produced by 30 minutes and 2 hours, PMA (12 nM) or DMSO (control, 1:500)-treated PMNs. (n=2). Pearson's correlation coefficient analysis. Results are shown as mean ± SEM. Unpaired Student's t-test. **p < 0.003, ****p < 0.00001.

CTSS cleaves ARG1 generating two major molecular forms

We demonstrated that ARG1 interacts with CTSS in the NETs released by stimulated PMNs and then we defined the thermodynamic values of this interaction. ITC analysis revealed that the binding of proCTSS, proteolitically inactive, (Fig. 12A) to ARG1 is thermodynamically favorable (Fig. 12A and Table 3), profiling an interaction of one ARG1 monomer binding to a single site on proCTSS with a kD of 2.1 µM. When mature proteolitically active CTSS was incubated with ARG1 (Fig. 12B and Table 3), the ΔH became more negative but was compensated by an increment in ΔS, which led to a net result of no changes in free energy and binding affinity compared to the proCTSS. The increment in the ΔH is likely the result of an increase in the number of hydrogen bonds and Van der Waals interactions between ARG1 and CTTS, while the loss in ΔS could be associated with a reduction on the degrees of freedom of CTSS. Altogether the ITC data suggest that the pro-peptide of CTSS is not required for the specific interaction with ARG1 but rather could be involved only in the catalytic activity of CTSS. Then, we evaluated whether CTSS was responsible for the molecular pattern of ARG1 observed in NETs of activated PMNs. We performed an in vitro digestion assay, based on the protocol published by Ljusberg et al. [308], and we observed a time dependent digestion of rhARG1 by rhCTSS. This resulted in the generation of two major cleaved products, corresponding to the 31 kDa and 25 kDa (Fig. 12C, blue arrows) which recapitulated the molecular pattern in NETs of activated PMNs (Fig.

7F). At later time point (12 hours), high molecular weight products were generated (Fig. 12C, red arrows), whose nature is currently under investigation and initial analysis revealed a complex mix of ARG1 and CTSS. In contrast, rhCTSG activity resulted in almost complete rhARG1 digestion after 12 h incubation (Fig. 12C). When we assessed the enzymatic activity of rhARG1 in the digestion mix at pH 7.3, we noticed a time-dependent increment only when rARG1 was incubated with rhCTSS while the activity in the presence of rhCTSG dropped to almost negligible levels (Fig. 12D). These results indicate that ARG1 gain of function at physiological pH occurs when incubated with rhCTSS and corresponds to the formation of 31 and 25 kDa forms.

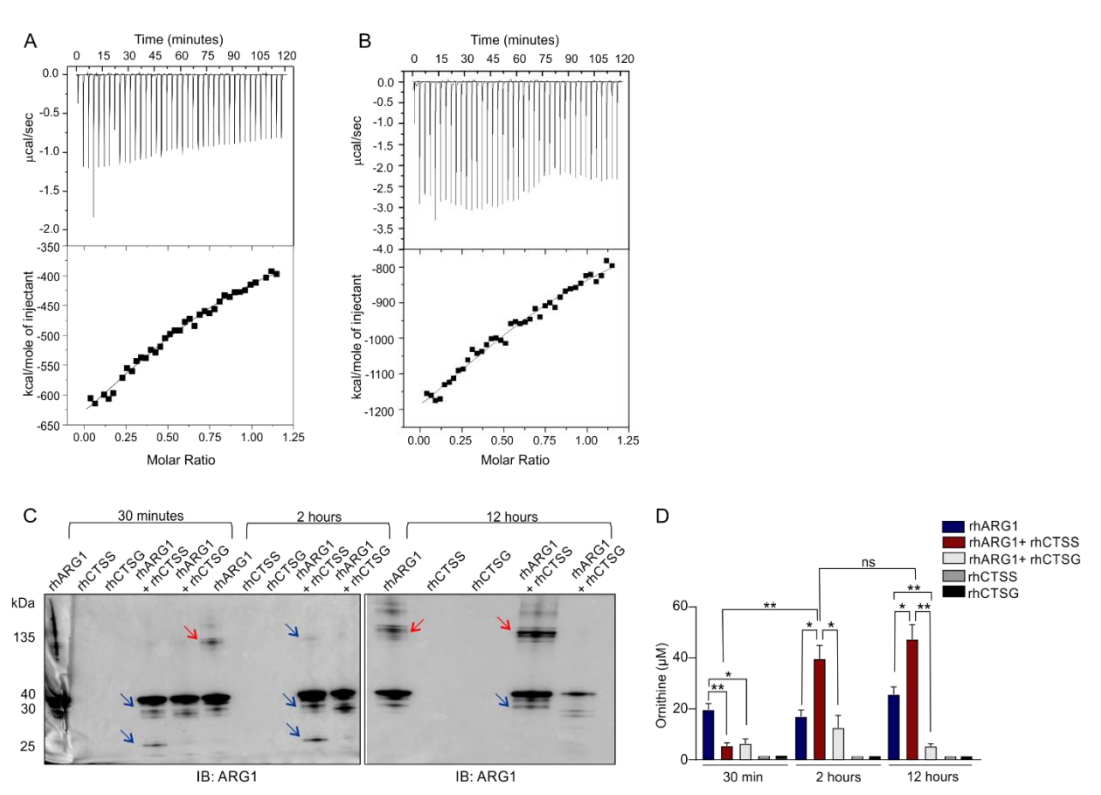

Figure 12. **CTSS cleaves ARG1 generating active forms of 31 and 25 kDa.**

A. Isothermal titration calorimetry (ITC) analysis of proCTSS interaction with rhARG1. B. Isothermal titration calorimetry (ITC) analysis of mature CTSS interaction with rhARG1. C. ARG1 immunoblot showing rhARG1 (200 ng) kinetic of digestion (30 minutes, 2 hours and 12 hours) in the presence or absence of rhCTSG (800 ng) or rhCTSS (800 ng). Red and blue arrows indicate generated bands. D. Activity of rhARG1 measured in the samples evaluated in C. rhARG1 activity analysis, based on ornithine production measured by colorimetric assay. The data are presented as mean ± SEM. One-way Anova, multiple comparisons with Tukey correction; *p < 0.05, **p < 0.01; ns, not significant.

ARG1 cleaved forms exhibit differential enzymatic properties

We argued that the partial inefficacy of classical ARG inhibitors on extracellularly released ARG1 could be linked to the presence of alternative molecular forms endowed with different functional activity. To test our hypothesis, we isolated and sequenced (Fig. 13A), cloned (Fig. 13B) and functionally tested (Fig. 13C-D) the 31 and 25 kDa molecular forms (thereafter indicated as ARG1-31 and ARG1-25, respectively). Both forms possess enzymatic activity (Fig. 13C-D), with the ARG1-31 being far more active (50 % of L-arginine converted in 5 min) than the full length protein, while the ARG1-25 showed a kinetic of L-arginine consumption lower than the uncleaved full length form (Fig. 13C-D and Fig. 10E). We then evaluated the ability of Ab clone 1.10 to interfere with the enzymatic function. We observed that ARG1-31 functional activity was unaffected at a molar ratio of 1:1 (Fig. 13C) but decreased at increasing molar ratios. Conversely, BEC and nor-NOHA were ineffective (Fig. 13C). Even though the ARG1-25 activity was minimal, the αARG1 clone 1.10 was only minimally delaying its function and only at the highest molar ratios (Fig. 13D). Both BEC and nor-NOHA confirmed to be ineffective. We then asked whether the ARG1 cleaved forms halt T cell proliferation, in vitro. After defining the doses and assessing the toxicity, we observed that ARG1-25 was not suppressive up to 100 ng/ml, with 200 ng/ml suppressing the proliferation of activated T cells by 30 % (Fig. 13E, left panel); furthermore, BEC and nor-NOHA confirmed their ineffectiveness also in this setting. Instead, ARG1-31 reached the same level of suppression achieved with 5 ng/ml of full length protein at concentration of just 0.1 ng/ml, in line with the enzymatic function (Fig. 13E, right panel). Thus, these experiments while underscoring the complexity of ARG1 regulation, they open a new way to understand and target ARG1 function.

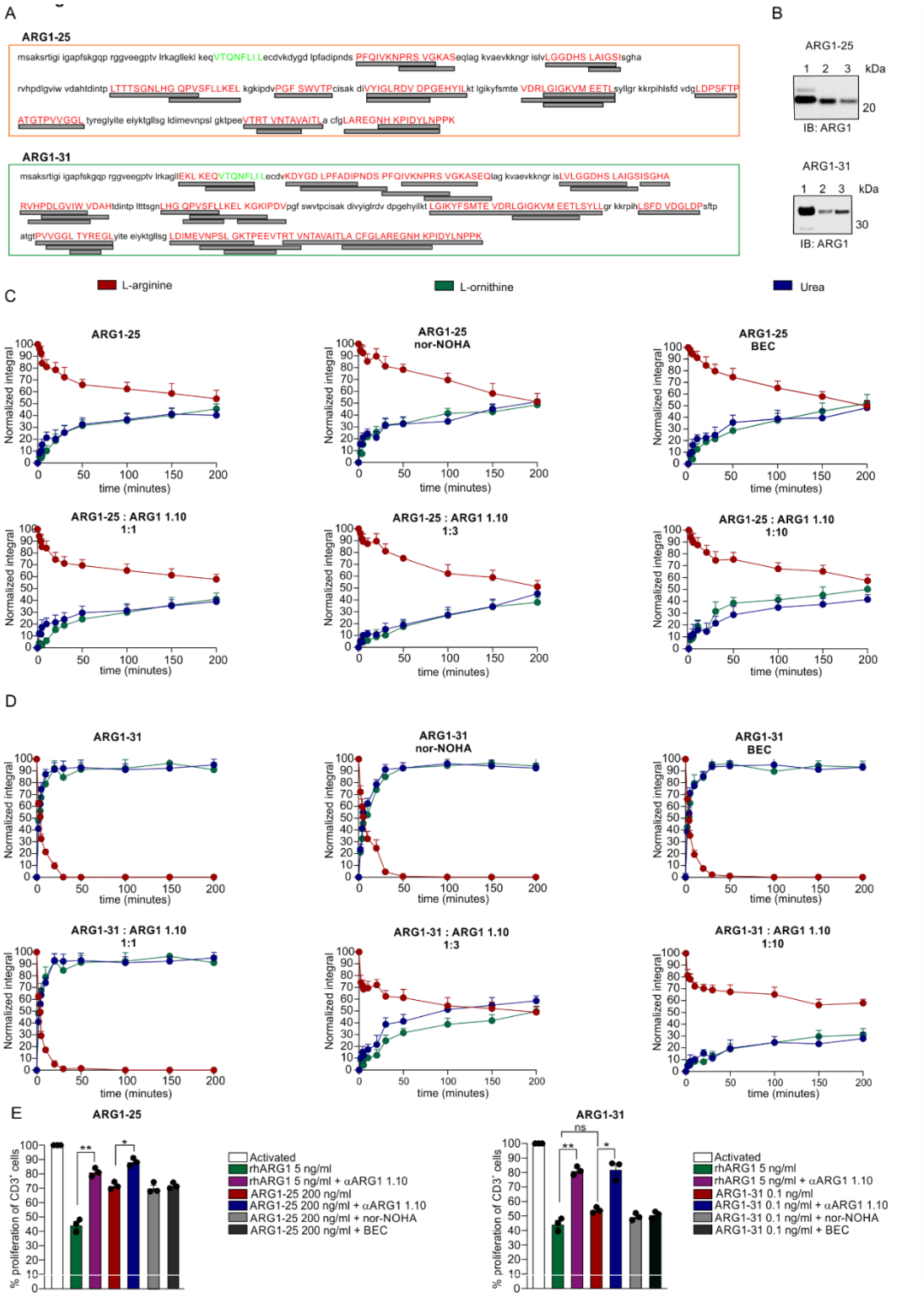

Figure 13. **ARG1 cleaved forms present different enzymatic activities and are differentially susceptible to the inhibition by mAb.**

A. Sequences of the 25 and 31 kDa forms derived from cleaved ARG1 were defined by Mascot analysis. Indicated are the peptides identified by the proteomic analysis. B. Immunoblot (anti-ARG1) representing different doses of the protein. Upper panel: ARG-1 25; Lower panel: ARG1-31. C. NMR evaluating the enzymatic ARG1-25 activity alone or in combination with BEC, nor-NOHA and anti-ARG1 clone 1.10 at a molar ratio of 1:1, 1:3 and 1:10. Data are obtained from two independent experiments with each time point read in triplicates. The levels of L-arginine (red), L-ornithine (green) and urea (blue) either consumed or formed by the time (minutes) are indicated. The data are presented as mean ± SD. D. NMR evaluating the enzymatic ARG1-31 activity alone or in combination with BEC, nor-NOHA and anti-ARG1 clone 1.10 at a molar ratio of 1:1, 1:3 and 1:10. Data are obtained from two independent experiments with each time point read in triplicates. The levels of L-arginine (red), L-ornithine (green) and urea (blue) either consumed or formed by the time (minutes) are indicated. The data are presented as mean ± SD. E. Proliferation of anti-CD3 and anti-CD28 activated T cells cultured with rhARG1 full length or ARG1-25 (left panel) or ARG1-31 (right panel) alone or in the presence of different inhibitors (n=3). Activated T cells are set as 100 % proliferation and used as control. Suppressive activity is represented as percentage of proliferation of $CD3^+$ $CellTrace^+$ cells. The data are presented as mean ± SEM. One-way Anova multiple comparisons with Tukey correction; *$p < 0.05$; **$p < 0.01$; ns, not significant.

ARG1 and CTSS are present in tumor tissues derived from PDAC patients

It is known that neutrophils recruited from the circulation help PDAC escape from immune responses [244, 314]. It remains though still unknown whether neutrophils recruited in the tumor sites release NETs and if ARG1 and CTSS are present and interact. To address these questions, we collected tumor tissues from a cohort of stage IIA, IIB PDAC patients (Table 4). By IF analysis, we evaluated the amount of tumor-infiltrating leucocytes (defined as $CD45^+$) and, specifically, the number of neutrophils (defined by $CD66b^+$) (Fig. 14A). PDAC patients presented a variable leukocyte infiltration (Fig. 14B; between 10 % and 50 % of total cells); however, on a closer look to neutrophils ($CD66b^+$), all the patients presented a significant amount, with levels ranging between 35% and 60% among $CD45^+$ cells, when compared to healthy pancreatic tissues (Fig. 14C; between 0 to 5.3% of $CD45^+$ cells). As expected, neutrophils were $ARG1^+$ (Fig. 14D). We then assessed the expression of CTSS in tumor tissues and we found that CTSS co-localized with ARG1 (Fig. 14E) in comparison with the surrounding, normal pancreatic tissue. The tumor tissue was, almost exclusively enriched in NETs (Fig. 14F-G) in which ARG1 and CTSS colocalized (Fig. 14H-J). Moreover, activated neutrophils generating NETs were found enriched at the tumor borders, and to a less extent in the stroma and in the inner part of

the tumor (Figure 14F). Overall, our data demonstrate that CD66b$^+$ neutrophils infiltrate PDAC tissues and release NETs in which ARG1 and CTSS interact, giving a biological relevance to our in vitro data.

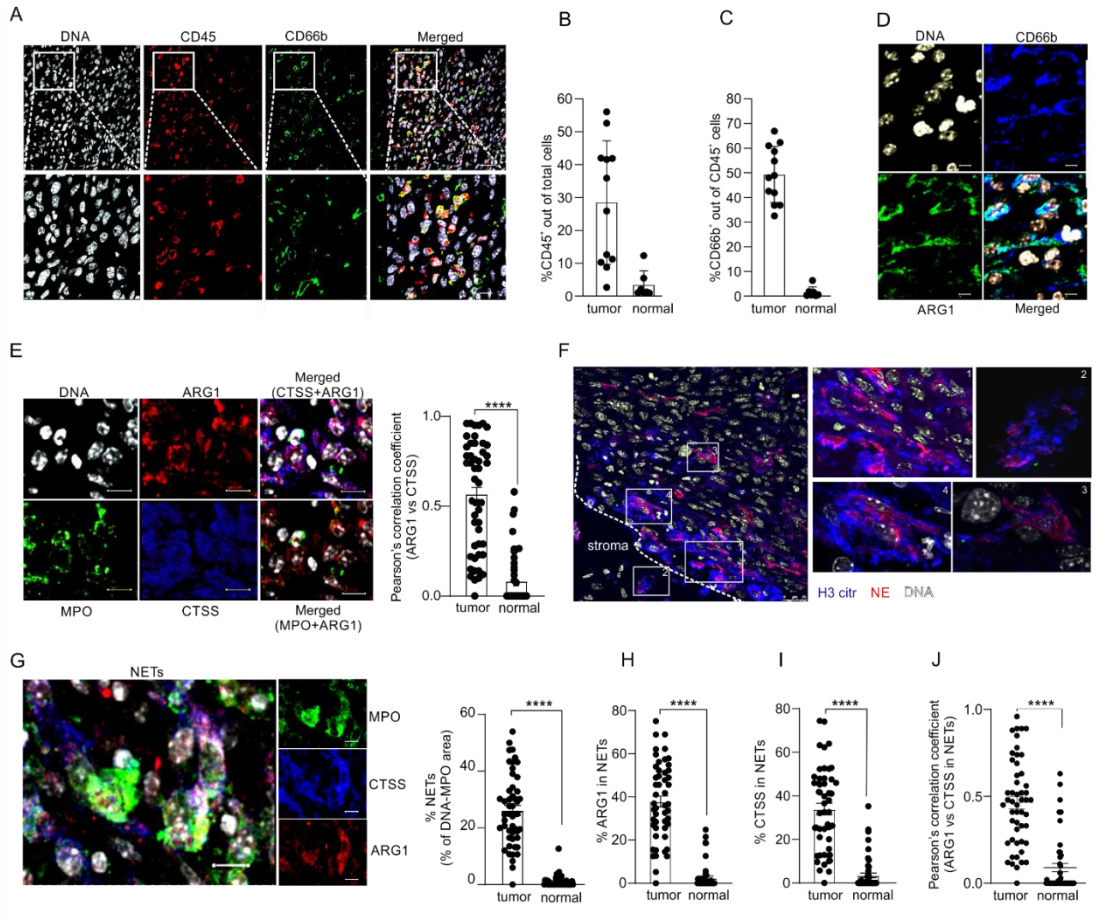

Figure 14. **PDAC patients present an enrichment in tumor-associated NETs containing ARG1 and CTSS.**

A. Representative immunofluorescence images of tumor tissues derived from PDAC patients showing CD45 (red, leukocytes), CD66b (green, neutrophils) and DNA (grey). Wide field shown on the upper panel and detailed zoom-in in the lower panel. Scale bars: 50 µm (upper panel) and 20 µm (lower panel). B-C. Quantification of the number of CD45$^+$ (B, calculated as % of CD45$^+$ out of total cells) and CD66b$^+$ cells (C, calculated as % of CD66b$^+$ out of CD45$^+$ cells) from (A), on a total of 15 patients. For each tissue section, 12 different regions were interrogated and analysed using ImageJ. Regions of pancreata not affected by the tumor were used as control (normal). The data are presented as mean ± SD. D. Representative immunofluorescence images of PDAC showing ARG1 (green), CD66b (red) and DNA (grey). Scale bar: 10 µM. E. Representative immunofluorescence images showing MPO (green), ARG1 (red), CTSS (blue) and DNA (grey) in PDAC tissue samples. Scale bar: 10 µM. Quantification of ARG1 and CTSS co-localization within the PDAC tissues. Pearson's correlation coefficient analysis. The data are presented as mean ± SEM. ****p < 0.0001. F. Representative immunofluorescence images detailing NE (red), H3 citrullinated (blue) and DNA (gray) in NETs present in PDAC tissues. Scale bar: 10 µm. G. Representative immunofluorescence images showing ARG1 (red) and CTSS (blue) in NETs (co-

localization of MPO, green, and DNA, grey) in PDAC tissues. Scale bar: 10 µm. Quantification of NETs (% of area DNA-MPO) in PDAC tissues. H-J. Quantification of (H) ARG1 and (I) CTSS intensity; (J) ARG1 and CTSS co-localization (Pearson's correlation coefficient analysis) in the NETs of PDAC tissues. The data are presented as mean ± SEM. ****p < 0.0001.

ARG1 and CTSS are present in serum of PDAC patients

The presence of neutrophils expressing ARG1 in the tumor stroma prompted us to evaluate the enzyme levels and activity also in patients' sera. As shown in Fig. 15A, we found that PDAC patients had high serum levels of ARG1 (mean value of 192 pg/ml vs 40 pg/ml in HDs). ARG1 activity at physiological pH 7.3 was higher in PDAC patients while the opposite was true for alkaline pH 9.5, indicating a shift in ARG1 function associated with tumor presence (Fig. 15B). Considering the increased levels of functionally active ARG1 in the sera of PDAC patients, we next determined the presence of ARG1 cleaved forms. To deal with the limited amount of sera from patients and the high demand of substrate to perform the assay, we collected 10-12 ml of serum from the fewest patients for whom we had ethical committee approval. As shown in Fig. 15C, ARG1 cleaved forms are present only in patients, even though to a less extent than the full length form, but absent in HD sera. This result was also supported by the fact that CTSS levels and activity were higher in PDAC sera (Fig. 15D-E) and NETs were increased (Fig. 15F). We then tested whether serum of PDAC patients was suppressive and, whether the αARG1 clone 1.10 was able to restore T cell proliferation. Indeed, proliferation of T cells cultured with PDAC serum was decreased by 40% compared to T cells cultured with HD-derived sera, and the αARG1 clone 1.10 restore T cell proliferation almost completely (Fig. 15G). Since these features are reminiscent of the activated PMNs observed in Fig. 6, we attempted to identify the systemic factors triggering neutrophil activation. We focused on IL-8, known activators of neutrophils (Fig. 8C-D); furthermore, increased levels of IL-8 in the serum of cancer patients were associated to reduced benefits of immunotherapy based on check point inhibitors [315]. Indeed, PDAC patients had higher levels of IL-8 than the HDs, indicating that these cytokines could mediate NETs release and ARG1 cleavage by CTSS in PDAC patients

(Fig. 15H). Indeed, IF experiments revealed that in NETs of IL-8-stimulated HD-derived PMNs, ARG1 and CTSS colocalize (Fig. 15I-J).

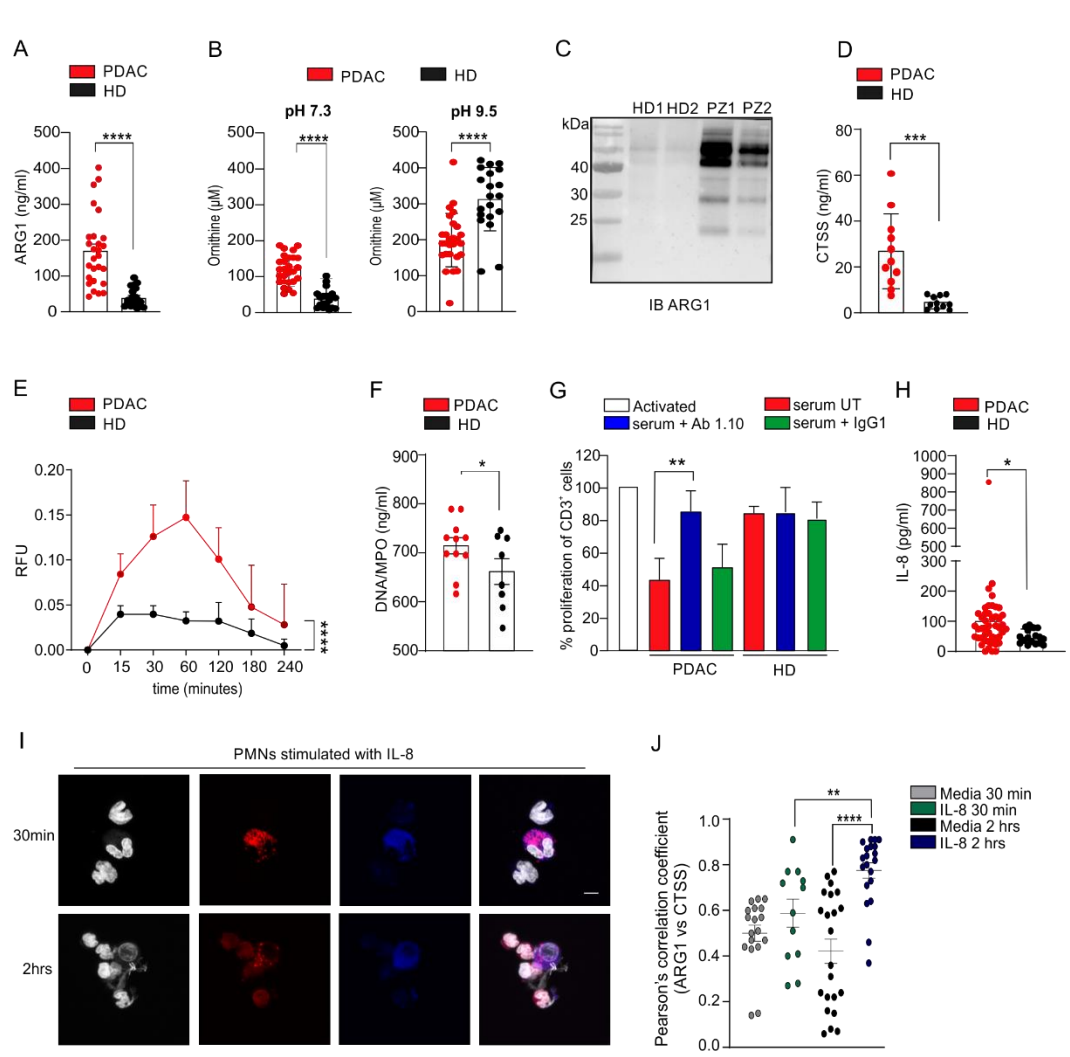

***Figure 15*. PDAC patients derived serum contains ARG1 endowed with suppressive capacity.**

A. Quantification of ARG1 levels (ng/ml) by ELISA in sera of PDAC patients and HDs. The data are presented as mean ± SEM. Paired Student's t-test. ****p < 0.0001. B. Determination of serum-derived ARG1 activity by colorimetric assay. The levels of ornithine obtained at pH 7.3 (left panel) and pH 9.5 (right panel) are shown. The data are presented as mean ± SEM. Paired Student's t-test. ****p < 0.0001. C. Representative immune blotting of ARG1 in sera derived from PDAC patients and HDs. D. Quantification of CTSS levels (ng/ml) by ELISA in sera of PDAC patients and HDs. The data are presented as mean ± SEM. Paired Student's t-test. ***p = 0.0015. E. Determination of serum-derived CTSS activity in kinetic assay in sera of PDAC patients and HDs. The data are presented as mean ± SD. Two-way ANOVA. ****p < 0,0001. F. Quantification of DNA-MPO complex levels (ng/ml) by ELISA in sera of PDAC patients and HDs. The data are presented as mean ± SD. G. Cumulative data of PDAC patients (n=52) and HDs (n=14) sera are shown. Sera from PDAC patients and HDs were either left untreated or incubated with neutralizing antibody αARG1 clone 1.10 (150 μg/ml) or IgG1 isotype

control. Activated T cells are set as 100 % proliferation and used as control. Suppressive activity is represented as percentage of proliferation of $CD3^+$ $CellTrace^+$ cells. The data are presented as mean ± SEM. Paired Student's t-test. **p = 0.0045. H. Quantification of IL-8 levels in sera of PDAC patients and HDs. The data are presented as mean ± SEM. Paired Student's t-test. *p < 0.05. I. Representative immunofluorescence images showing ARG1 (red), CTSS (blue) and nucleus (grey) of PMNs treated with 20 nM IL-8 for 30 minutes and 2 hours (n=3). Scale bars: 10 μm. J. Quantification of ARG1 and CTSS co-localization within the NETs produced by either IL-8 –stimulated (30 minutes and 2 hours) or untreated PMNs. Pearsons 'correlation coefficient analysis. The data are presented as mean ± SEM. Unpaired Student's t-test; **p = 0,0065, ****p < 0.0001.

αARG1 clone 1.10 enhances the effect of the immunotherapy with checkpoint inhibitors in PDAC tumor homogenates

Immune checkpoint inhibitors (ICI) targeting CTLA-4 and the PD-1/PD-L1 axis have shown unprecedented clinical activity in several types of cancer and are rapidly transforming the practice of medical oncology [316, 317]. However, initial resistance, non-response to single-agent ICI and tumor relapse represent big challenges for the effectiveness of this type of immunotherapy [318, 319]. PDAC is among the ICI-resistant tumors and the immunological challenges to override are the insufficient immune activation and the excessive immune suppression [244, 314]. We set up an *ex vivo* experiment using resected PDAC tumors from naïve-treatment patients. Tumors were mechanically digested, debris was removed, and the tumor composition was evaluated by FACS analysis for CD45, CD3, CD8 and CD66b. Purified $CD45^+$ cells were incubated with ICI, αARG1 clone 1.10, either alone or in combination (Fig. 16A) [320] As shown in Fig. 16B, after 24 hrs the combinatorial treatment nivolumab+ipilimumab+αARG1 resulted in a significant decrease in the amount of $CD8^+$ T cells expressing PD-1, which was paralleled by an increment in IFN-γ and IL-2 release (Fig. 16C) while the levels of several leucocyte subsets were unaltered among the various treatment groups (Fig. 16D). These data suggest that harnessing ARG1 activity in PDAC might enhance the efficacy of ICI therapy, which is currently confined to a minority of patients [321].

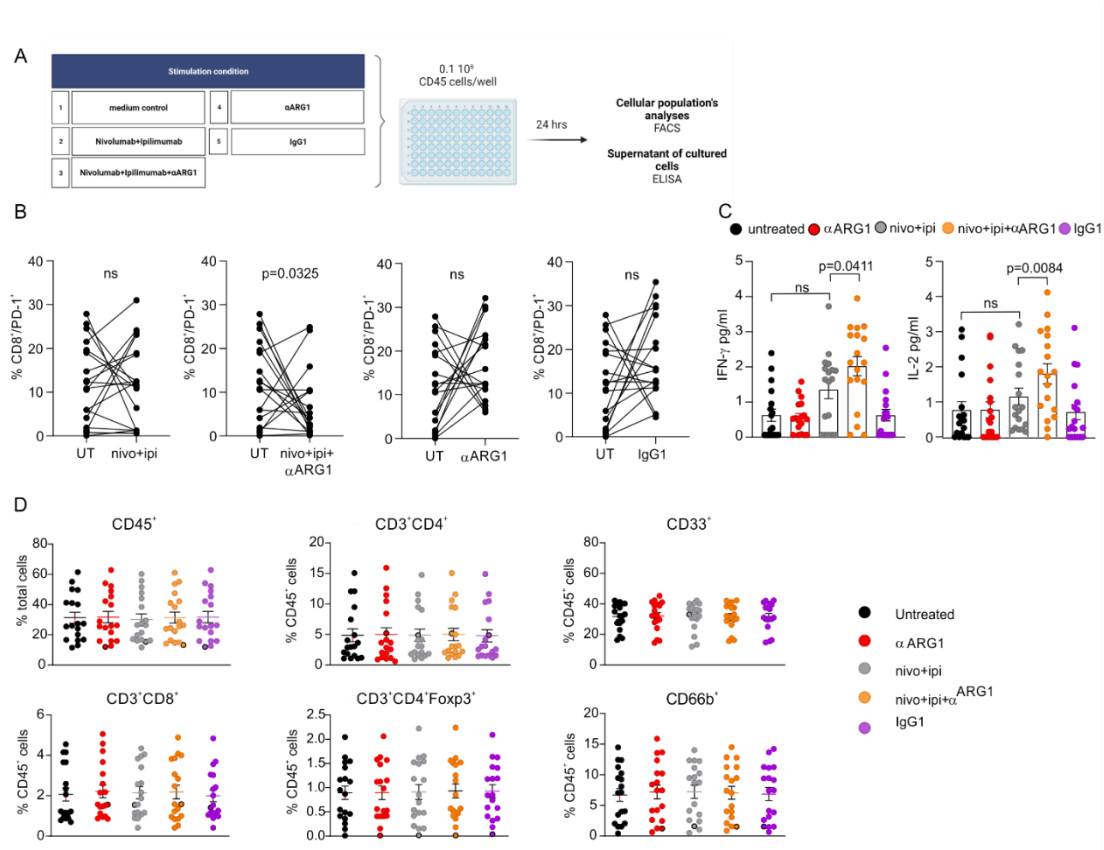

***Figure 16*. In PDAC tumor homogenates, blockade of ARG1 by monoclonal antibody improved the efficacy of ICI.**

A. Experimental setting of the ex vivo human PDAC assay. Tumor homogenate was cultured either with nivo+ipi, nivo+ipi+αARG1, αARG1, IgG1 or left untreated for 24 hrs. Then FACS analysis on the cells was performed and the supernatants were evaluated for the presence of IFN-γ and IL-2. B. FACS analysis of $CD8^+PD\text{-}1^+$ cells in tumor tissue homogenate, derived from naïve-treatment PDAC patients, cultured for 24 hrs with either nivo+ipi, nivo+ipi+αARG1,αARG1, isotype IgG1 control or left untreated. (n=18) The data are presented as mean ± SEM. Paired Student's t-test. C. Quantification, by ELISA, of IFN-γ and IL-2 secreted in the supernatants of cells treated for 24 hrs as in A. The data are presented as mean ± SEM. One-way Anova, multiple comparisons with Tukey correction; *p=0.0411, **p=0.0084; ns, not significant. D. FACS analysis for the detection of $CD45^+$, $CD3^+CD4^+$, $CD33^+$, $CD3^+CD8^+$, $CD3^+CD4^+Foxp3^+$ and $CD66b^+$ cells was performed after 24 hours.

ARG1 and CTSS are released by myeloid cells of PDAC patients and blocking of ARG1 can block neutrophils and CD14 cells suppressive activity

It is known that MDSCs are one of the main populations that shape the tumor microenvironment, suppress anti-tumor immune responses of T cells and block the effect of immunotherapy [44]. Therefore, we wanted to investigate the immune suppressive activity of myeloid populations derived from the peripheral blood of PDAC patients and HDs (Table 4). We selected to isolate populations that express ARG1, such as LDN and NDN neutrophils. We also isolated CD14 cells, since there are newly described immunosuppressive $CD14^+$ monocytes and PMNs expressing CD14 subsets [322]. Cells were plated for 12 hours without any stimulation, and then cells and culture supernatants were collected separately and added on T cells. After 4 days we evaluated as before T cell proliferation. Regarding cells suppressive capacity, we can understand from Fig. 17A (left panel) that $CD14^+$ cells from patients clustered in two groups, the suppressive (Fig. 17A, black dots) and the non-suppressive (Fig. 17A, red dots), while few LDNs and even fewer NDNs were suppressive. As expected, cells isolated form HDs did not have suppressive capacity, unless stimulated (Fig. 17A, right panel and Figure 7L). On the other hand, supernatants from almost all LDNs and several NDNs derived from PDAC patients suppressed as the ones from CD14 (Fig.17B, left panel), while supernatants from HDs did not impact T cell proliferation (Fig. 17B, right panel). These results indicated that NDNs and LDNs did not suppress in a cell-to-cell contact manner and that CD14 cells were capable to suppress either by contact with T cells or by secreting inhibitory molecules in the extracellular environment. With view to prove that the cells suppress in an ARG1-dependent manner, we examined the presence of NETs and ARG1 in the supernatants of each group. As expected, NDNs produced higher levels of NETs, compared to LDNs and $CD14^+$ cells, but ARG1 levels in the supernatants had no difference among the three populations (Fig. 17C-D). Then, ARG1 enzymatic activity was evaluated and surprisingly ARG1 secreted from $CD14^+$ cells was more active than the one released

from neutrophils' populations (Fig. 17E). This phenomenon was also correlated with higher levels of CTSS in CD14-derived supernatants (Fig. 17F). Finally, we evaluated if the observed suppression was ARG1 dependent and if so, whether αARG1 clone 1.10 was able to reverse this situation. We noticed that αARG1 clone 1.10 had no effect on the suppression exerted by all the three groups of cells when cultured with T cells (Fig. 17G). Nevertheless, αARG1 clone 1.10 was effective on unleashing the proliferation of T cells cultured with supernatants, even if this was observed in different potency in each population (Fig. 17H). Overall, myeloid cells isolated from PDAC patients secrete ARG1, with differential activity probably due to different concentration of CTSS released by the three population, and αARG1 clone 1.10 is able to block its activity when released in the supernatants.

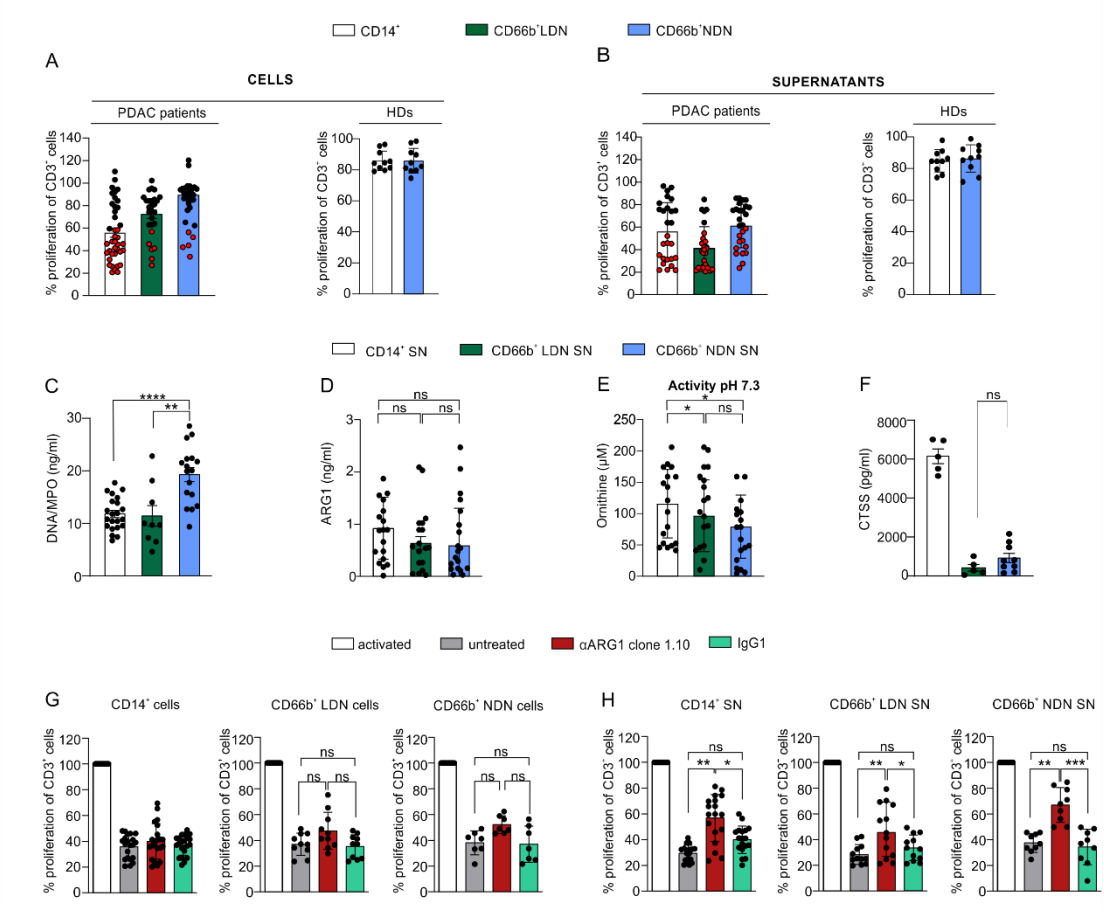

Figure 17. **Blockade of ARG1 with monoclonal antibody dampened the immune suppressive function of neutrophils and CD14$^+$ cells isolated from PDAC patients.**

A-B. Proliferation assay showing the percentage of anti-CD3 and anti-CD28 activated T cells cultured with myeloid cells isolated from the peripheral blood by density gradient. The $CD14^+$ cells (PDAC patients, n=40; HDs, n=3), low density $CD66b^+$ neutrophils (LDNs, PDAC patients, n=40) and normal density $CD66b^+$ neutrophils (NDNs, PDAC patients, n=40; HDs, n=3) were added as either cells (C, at the 3:1 effector:target ratio) or as supernatants (D, $CD14^+$, PDAC patients, n=27; HDs, n=3; $CD66b^+$ LDNs, PDAC patients, n=27; HDs, n=3; $CD66b^+$ NDNs, PDAC patients, n=27; HDs, n=3). Activated T cells are set as 100 % proliferation and used as control. Suppressive activity is represented as percentage of proliferation of $CD3^+$ $CellTrace^+$ cells. The data are presented as mean ± SEM. Red dots represent the suppressive samples. C. Quantification of DNA/MPO complex levels (ng/ml) by ELISA in the supernatants of $CD14^+$ (n=22), $CD66b^+$ LDN (n=9), and $CD66b^+$ NDN cells (n=17). The data are presented as mean ± SEM. One-way Anova multiple comparisons with Tukey correction; $^{**}p < 0.010$; $^{****}p < 0.0001$. D. Quantification of ARG1 levels (ng/ml) by ELISA in the supernatants of $CD14^+$, $CD66b^+$ LDN and $CD66b^+$ NDN cells (n=18). The data are presented as mean ± SEM. One-way Anova multiple comparisons with Tukey correction; ns, not significant. E. Determination of ARG1 activity in the supernatants of $CD14^+$, $CD66b^+$ LDN and $CD66b^+$ NDN cells (n=18). Ornithine levels are evaluated by colorimetric assay at pH 7.3. The data are presented as mean ± SEM. One-way Anova multiple comparisons with Tukey correction; $^{*}p < 0.05$; ns, not significant. F. Quantification of CTSS levels (ng/ml) by ELISA in the supernatants of $CD14^+$ (n=5), $CD66b^+$ LDN (n=5) and $CD66b^+$ NDN cells (n=9). The data are presented as mean ± SEM. One-way Anova multiple comparisons with Tukey correction; ns, not significant. G-H. Proliferation assay showing the percentage of anti-CD3 and anti-CD28 activated T cells, cultured with suppressive $CD14^+$ (n=18), $CD66b^+$ LDNs (n=10) or $CD66b^+$ NDNs cells (G, n=7) or cell-derived suppressive supernatants (H, $CD14^+$ SN, n=18; $CD66b^+$ LDN SN, n=13; $CD66b^+$ NDN SN, n=9. To verify the efficacy of ARG1 neutralizing antibodies, either cells or the supernatants were cultured with the antibody anti-ARG1 clone 1.10 or IgG1 isotype control (150 µg/ml). Activated T cells are set as 100 % proliferation and used as control. Suppressive activity is represented as percentage of proliferation of $CD3^+$ $CellTrace^+$ cells. The data are presented as mean ± SEM. One-way Anova multiple comparisons with Tukey correction. $^{*}p < 0.05$; $^{**}p < 0.01$; $^{***}p = 0.001$; ns, not significant.

Neutralization of ARG1 increases the trafficking and function of adoptively transferred $hTERT_{865-873}$-specific T cells in humanized mouse model of human cancers

The profound dissimilarity between humans and mice, regarding ARG1 cellular source and its species specific regulation, prompted us to exploit a humanized mouse model, in which, the concomitant presence of neutrophils and expression of ARG1, could be used to assess the *in vivo* efficacy of the anti hARG1 clone 1.10, in combination with ACT based on T cells genetically-engineered with a TCR specific for $hTERT_{865-873}$ peptide [323]. NOG mice were γ-irradiated and subsequently engrafted with human HLA-$A2^+CD34^+$ HSCs, as previously reported [324]. To favor the expansion of neutrophils, recombinant AAV9 coding for human CSF3, IL-3, IL-8 and HGF [325], were administered intramuscularly at week 4 to sustain the systemic release of these

cytokines [326]. Ten weeks later, tumor cells were subcutaneously injected (Fig. 18A). The humanization protocol led to a robust reconstitution of human leukocytes in mouse peripheral blood (Fig. 18B) and lymphoid organs (Fig. 18C-D). We found that all mice exhibited high, stable engraftment of $hCD45^+$ cells, with $CD19^+$ B lymphocytes detected during the earlier phases (peak at week 8) (Fig. 18B). The percentage of human $CD3^+$ T cells started to be detectable only at later time points and it was paralleled by a drop in B lymphocytes. Interestingly, myeloid $CD33^+$ cells maintained a constant level throughout the study (for both $CD15^+$ and $CD14^+$ cells). We could not find a suitable PDAC cell line, i.e. expressing hTERT, HLA-$A2^+$ and infiltrated by neutrophils. Thus, we screened a number of human lines of various histology. SK-MEL-5 melanoma met the criteria for being used in humanized mice. Indeed, it expressed hTERT (Fig. 18E) and displayed hTERT peptide-HLA-A02 complexes on the cell surface, as demonstrated by the IFN-γ secretion of $hTERT_{865-873}$-specific TCR transgenic T cells (Fig. 18F-G). Furthermore, SK-MEL-5 tumors established in humanized mice were infiltrated with both human neutrophils and monocytes (Fig. 18H-I). Additional analysis of tumor tissues allowed detecting $CD66b^+$ neutrophils expressing ARG1 at levels that were independent from the treatments.

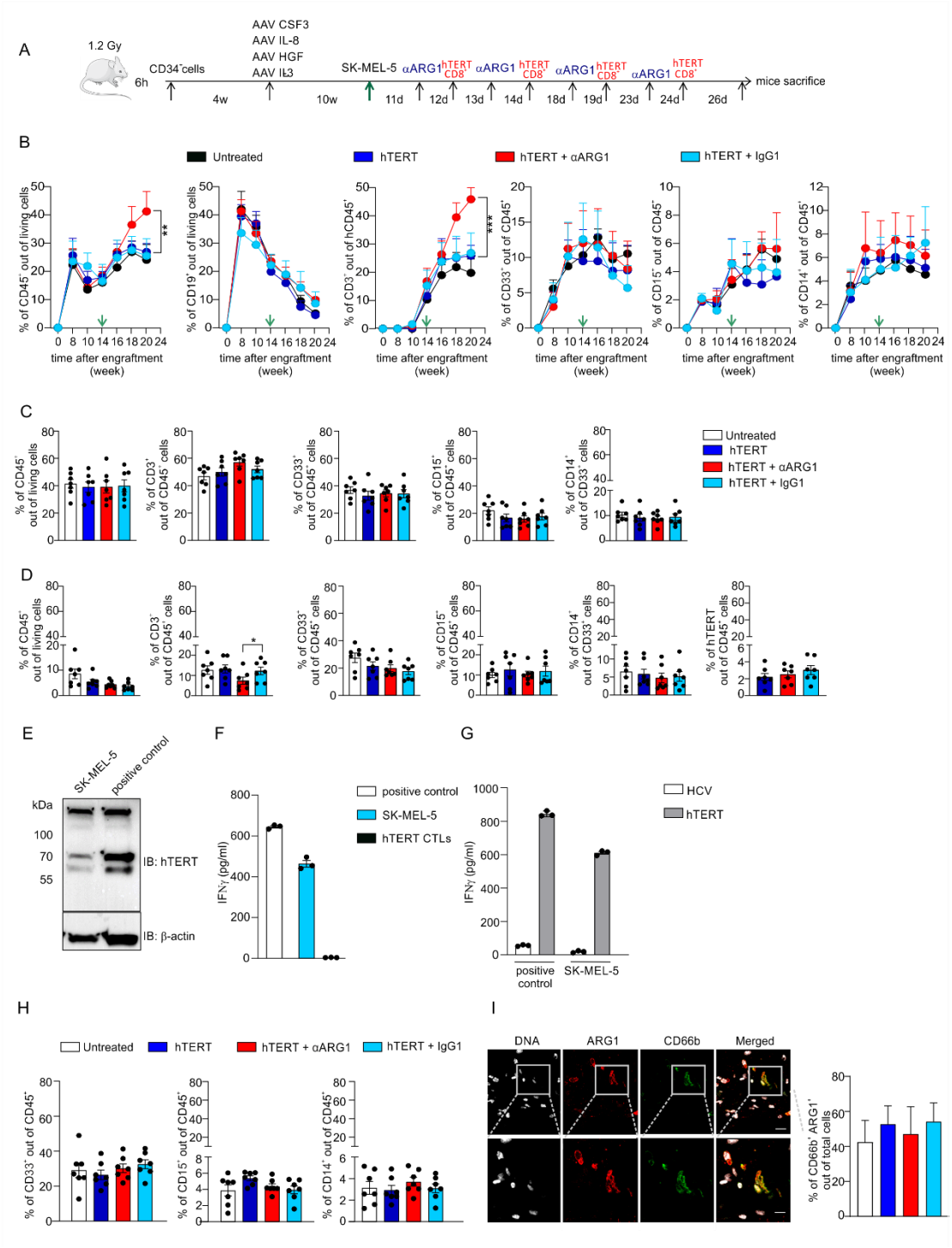

Figure 18. **Functional characterization of hTERT$_{865-873}$ specific T cells and analysis of human cells infiltrating myeloid organs in SK-MEL-5 humanized mouse model.**

A. Experimental layout of humanized mice generation. NOG mice were γ-irradiated (1.2 Gy) and subsequently engrafted with 105 hHLA A2-CD34$^+$ cells via tail vein injection. At week four recombinant

AAV9 vectors coding for human CSF3, IL-3, IL-8 and HGF were administered intramuscularly. After 10 weeks, mice were inoculated s.c. either with SK-MEL-5 cell line (1 x 10^6 cells). When the tumor reached 200 mm^3, mice received tail vein 2.5 x 10^6 $hTERT_{865-873}$-specific, TCR-engineered T cells and rhIL-2 (20 IU/mL) given i.p. IL-2 was then given every other day. The day before the hTERT-specific T cell injection, mice received the antibody αARG1 clone 1.10, 0.5 mg/g, or IgG1 isotype control (i.p.). 2.5 x 10^6 $hTERT_{865-873}$-TCR-engineered T cells were injected every 5 days for the first two injections, then once a week for the last two injections. Two days after the last injection, the mice were sacrificed. *B.* The kinetic of human immune cell reconstitution analyzed in peripheral blood of humanized mice was evaluated by FACS analysis of hCD45, hCD19, hCD3, hCD33, hCD15 and hCD14. Humanized mice, carrying a SK-MEL-5 melanoma, were treated with $hTERT_{865-873}$ tumor-specific T cells alone or in combination with neutralizing antibody αARG1 clone 1.10 or IgG1 isotype control (n=7 mice per group). The data are presented as mean ± SD. Two-way Anova. **p = 0.0125; ***p = 0.00185. Green arrow indicates the day of tumor inoculation. C-D. FACS analysis showing the percentages of human immune cells in C) bone marrow and D) spleen of mice bearing a SK-MEL-5 tumors. Cells were defined based on the expression of hCD45, hCD3, hCD33, hCD15, hCD14 and hTERT-specific T cells. Humanized mice were treated, either with hTERT-specific T cells alone or in combination with neutralizing antibody αARG1 clone 1.10 or IgG1 isotype control. (n=7 mice per group). The data are presented as mean ± SEM. Paired Student's *t*-test. *p = 0.03. E. Immunoblot detailing hTERT expression by SK-MEL-5 and positive control (T2) cell lines. β-actin: loading control. *F*. Quantification of IFN□ levels (ng/ml) by ELISA in hTERT-specific transgenic T cells. The IFNγ secretion was assessed upon co-culturing hTERT-specific T cells with PT-45and positive control (T2) cell lines; 10^5 engineered CTLs were co-cultured at 1:1 ratio, for 24 hrs. *G*. Quantification of IFNγ levels (ng/ml) by ELISA in hTERT-specific transgenic T cells. Transgenic T cells specific for $hTERT_{865-873}$ peptide were co-cultured with T2, *SK-MEL-5* cells pulsed with either $hTERT_{865-873}$ peptide (10^{-10} M) or irrelevant $hHCV_{1406-1415}$ peptide (10^{-10} M). *H.* FACS analysis showing the percentages of tumor–infiltrating human immune cells in the PT-45 mouse model. Cells were defined based on the expression of hCD45, hCD33, hCD15 and hCD14. I. Representative immunofluorescence images of tumors derived from PT-45 tumor-bearing mice showing ARG1 (red), CD66b (green) and DNA (grey) from tumors of mice treated with hTERT-specific T cells alone or in combination with either neutralizing antibody αARG1 clone 1.10 or IgG1 isotype control. Wide field shown in the top panel and detailed zoom-in in the bottom panel. Scale bar: 50 µm (top panel) and 10 µm (lower panel). I. Quantification of $CD66b^+$ $ARG1^+$ cell percentages from H. The data are presented as mean ± SEM.

A therapeutic effect of $hTERT_{865-873}$-specific T cells in controlling the tumor growth (Fig. 19A) was associated with changes in lymphoid but not myeloid compartment in tumor and lymphoid organs (Fig. 19B). Indeed, combination therapy (i.e. hTERT ACT and αARG1 clone 1.10) increased the amount of $CD3^+$ T cells within the tumor (Fig. 19B-C), which correlated with a higher tumor infiltration of hTERT-specific T cells and improved control of tumor growth. The hTERT-specific T cells were identified as positive for the transgene CD34 present in the TCR-expressing lymphocytes, as previously published [305]. We then evaluated the functional features of hTERT-specific T cells isolated from SK-MEL-5 tumors and found that T cells had a higher proliferation capacity, as well as higher expression of CD69 and CD25, but not PD-1, suggesting a shift towards activation in mice treated with the combination therapy (Fig.

19D). These results recapitulate the *in vitro* data with PDAC biopsies (Fig. 16B). Thus, ACT and ARG1 blockade can lead to an increase in $CD3^+$ T cells, and among them hTERT-specific T cells.

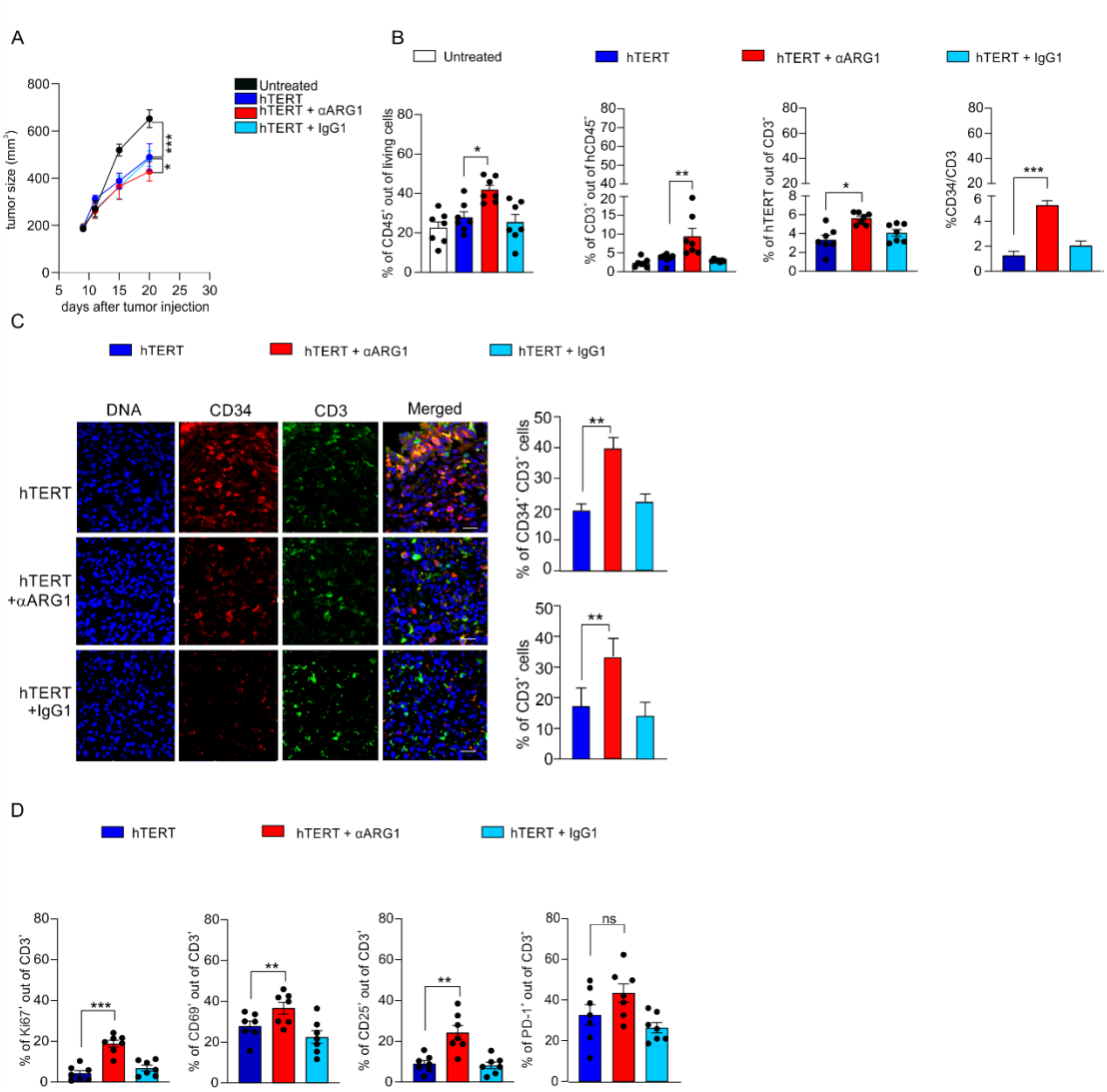

Figure 19. **Neutralization of ARG1 increases the infiltration and function of hTERT$_{865-873}$-specific T cells.**

A. Determination of the tumor volume (mm3), in the SK-MEL-5 tumor model, injected s.c. in humanized mice. Cumulative tumor size curves of the different treatment groups are shown. The data are presented as mean ± SD. Mann-Whitney non parametric test. *p = 0.042, ***p = 0.0004. B. FACS analysis of the percentages of tumor–infiltrating human immune cells in the PT-45 tumors. Cells were defined as before, based on the expression of hCD45 and hCD3; hTERT-specific T cells and the CD34/CD3 ratio was also defined. Humanized mice were treated, as before, with hTERT-specific T cells alone or in combination with neutralizing antibody αARG1 clone 1.10, or IgG1 isotype control (n=7 mice per group). The data are presented as mean ± SEM. Paired Student's *t*-test. *p <0.036, **p = 0.00204, ***p = 0.0002. C.

Representative immunofluorescence images of tumors derived from PT-45 tumor-bearing mice showing CD34 (red), CD3 (green) and DNA (blue) from tumors of mice treated with hTERT-specific T cells alone or in combination with neutralizing antibody αARG1 clone 1.10 or IgG1 control. Scale bar: 50μm. Quantification of percentage of cells $CD3^+CD34^+$ (top panel) and $CD3^+$ (bottom panel). Results are shown as mean ± SEM. Paired Student's *t*-test. **p < 0.0248. D. FACS analysis of $hCD3^+hCD34^+$ hTERT-specific T cells, isolated from PT-45 tumors, evaluating the expression of proliferation (Ki67) and activation (CD25, CD69 and PD-1) markers. $hTERT_{865-873}$ transgenic T cells were isolated from SK-MEL-5 tumors of mice treated with hTERT-specific T cells alone or in combination with neutralizing antibody αARG1 clone 1.10, or IgG1 isotype control (n=7 mice per group). The data are presented as mean ± SEM. Paired Student's *t*-test. **p< 0.00356.

Immune checkpoint inhibitors in combination with ARG1 blockade enhance survival of humanized mice bearing a melanoma

Mounting evidence suggests that a major constrain to ICI includes either the absence of preexisting tumor-specific T-cells or their exclusion from the tumor microenvironment. Analyses of pretreatment melanoma biopsies have shown that clinical response to anti-PD-1 [327] and anti-CTLA4 [328] is correlated with the presence of tumor infiltrating lymphocytes prior to the therapy, specifically $CD8^+$ T-cells. In the SK-MEL-5 model, endogenous $CD3^+$ T cells are significantly present in both peripheral blood and tumor site (Fig. 18B and 19B) and blocking ARG1 function resulted in further increase compared to the controls, laying the rationale for using ICI in combination with ARG1 blockade. NOG mice were engrafted with $HLA\text{-}A2^+CD34^+$ HSCs and received AAV9 vectors (Fig. 20A). We performed tumor cell inoculation as before, i.e. when the levels of $CD3^+$ T cells started to increase in peripheral blood. As shown in Fig. 20B-C, nivolumab + ipilimumab (ICI) affected the tumor growth, yet the combinatorial therapy ICI + αARG1 was more effective in controlling tumor growth, with a positive impact on mouse survival (Fig. 20D).

Thus, these data suggest that combination of ICI and ARG1 blockade by neutralizing antibody could represent a safe and effective strategy for harnessing tumors growth.

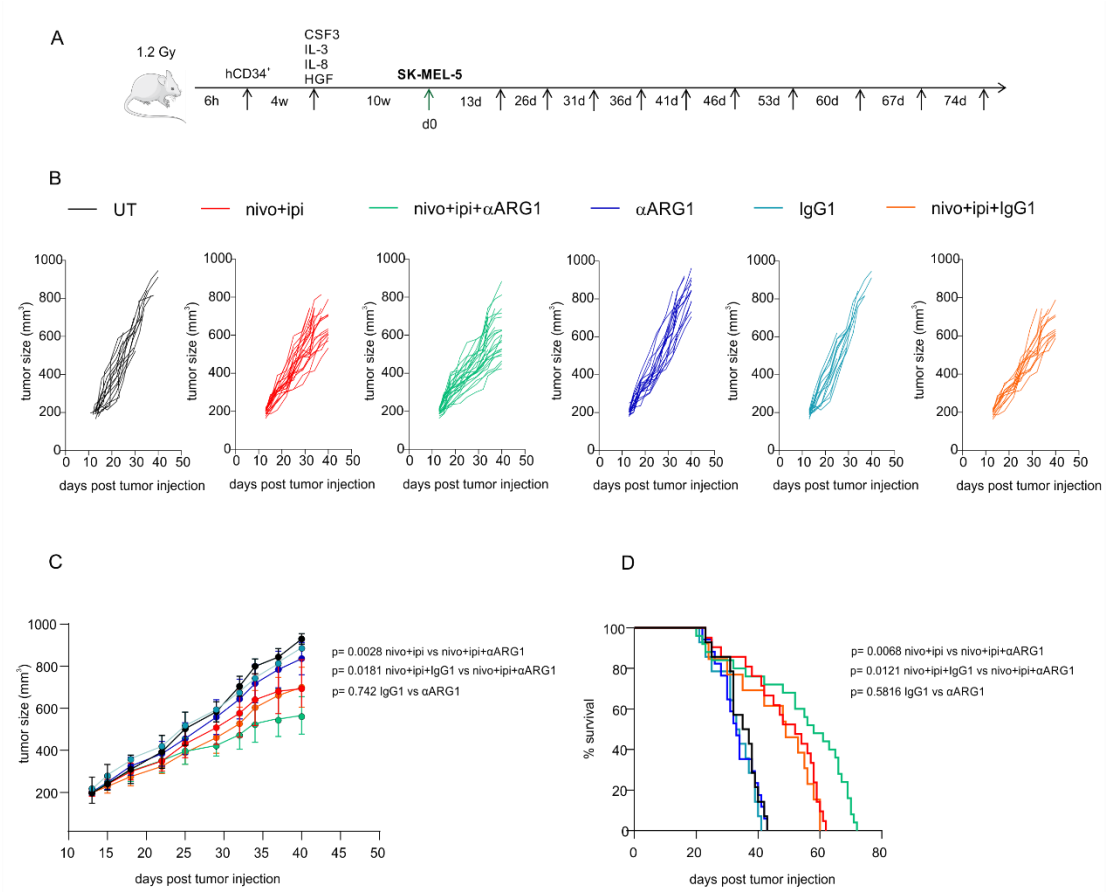

Figure 20. **Neutralization of ARG1 increases the efficacy of ICI therapy.**

A. Experimental layout of humanized mice generation, followed by challenge with SK-MEL-5 melanoma. Mice were treated with neutralizing antibody αARG1 clone 1.10 (20 mg/kg) alone or in combination with nivolumab (10 mg/kg) and ipilimumab (5 mg/kg), or a combination of nivolumab and ipilimumab or left untreated. All the groups received i.p. injections every 5 days up to end stage of life. B. Single tumor size curves of SK-MEL-5 bearing humanized mice treated as in A (untreated, n=14; nivo+ipi, n=25; nivo+ipi+αARG1, n=25; αARG1, n=17; nivo+ipi+IgG1, n=18; IgG1, n=14). C. Cumulative curves of tumor size in SK-MEL-5 bearing humanized mice treated as in A. The data are presented as mean ± SD. Mann-Whitney non parametric test. nivo+ipi vs nivo+ipi+αARG1, **p=0.0028; nivo+ipi+IgG1 vs nivo+ipi+αARG1, *p=0.0181; IgG1 vs αARG1, not significant, p=0.742 D. Kaplan-Meier plots estimating the survival of SK-MEL-5 bearing humanized mice treated as in A. The data are presented as percent survival. Log-rank test.

Discussion

In spite of the development of many promising immunotherapeutic treatments for solid malignancies, the efficiency of anti-tumor therapies is restrained to a small fraction of patients while they have poor to no beneficial effect in the majority of cancer patients [1]. This can be explained by the fact that most of the immunotherapeutic approaches target only one component among the highly complex network of cells and factors that constitute the TME. Accumulating evidence shows that cellular and acellular components in TME can reprogram tumor initiation, growth, invasion, metastasis, and response to therapies. TME is shaped and trained by cancer cells to assist the development of cancer hallmarks, respond to intrinsic or extrinsic stress, stimulation and treatment, and ultimately assist tumor cells' survival and migration. Nonetheless, the clinical efficacy of therapeutic strategies targeting TME, especially the specific cells or pathways of TME, remains unsatisfactory. Among the immunosuppressive mechanisms in place, the deprivation of nutrients and the accumulation of products with pro-tumor and immune-suppressive activities (e.g. kynurenines and lactate) is an active field of cancer research. Tumors consume large amounts of glucose, to sustain their anaerobic glycolysis, and nutrients, like amino acids (e.g. tryptophan, glutamine, arginine) and lipids, to support proliferation and survival [19, 329, 330]. These limitations restrain anti-tumor T cell activation and effector functions, thus hampering a proper anti-tumor immune response [331]. The demonstration that sustained intratumor availability of L-arginine, by engineered bacteria strain, increased the number of tumor-infiltrating T cells and had marked synergistic effects with PD-L1 blocking antibodies in the clearance of tumors [332], reinforce the concept that modulation of the tumor microenvironment is an essential step of an effective anti-tumor therapy.

ARG1 and ARG2 are the responsible enzymes for the hydrolysis of L-arginine and they are expressed by both tumors and cells of the TME. The role of ARG2 in cancer has only recently gain attention. Preclinical studies confirmed that ARG2 promotes the proliferation of cancer cells and the growth of tumor xenografts independently of its immunosuppressive activity. Generation of polyamines to facilitate the growth of

hypoxic and nutrient-deprived tumors**,** as well as specific metabolic adaptations including increased reliance on protein catabolism are the major mechanisms underlying the tumorigenic activity of ARG2**.**

Instead, ARG1 and its tumor promoting effects have been extensively analyzed in the last decades. Despite the intense research, targeting ARG1 remains a challenge. On the light of the unique hARG1 biology, it is compulsory to reconsider its targeting and better contextualize the findings about the inhibitors so far developed.

In our study, we have found that, upon PMNs stimulation, ARG1 is released and localizes in NETs, where it shows an unprecedented defined molecular pattern. This pattern present only in the NETs of stimulated PMNs, is associated with a gain of activity at physiological pH assessed in term of both downstream ornithine production and immunosuppressive activity towards activated T cells.

We showed that classical ARG1 inhibitors (e.g. BEC and Nor-NOHA) have no effect on soluble cleaved forms, differently from newly generated monoclonal antibody. Even though small molecule ARG1 inhibitors are being tested in phase I/II clinical trials (e.g INCB001158, clinical trial identifier: NCT02903914), several issues argue that this approach might be biased and not entirely focused. As side effect, small inhibitors can affect the urea cycle in the liver causing hyperammonemia, with unpredictable results on the overall antitumor immune response. Moreover, as we showed the inhibitors are not active on hARG1 cleaved forms or high molecular weight complexes derived from them. The simple explanation is that they were designed and synthesized based on the know-how acquired, over several decades, on the full-length enzyme, which is not active at physiologic pH. Furthermore, molecular complexity of the cleaved forms might interfere with the accessibility of small molecule inhibitors to the catalytic site and/or substrate-binding pocket. In line with these considerations, the availability of the recombinant cleaved forms should offer a simple way to test and screen *in vitro* different inhibitors from complex libraries of small synthetic molecules.

We have also proven that biological relevant stimuli (e.g. IL-8) induce ARG1-controlled release in NETs; however, whether this results in ARG1 cleavage and gain of function at physiological pH remains to be investigated. In line, initial work done by

our laboratory demonstrated that PMNs stimulated with TNFα secrete ARG1 lacking functional activity at physiological pH [83]. A possible explanation is that TNFα triggers the release of NETs with different molecular components that might have different impact on ARG1 structure and function. Ongoing experiments in our laboratory are trying to address these questions.

Indeed, we have demonstrated that in NETs released by ionomycin-stimulated PMNs, ARG1 has several specific interacting partners. We selected CTSS, as it is a protease with *in silico* potential cleavage sites in ARG1, known activity at physiological pH and implication in tumor progression. As shown our data confirmed that rhCTSS binds and cleaves rhARG1, generating the same molecular pattern observed in ionomycin-stimulated PMNs. Interestingly, the appearance of ARG1 high molecular weight bands at late time points of NET assembly envisions a situation in which products of the cleavage and/or uncut full length protein assemble into molecular complexes that are thermodynamically favored and stable, as suggested by the higher catalytic activity. In this sense, antibodies directed to the truncated forms (rhARG1-25 and rhARG1-31) will be useful to dissect this heterogeneity.

Our data clearly indicate that rhARG1-31 and rhARG1-25 have enzymatic activity, with the rhARG1-31 far more active to convert L-arginine into ornithine, than rhARG1 and rhARG-25. This difference translated into a more efficient T cell suppression, with BEC and nor-NOHA ineffective on both cleaved forms while our antibody clone 1.10 was effective in a dose dependent manner.

Cysteine cathepsins are known for their role in tumor progression. Among the other members, CTSS supports the progression of pancreatic tumor in mice and its high levels are also correlated with poor prognosis in cancer patients. Our study points out a previously undescribed role of CTSS, that in this case indirectly facilitates tumor progression through the cleavage of ARG1 favoring a net gain of function at physiological pH which is subsequently translated in ARG1-mediated T cell suppression. Therefore, blocking CTSS could block the generation of ARG1 cleaved forms and unleash T cells anti-tumor activity.

Recently published studies have demonstrated that NETs mediated cancer cell awakening and metastatic spread [221, 222]. Despite the advances, the role of NETs in human cancer progression and resistance to therapy remain poorly investigated [333]. Therefore, in this study, we evaluated, in PDAC patients, the presence of NETs in serum and tumor tissue and then we evaluated the ability of freshly isolated circulating myeloid cells to release NETs. Specifically, NETs-associated ARG1 was present in increased levels in tumor tissues, serum and myeloid cell-derived supernatants compared to healthy donors. Undoubtedly, ARG1 was found co-localized with CTSS in tumor tissues or co-present in serums and cell-derived supernatants. Moreover, ARG1 elevated levels were accompanied by increased activity at physiological pH, indicating anew that CTSS has performed its cleavage on ARG1. PDAC-derived myeloid cells, notably NDNs and LDNs and $CD14^+$ cells release NETs, in which ARG1 localizes and functions. In spite of these similarities, ARG1 released from a new subset of $CD14^+$ cells, recently described by our group and by [322], was far more active than the one released by PMNs. Future analysis will reveal whether in NETs produced by PDAC-derived myeloid cells, ARG1 presents a similar cleavage pattern, that might infer to its function.

Given the ability of IL-8 to act as a pro-inflammatory and pro-angiogenic factor and to induce the release of ARG1 by PMNs [102], we evaluated the protein levels of this cytokine in the serum of patients with PDAC. We observed increased levels of IL-8 in sera, which could function as activator of myeloid cells resulting in subsequent release of ARG1-containing NETs. We have highlighted how patients with PDAC have higher IL-8 levels than healthy donors, underlining even more the inflammatory state that the presence of the tumor determines in these patients.

NETs were also identified in PDAC tumor tissue. Still open remains the question whether in the tumor contest IL-8 is present and is active. It is known that the binding and effect of IL-8 to receptors expressed in neutrophils (such as CXCR1 and CXCR2) can be modulated by its proteolytic cut [334]. There are forms of IL-8, such as that at 72aa, (devoid of the 6 amino acids positioned at the N-terminus of the protein), which have a high activity on neutrophils. The 72aa form was used in our neutrophil

stimulation assays to evaluate their immunosuppressive effect. Proteases, such as metal protease 9 (MMP-9), secreted by neutrophils appear to be responsible for generating, on site, the formation of the more active form of IL-8 [335]. Therefore, even if our experiments showed high systemic levels of IL-8, we can hypothesize an equally relevant function of this cytokine in the tumor microenvironment, stimulating the neutrophils to release NETs.

In PDAC patients, the neutralizing antibody clone 1.10 unleashes the inhibitory effect of ARG1 on T cells proliferation only on NET-derived ARG1 but is ineffective when myeloid cells are co-cultured with T cells. This indicates that the αARG1 can block soluble ARG1 function. Moreover, the combinatory administration of αARG1 and ICI in PDAC tumor tissues isolated from patients showed a beneficial effect compared to the ICI alone, resulting in more activated T cells. Therefore, these results suggest that targeting the immunosuppresive TME could enhance the efficacy of ICI.

Finally, in order to test the *in vivo* efficacy of αARG1 we have generated a HIR mouse model, with constant presence of neutrophils in the circulation. SK-MEL-5-bearing HIR mice treated with αARG1 in combination with ACT showed decreased tumor growth compared to the other groups, which was accompanied by an increased in tumor antigen-specific T cells infiltration. Although we did not observe any differences in T cells function between the combinatory treatment and ACT alone, our results suggest that blocking ARG1 could favor the accessibility of tumor specific T cells. Blocking ARG1 was also effective in combination with ICI, were we observed a reduction in tumor size and increased survival in mice treated with nivo+ipi+αARG1, as compared to other groups. These data might pave the way to a rapid translation of the combination therapy to the clinic.

In conclusion, our study revealed a new molecular pattern of NET-associated ARG1, in which ARG1 is cleaved by CTSS resulting in the generation of ARG1 cleaved form endowed with enzymatic activity at physiological pH. The generated truncated forms contribute significantly in ARG1-mediated immunosuppression of T cells. We have also established that a newly generated neutralizing monoclonal antibody, blocks the

enzymatic function of both full length and cleaved ARG1 forms, while the commercially available ARG inhibitors are ineffective. This neutralizing effect was maintained *in vivo* in HIR mice and in myeloid cells derived from PDAC patients (Fig.21).

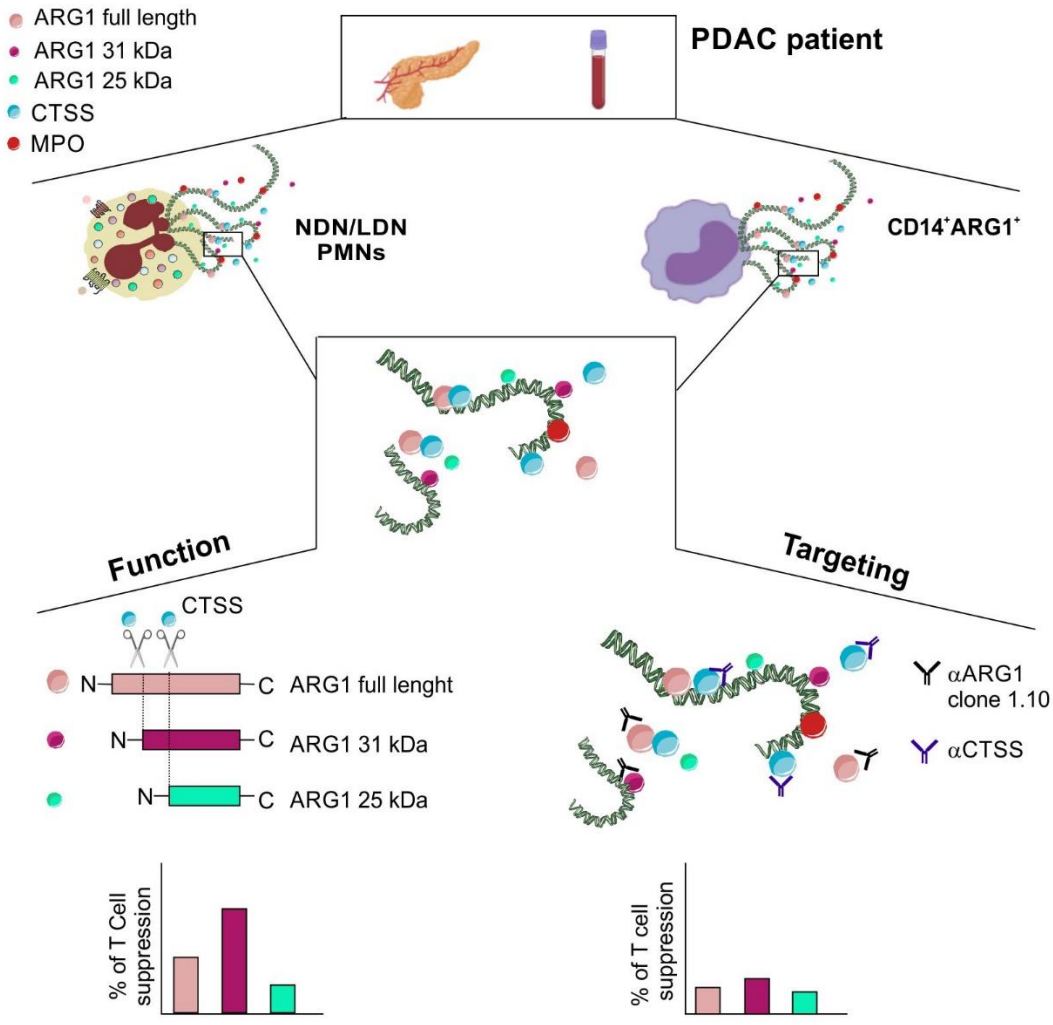

Figure 21. **Neutralization of NET-associated human ARG1 enhances cancer immunotherapy.** A newly described molecular pattern of NET-associated ARG1 generated by CTSS cleavage is correlated with increased activity of ARG1 in physiological pH and subsequently enhanced ARG1-mediated suppression of T cells. The neutralizing αARG1 clone 1.10 is able to recognize and inhibit all the forms of ARG1 restoring T cells proliferation, as also to boost the effect of immunotherapy.

Tables

Type	Start	End	Epitope Candidate	Value
LIN 9	14	22	HKPIDYLNP	2595
	15	23	KPIDYLNPP	2872
	16	24	PIDYLNPPK	2693
	17	25	IDYLNPPKG	2579
	18	26	DYLNPPKGG	1272
LIN 12	11	22	EGNHKPIDYLNP	2412
	12	23	GNHKPIDYLNPP	2887
	13	24	NHKPIDYLNPPK	2703
	14	25	HKPIDYLNPPKG	2733
	15	26	KPIDYLNPPKGG	2693
LIN 15	8	22	LAREGNHKPIDYLNP	2149
	9	23	AREGNHKPIDYLNPP	2888
	10	24	REGNHKPIDYLNPPK	2769
	11	25	EGNHKPIDYLNPPKG	2758
	12	26	GNHKPIDYLNPPKGG	2775

Table 1. **List of epitope candidates found for anti-ARG1.**
The binding region, containing all overlapping peptides, is indicated by residue numbers. Peptides considered are at least 2x the background (defined as the 15th percentile value of the mimic type). Core epitopes (highlighted in yellow), are based on common sequences in overlapping peptides.

Constant	Site 1	Site 2	Site 3
Kd (M)	$3.28 \times 10^{-11} \pm 7.30 \times 10^{-13}$	$1.37 \times 10^{-10} \pm 2.80 \times 10^{-12}$	$1.05 \times 10^{-5} \pm 9.00 \times 10^{-7}$
ΔH (kcal/mol)	$-1.75 \times 10^{3} \pm 7.6$	$-8.32 \times 10^{2} \pm 7.72$	$-4.30 \times 10^{3} \pm 262$
-TΔS (kcal/mol)	1.74×10^{3}	8.19×10^{2}	4.29×10^{2}

Table 2. **Thermodynamic constants of binding interaction between ARG1 and αARG1 clone 1.10.**
In the table are indicated the thermodynamic parameters derived from the best fit of ITC profile of ARG1 and Ab clone 1.10 binding obtained using three site-sequential binding model.

Constant	procathepsin S	mature cathepsin S
Kd (M)	$2.16 \times 10^{-6} \pm 1.41 \times 10^{-6}$	$2.10 \times 10^{-6} \pm 1.77 \times 10^{-6}$
ΔH (kcal/mol)	-565 ± 201	-1000 ± 561
-TΔS (kcal/mol)	557	992

Table 3. **Thermodynamic constants of rhARG1 and rhCTSS binding.**
In the table are indicated the thermodynamic parameters derived from the best fit of ITC profile of CTSS titrated with ARG1 obtained using one-site sequential binding model. The binding was assessed with rhCTSS as proprotein and mature enzyme.

	patient cohort	HD cohort
	(n=52)	(n=55)
gender		
female	45.3%	39.6%
male	62.7%	60.4%
age	44-86 (average 65)	47-80 (average 63.5)
stage		
IV	36.9	
III	48.6	
IIA-IIB	14.5	
tumor site		
head	75.8	
body	18.9	
tail	5.5	

Table 4. **Clinical characteristics of the PDAC patient cohort and healthy donor control group evaluated in the study.**
In the PDAC patient cohort table are reported the gender (%), age, tumor stage and localization of the tumor.

Bibliography

1. Boumahdi, S. & de Sauvage, F.J. The great escape: tumour cell plasticity in resistance to targeted therapy. *Nat Rev Drug Discov* **19**, 39-56 (2020).

2. De Sanctis, F. *et al.* MDSCs in cancer: Conceiving new prognostic and therapeutic targets. *Biochim Biophys Acta* **1865**, 35-48 (2016).

3. Sadeghi Rad, H. *et al.* Understanding the tumor microenvironment for effective immunotherapy. *Med Res Rev* **41**, 1474-1498 (2021).

4. Baghban, R. *et al.* Tumor microenvironment complexity and therapeutic implications at a glance. *Cell Commun Signal* **18**, 59 (2020).

5. Laplane, L., Duluc, D., Larmonier, N., Pradeu, T. & Bikfalvi, A. The Multiple Layers of the Tumor Environment. *Trends Cancer* **4**, 802-809 (2018).

6. Maman, S. & Witz, I.P. A history of exploring cancer in context. *Nat Rev Cancer* **18**, 359-376 (2018).

7. Manoukian, P., Bijlsma, M. & van Laarhoven, H. The Cellular Origins of Cancer-Associated Fibroblasts and Their Opposing Contributions to Pancreatic Cancer Growth. *Front Cell Dev Biol* **9**, 743907 (2021).

8. Flint, T.R. *et al.* Tumor-Induced IL-6 Reprograms Host Metabolism to Suppress Anti-tumor Immunity. *Cell Metab* **24**, 672-684 (2016).

9. Krisnawan, V.E., Stanley, J.A., Schwarz, J.K. & DeNardo, D.G. Tumor Microenvironment as a Regulator of Radiation Therapy: New Insights into Stromal-Mediated Radioresistance. *Cancers (Basel)* **12** (2020).

10. Monteran, L. & Erez, N. The Dark Side of Fibroblasts: Cancer-Associated Fibroblasts as Mediators of Immunosuppression in the Tumor Microenvironment. *Front Immunol* **10**, 1835 (2019).

11. Fearon, D.T. The carcinoma-associated fibroblast expressing fibroblast activation protein and escape from immune surveillance. *Cancer Immunol Res* **2**, 187-193 (2014).

12. Elyada, E. *et al.* Cross-Species Single-Cell Analysis of Pancreatic Ductal Adenocarcinoma Reveals Antigen-Presenting Cancer-Associated Fibroblasts. *Cancer Discov* **9**, 1102-1123 (2019).

13. Lakins, M.A., Ghorani, E., Munir, H., Martins, C.P. & Shields, J.D. Cancer-associated fibroblasts induce antigen-specific deletion of CD8 (+) T Cells to protect tumour cells. *Nat Commun* **9**, 948 (2018).

14. Costa, A. *et al.* Fibroblast Heterogeneity and Immunosuppressive Environment in Human Breast Cancer. *Cancer Cell* **33**, 463-479 e410 (2018).

15. Feig, C. *et al.* Targeting CXCL12 from FAP-expressing carcinoma-associated fibroblasts synergizes with anti-PD-L1 immunotherapy in pancreatic cancer. *Proc Natl Acad Sci U S A* **110**, 20212-20217 (2013).

16. Sanford-Crane, H., Abrego, J. & Sherman, M.H. Fibroblasts as Modulators of Local and Systemic Cancer Metabolism. *Cancers (Basel)* **11** (2019).

17. Bertero, T. *et al.* Tumor-Stroma Mechanics Coordinate Amino Acid Availability to Sustain Tumor Growth and Malignancy. *Cell Metab* **29**, 124-140 e110 (2019).

18. Sousa, C.M. *et al.* Pancreatic stellate cells support tumour metabolism through autophagic alanine secretion. *Nature* **536**, 479-483 (2016).

19. Auciello, F.R. *et al.* A Stromal Lysolipid-Autotaxin Signaling Axis Promotes Pancreatic Tumor Progression. *Cancer Discov* **9**, 617-627 (2019).

20. Valencia, T. *et al.* Metabolic reprogramming of stromal fibroblasts through p62-mTORC1 signaling promotes inflammation and tumorigenesis. *Cancer Cell* **26**, 121-135 (2014).

21. Sakaguchi, S., Miyara, M., Costantino, C.M. & Hafler, D.A. FOXP3+ regulatory T cells in the human immune system. *Nat Rev Immunol* **10**, 490-500 (2010).

22. Miyara, M. *et al.* Functional delineation and differentiation dynamics of human CD4+ T cells expressing the FoxP3 transcription factor. *Immunity* **30**, 899-911 (2009).

23. Thornton, A.M. & Shevach, E.M. CD4+CD25+ immunoregulatory T cells suppress polyclonal T cell activation in vitro by inhibiting interleukin 2 production. *J Exp Med* **188**, 287-296 (1998).

24. Wing, K. *et al.* CTLA-4 control over Foxp3+ regulatory T cell function. *Science* **322**, 271-275 (2008).

25. Steinbrink, K., Wolfl, M., Jonuleit, H., Knop, J. & Enk, A.H. Induction of tolerance by IL-10-treated dendritic cells. *J Immunol* **159**, 4772-4780 (1997).

26. Turnis, M.E. *et al.* Interleukin-35 Limits Anti-Tumor Immunity. *Immunity* **44**, 316-329 (2016).

27. Jarnicki, A.G., Lysaght, J., Todryk, S. & Mills, K.H. Suppression of antitumor immunity by IL-10 and TGF-beta-producing T cells infiltrating the growing tumor: influence of tumor environment on the induction of CD4+ and CD8+ regulatory T cells. *J Immunol* **177**, 896-904 (2006).

28. Wilson, J.M. *et al.* The A2B adenosine receptor impairs the maturation and immunogenicity of dendritic cells. *J Immunol* **182**, 4616-4623 (2009).

29. Grossman, W.J. *et al.* Human T regulatory cells can use the perforin pathway to cause autologous target cell death. *Immunity* **21**, 589-601 (2004).

30. Vignali, D.A., Collison, L.W. & Workman, C.J. How regulatory T cells work. *Nat Rev Immunol* **8**, 523-532 (2008).

31. De Simone, M. *et al.* Transcriptional Landscape of Human Tissue Lymphocytes Unveils Uniqueness of Tumor-Infiltrating T Regulatory Cells. *Immunity* **45**, 1135-1147 (2016).

32. Maj, T. *et al.* Oxidative stress controls regulatory T cell apoptosis and suppressor activity and PD-L1-blockade resistance in tumor. *Nat Immunol* **18**, 1332-1341 (2017).

33. Togashi, Y. & Nishikawa, H. Suppression from beyond the grave. *Nat Immunol* **18**, 1285-1286 (2017).

34. Zhou, J. *et al.* Tumor-Associated Macrophages: Recent Insights and Therapies. *Front Oncol* **10**, 188 (2020).

35. Ojalvo, L.S., King, W., Cox, D. & Pollard, J.W. High-density gene expression analysis of tumor-associated macrophages from mouse mammary tumors. *Am J Pathol* **174**, 1048-1064 (2009).

36. Balkwill, F. Cancer and the chemokine network. *Nat Rev Cancer* **4**, 540-550 (2004).

37. Mantovani, A. *et al.* The chemokine system in diverse forms of macrophage activation and polarization. *Trends Immunol* **25**, 677-686 (2004).

38. Buchbinder, E.I. & Desai, A. CTLA-4 and PD-1 Pathways: Similarities, Differences, and Implications of Their Inhibition. *Am J Clin Oncol* **39**, 98-106 (2016).

39. Noy, R. & Pollard, J.W. Tumor-associated macrophages: from mechanisms to therapy. *Immunity* **41**, 49-61 (2014).

40. Mbongue, J.C. *et al.* The Role of Indoleamine 2, 3-Dioxygenase in Immune Suppression and Autoimmunity. *Vaccines (Basel)* **3**, 703-729 (2015).

41. Ostuni, R., Kratochvill, F., Murray, P.J. & Natoli, G. Macrophages and cancer: from mechanisms to therapeutic implications. *Trends Immunol* **36**, 229-239 (2015).

42. Kitamura, T. *et al.* Monocytes Differentiate to Immune Suppressive Precursors of Metastasis-Associated Macrophages in Mouse Models of Metastatic Breast Cancer. *Front Immunol* **8**, 2004 (2017).

43. Gabrilovich, D.I. & Nagaraj, S. Myeloid-derived suppressor cells as regulators of the immune system. *Nat Rev Immunol* **9**, 162-174 (2009).

44. Bronte, V. *et al.* Recommendations for myeloid-derived suppressor cell nomenclature and characterization standards. *Nat Commun* **7**, 12150 (2016).

45. Solito, S. *et al.* Myeloid-derived suppressor cell heterogeneity in human cancers. *Ann N Y Acad Sci* **1319**, 47-65 (2014).

46. Veglia, F., Perego, M. & Gabrilovich, D. Myeloid-derived suppressor cells coming of age. *Nat Immunol* **19**, 108-119 (2018).

47. Vasievich, E.A. & Huang, L. The suppressive tumor microenvironment: a challenge in cancer immunotherapy. *Mol Pharm* **8**, 635-641 (2011).

48. Grzywa, T.M. *et al.* Myeloid Cell-Derived Arginase in Cancer Immune Response. *Front Immunol* **11**, 938 (2020).

49. Patel, H., Nilendu, P., Jahagirdar, D., Pal, J.K. & Sharma, N.K. Modulating secreted components of tumor microenvironment: A masterstroke in tumor therapeutics. *Cancer Biol Ther* **19**, 3-12 (2018).

50. Bejarano, L., Jordao, M.J.C. & Joyce, J.A. Therapeutic Targeting of the Tumor Microenvironment. *Cancer Discov* **11**, 933-959 (2021).

51. Jakos, T., Pislar, A., Jewett, A. & Kos, J. Cysteine Cathepsins in Tumor-Associated Immune Cells. *Front Immunol* **10**, 2037 (2019).

52. Olson, O.C. & Joyce, J.A. Cysteine cathepsin proteases: regulators of cancer progression and therapeutic response. *Nat Rev Cancer* **15**, 712-729 (2015).

53. Reiser, J., Adair, B. & Reinheckel, T. Specialized roles for cysteine cathepsins in health and disease. *J Clin Invest* **120**, 3421-3431 (2010).

54. Rudzinska, M. *et al.* The Role of Cysteine Cathepsins in Cancer Progression and Drug Resistance. *Int J Mol Sci* **20** (2019).

55. Kramer, L., Turk, D. & Turk, B. The Future of Cysteine Cathepsins in Disease Management. *Trends Pharmacol Sci* **38**, 873-898 (2017).

56. Rorvig, S., Ostergaard, O., Heegaard, N.H. & Borregaard, N. Proteome profiling of human neutrophil granule subsets, secretory vesicles, and cell membrane: correlation with transcriptome profiling of neutrophil precursors. *J Leukoc Biol* **94**, 711-721 (2013).

57. Hsing, L.C. & Rudensky, A.Y. The lysosomal cysteine proteases in MHC class II antigen presentation. *Immunol Rev* **207**, 229-241 (2005).

58. Mahiddine, K., Hassel, C., Murat, C., Girard, M. & Guerder, S. Tissue-Specific Factors Differentially Regulate the Expression of Antigen-Processing Enzymes During Dendritic Cell Ontogeny. *Front Immunol* **11**, 453 (2020).

59. Perisic Nanut, M., Sabotic, J., Jewett, A. & Kos, J. Cysteine cathepsins as regulators of the cytotoxicity of NK and T cells. *Front Immunol* **5**, 616 (2014).

60. McDowell, S.H., Gallaher, S.A., Burden, R.E. & Scott, C.J. Leading the invasion: The role of Cathepsin S in the tumour microenvironment. *Biochim Biophys Acta Mol Cell Res* **1867**, 118781 (2020).

61. Wilkinson, R.D., Williams, R., Scott, C.J. & Burden, R.E. Cathepsin S: therapeutic, diagnostic, and prognostic potential. *Biol Chem* **396**, 867-882 (2015).

62. Small, D.M. *et al.* Cathepsin S from both tumor and tumor-associated cells promote cancer growth and neovascularization. *Int J Cancer* **133**, 2102-2112 (2013).

63. Joyce, J.A. *et al.* Cathepsin cysteine proteases are effectors of invasive growth and angiogenesis during multistage tumorigenesis. *Cancer Cell* **5**, 443-453 (2004).

64. Gocheva, V. *et al.* Distinct roles for cysteine cathepsin genes in multistage tumorigenesis. *Genes Dev* **20**, 543-556 (2006).

65. Gocheva, V. *et al.* IL-4 induces cathepsin protease activity in tumor-associated macrophages to promote cancer growth and invasion. *Genes Dev* **24**, 241-255 (2010).

66. Fuchs, N., Meta, M., Schuppan, D., Nuhn, L. & Schirmeister, T. Novel Opportunities for Cathepsin S Inhibitors in Cancer Immunotherapy by Nanocarrier-Mediated Delivery. *Cells* **9** (2020).

67. Reina-Campos, M., Moscat, J. & Diaz-Meco, M. Metabolism shapes the tumor microenvironment. *Curr Opin Cell Biol* **48**, 47-53 (2017).

68. Renner, K. *et al.* Metabolic Hallmarks of Tumor and Immune Cells in the Tumor Microenvironment. *Front Immunol* **8**, 248 (2017).

69. Fallarino, F. *et al.* The combined effects of tryptophan starvation and tryptophan catabolites down-regulate T cell receptor zeta-chain and induce a regulatory phenotype in naive T cells. *J Immunol* **176**, 6752-6761 (2006).

70. Pacheco, R., Gallart, T., Lluis, C. & Franco, R. Role of glutamate on T-cell mediated immunity. *J Neuroimmunol* **185**, 9-19 (2007).

71. Murray, P.J. Amino acid auxotrophy as a system of immunological control nodes. *Nat Immunol* **17**, 132-139 (2016).

72. Caldwell, R.B., Toque, H.A., Narayanan, S.P. & Caldwell, R.W. Arginase: an old enzyme with new tricks. *Trends Pharmacol Sci* **36**, 395-405 (2015).

73. Gotoh, T. *et al.* Molecular cloning of cDNA for nonhepatic mitochondrial arginase (arginase II) and comparison of its induction with nitric oxide synthase in a murine macrophage-like cell line. *FEBS Lett* **395**, 119-122 (1996).

74. Dizikes, G.J., Grody, W.W., Kern, R.M. & Cederbaum, S.D. Isolation of human liver arginase cDNA and demonstration of nonhomology between the two human arginase genes. *Biochem Biophys Res Commun* **141**, 53-59 (1986).

75. Vockley, J.G. *et al.* Cloning and characterization of the human type II arginase gene. *Genomics* **38**, 118-123 (1996).

76. Dowling, D.P., Di Costanzo, L., Gennadios, H.A. & Christianson, D.W. Evolution of the arginase fold and functional diversity. *Cell Mol Life Sci* **65**, 2039-2055 (2008).

77. Dzik, J.M. Evolutionary roots of arginase expression and regulation. *Front Immunol* **5**, 544 (2014).

78. Pandey, D. *et al.* OxLDL triggers retrograde translocation of arginase2 in aortic endothelial cells via ROCK and mitochondrial processing peptidase. *Circ Res* **115**, 450-459 (2014).

79. Wu, G. *et al.* Arginine metabolism and nutrition in growth, health and disease. *Amino Acids* **37**, 153-168 (2009).

80. Morris, S.M., Jr. Recent advances in arginine metabolism: roles and regulation of the arginases. *Br J Pharmacol* **157**, 922-930 (2009).

81. Cane, S. & Bronte, V. Detection and functional evaluation of arginase-1 isolated from human PMNs and murine MDSC. *Methods Enzymol* **632**, 193-213 (2020).

82. Jacobsen, L.C., Theilgaard-Monch, K., Christensen, E.I. & Borregaard, N. Arginase 1 is expressed in myelocytes/metamyelocytes and localized in gelatinase granules of human neutrophils. *Blood* **109**, 3084-3087 (2007).

83. Rotondo, R. *et al.* Exocytosis of azurophil and arginase 1-containing granules by activated polymorphonuclear neutrophils is required to inhibit T lymphocyte proliferation. *J Leukoc Biol* **89**, 721-727 (2011).

84. Kanyo, Z.F., Scolnick, L.R., Ash, D.E. & Christianson, D.W. Structure of a unique binuclear manganese cluster in arginase. *Nature* **383**, 554-557 (1996).

85. Di Costanzo, L. *et al.* Crystal structure of human arginase I at 1.29-A resolution and exploration of inhibition in the immune response. *Proc Natl Acad Sci U S A* **102**, 13058-13063 (2005).

86. Cama, E. *et al.* Human arginase II: crystal structure and physiological role in male and female sexual arousal. *Biochemistry* **42**, 8445-8451 (2003).

87. Ash, D.E. Structure and function of arginases. *J Nutr* **134**, 2760S-2764S; discussion 2765S-2767S (2004).

88. Kim, S.H., Roszik, J., Grimm, E.A. & Ekmekcioglu, S. Impact of l-Arginine Metabolism on Immune Response and Anticancer Immunotherapy. *Front Oncol* **8**, 67 (2018).

89. Rodriguez, P.C. *et al.* Regulation of T cell receptor CD3zeta chain expression by L-arginine. *J Biol Chem* **277**, 21123-21129 (2002).

90. Lee, J., Ryu, H., Ferrante, R.J., Morris, S.M., Jr. & Ratan, R.R. Translational control of inducible nitric oxide synthase expression by arginine can explain the arginine paradox. *Proc Natl Acad Sci U S A* **100**, 4843-4848 (2003).

91. Bronte, V. & Zanovello, P. Regulation of immune responses by L-arginine metabolism. *Nat Rev Immunol* **5**, 641-654 (2005).

92. Munn, D.H. & Mellor, A.L. Indoleamine 2,3 dioxygenase and metabolic control of immune responses. *Trends Immunol* **34**, 137-143 (2013).

93. Rodriguez, P.C., Quiceno, D.G. & Ochoa, A.C. L-arginine availability regulates T-lymphocyte cell-cycle progression. *Blood* **109**, 1568-1573 (2007).

94. Van de Velde, L.A. *et al.* Stress Kinase GCN2 Controls the Proliferative Fitness and Trafficking of Cytotoxic T Cells Independent of Environmental Amino Acid Sensing. *Cell Rep* **17**, 2247-2258 (2016).

95. Van de Velde, L.A. & Murray, P.J. Proliferating Helper T Cells Require Rictor/mTORC2 Complex to Integrate Signals from Limiting Environmental Amino Acids. *J Biol Chem* **291**, 25815-25822 (2016).

96. Geiger, R. *et al.* L-Arginine Modulates T Cell Metabolism and Enhances Survival and Anti-tumor Activity. *Cell* **167**, 829-842 e813 (2016).

97. Lemos, H., Huang, L., Prendergast, G.C. & Mellor, A.L. Immune control by amino acid catabolism during tumorigenesis and therapy. *Nat Rev Cancer* **19**, 162-175 (2019).

98. Rodriguez, P.C. *et al.* Arginase I production in the tumor microenvironment by mature myeloid cells inhibits T-cell receptor expression and antigen-specific T-cell responses. *Cancer Res* **64**, 5839-5849 (2004).

99. Duque-Correa, M.A. *et al.* Macrophage arginase-1 controls bacterial growth and pathology in hypoxic tuberculosis granulomas. *Proc Natl Acad Sci U S A* **111**, E4024-4032 (2014).

100. Pesce, J.T. *et al.* Arginase-1-expressing macrophages suppress Th2 cytokine-driven inflammation and fibrosis. *PLoS Pathog* **5**, e1000371 (2009).

101. Munder, M. *et al.* Suppression of T-cell functions by human granulocyte arginase. *Blood* **108**, 1627-1634 (2006).

102. Rotondo, R. *et al.* IL-8 induces exocytosis of arginase 1 by neutrophil polymorphonuclears in nonsmall cell lung cancer. *Int J Cancer* **125**, 887-893 (2009).

103. Pudlo, M., Demougeot, C. & Girard-Thernier, C. Arginase Inhibitors: A Rational Approach Over One Century. *Med Res Rev* **37**, 475-513 (2017).

104. Mortier, J. *et al.* Arginase Structure and Inhibition: Catalytic Site Plasticity Reveals New Modulation Possibilities. *Sci Rep* **7**, 13616 (2017).

105. Ilies, M., Di Costanzo, L., North, M.L., Scott, J.A. & Christianson, D.W. 2-aminoimidazole amino acids as inhibitors of the binuclear manganese metalloenzyme human arginase I. *J Med Chem* **53**, 4266-4276 (2010).

106. Boucher, J.L. *et al.* N omega-hydroxyl-L-arginine, an intermediate in the L-arginine to nitric oxide pathway, is a strong inhibitor of liver and macrophage arginase. *Biochem Biophys Res Commun* **203**, 1614-1621 (1994).

107. Di Costanzo, L., Ilies, M., Thorn, K.J. & Christianson, D.W. Inhibition of human arginase I by substrate and product analogues. *Arch Biochem Biophys* **496**, 101-108 (2010).

108. Steggerda, S.M. *et al.* Inhibition of arginase by CB-1158 blocks myeloid cell-mediated immune suppression in the tumor microenvironment. *J Immunother Cancer* **5**, 101 (2017).

109. Lu, M. *et al.* Structure-Based Discovery of Proline-Derived Arginase Inhibitors with Improved Oral Bioavailability for Immuno-Oncology. *ACS Med Chem Lett* **12**, 1380-1388 (2021).

110. Mitcheltree, M.J. *et al.* Discovery and Optimization of Rationally Designed Bicyclic Inhibitors of Human Arginase to Enhance Cancer Immunotherapy. *ACS Med Chem Lett* **11**, 582-588 (2020).

111. Palte, R.L. *et al.* Cryo-EM structures of inhibitory antibodies complexed with arginase 1 provide insight into mechanism of action. *Commun Biol* **4**, 927 (2021).

112. Mantovani, A., Cassatella, M.A., Costantini, C. & Jaillon, S. Neutrophils in the activation and regulation of innate and adaptive immunity. *Nat Rev Immunol* **11**, 519-531 (2011).

113. Coffelt, S.B., Wellenstein, M.D. & de Visser, K.E. Neutrophils in cancer: neutral no more. *Nat Rev Cancer* **16**, 431-446 (2016).

114. Nemeth, T., Sperandio, M. & Mocsai, A. Neutrophils as emerging therapeutic targets. *Nat Rev Drug Discov* **19**, 253-275 (2020).

115. Lawrence, S.M., Corriden, R. & Nizet, V. The Ontogeny of a Neutrophil: Mechanisms of Granulopoiesis and Homeostasis. *Microbiol Mol Biol Rev* **82** (2018).

116. Mortaz, E., Alipoor, S.D., Adcock, I.M., Mumby, S. & Koenderman, L. Update on Neutrophil Function in Severe Inflammation. *Front Immunol* **9**, 2171 (2018).

117. Segal, A.W. How neutrophils kill microbes. *Annu Rev Immunol* **23**, 197-223 (2005).

118. Ley, K. *et al.* Neutrophils: New insights and open questions. *Sci Immunol* **3** (2018).

119. Akashi, K., Traver, D., Miyamoto, T. & Weissman, I.L. A clonogenic common myeloid progenitor that gives rise to all myeloid lineages. *Nature* **404**, 193-197 (2000).

120. Paul, F. *et al.* Transcriptional Heterogeneity and Lineage Commitment in Myeloid Progenitors. *Cell* **163**, 1663-1677 (2015).

121. Evrard, M. *et al.* Developmental Analysis of Bone Marrow Neutrophils Reveals Populations Specialized in Expansion, Trafficking, and Effector Functions. *Immunity* **48**, 364-379 e368 (2018).

122. Zhu, Y.P. *et al.* Identification of an Early Unipotent Neutrophil Progenitor with Pro-tumoral Activity in Mouse and Human Bone Marrow. *Cell Rep* **24**, 2329-2341 e2328 (2018).

123. Faurschou, M. & Borregaard, N. Neutrophil granules and secretory vesicles in inflammation. *Microbes Infect* **5**, 1317-1327 (2003).

124. Cowland, J.B. & Borregaard, N. Granulopoiesis and granules of human neutrophils. *Immunol Rev* **273**, 11-28 (2016).

125. Perera, N.C. *et al.* NSP4 is stored in azurophil granules and released by activated neutrophils as active endoprotease with restricted specificity. *J Immunol* **191**, 2700-2707 (2013).

126. Kjeldsen, L., Sengelov, H., Lollike, K., Nielsen, M.H. & Borregaard, N. Isolation and characterization of gelatinase granules from human neutrophils. *Blood* **83**, 1640-1649 (1994).

127. Borregaard, N., Sorensen, O.E. & Theilgaard-Monch, K. Neutrophil granules: a library of innate immunity proteins. *Trends Immunol* **28**, 340-345 (2007).

128. Gullberg, U., Andersson, E., Garwicz, D., Lindmark, A. & Olsson, I. Biosynthesis, processing and sorting of neutrophil proteins: insight into neutrophil granule development. *Eur J Haematol* **58**, 137-153 (1997).

129. Faurschou, M., Sorensen, O.E., Johnsen, A.H., Askaa, J. & Borregaard, N. Defensin-rich granules of human neutrophils: characterization of secretory properties. *Biochim Biophys Acta* **1591**, 29-35 (2002).

130. Sengelov, H., Kjeldsen, L. & Borregaard, N. Control of exocytosis in early neutrophil activation. *J Immunol* **150**, 1535-1543 (1993).

131. Scapini, P., Marini, O., Tecchio, C. & Cassatella, M.A. Human neutrophils in the saga of cellular heterogeneity: insights and open questions. *Immunol Rev* **273**, 48-60 (2016).

132. Ng, L.G., Ostuni, R. & Hidalgo, A. Heterogeneity of neutrophils. *Nat Rev Immunol* **19**, 255-265 (2019).

133. Adrover, J.M., Nicolas-Avila, J.A. & Hidalgo, A. Aging: A Temporal Dimension for Neutrophils. *Trends Immunol* **37**, 334-345 (2016).

134. Casanova-Acebes, M. *et al.* Rhythmic modulation of the hematopoietic niche through neutrophil clearance. *Cell* **153**, 1025-1035 (2013).

135. Adrover, J.M. *et al.* A Neutrophil Timer Coordinates Immune Defense and Vascular Protection. *Immunity* **51**, 966-967 (2019).

136. Ella, K., Csepanyi-Komi, R. & Kaldi, K. Circadian regulation of human peripheral neutrophils. *Brain Behav Immun* **57**, 209-221 (2016).

137. Ballesteros, I. *et al.* Co-option of Neutrophil Fates by Tissue Environments. *Cell* **183**, 1282-1297 e1218 (2020).

138. Khoyratty, T.E. *et al.* Distinct transcription factor networks control neutrophil-driven inflammation. *Nat Immunol* **22**, 1093-1106 (2021).

139. Chorny, A. *et al.* The soluble pattern recognition receptor PTX3 links humoral innate and adaptive immune responses by helping marginal zone B cells. *J Exp Med* **213**, 2167-2185 (2016).

140. Puga, I. *et al.* B cell-helper neutrophils stimulate the diversification and production of immunoglobulin in the marginal zone of the spleen. *Nat Immunol* **13**, 170-180 (2011).

141. Silvestre-Roig, C., Hidalgo, A. & Soehnlein, O. Neutrophil heterogeneity: implications for homeostasis and pathogenesis. *Blood* **127**, 2173-2181 (2016).

142. Silvestre-Roig, C., Fridlender, Z.G., Glogauer, M. & Scapini, P. Neutrophil Diversity in Health and Disease. *Trends Immunol* **40**, 565-583 (2019).

143. Pillay, J. *et al.* A subset of neutrophils in human systemic inflammation inhibits T cell responses through Mac-1. *J Clin Invest* **122**, 327-336 (2012).

144. Choi, J. *et al.* CD15+/CD16low human granulocytes from terminal cancer patients: granulocytic myeloid-derived suppressor cells that have suppressive function. *Tumour Biol* **33**, 121-129 (2012).

145. Jaillon, S. *et al.* Neutrophil diversity and plasticity in tumour progression and therapy. *Nat Rev Cancer* **20**, 485-503 (2020).

146. Moses, K. & Brandau, S. Human neutrophils: Their role in cancer and relation to myeloid-derived suppressor cells. *Semin Immunol* **28**, 187-196 (2016).

147. Brandau, S. *et al.* Myeloid-derived suppressor cells in the peripheral blood of cancer patients contain a subset of immature neutrophils with impaired migratory properties. *J Leukoc Biol* **89**, 311-317 (2011).

148. Shaul, M.E. & Fridlender, Z.G. Cancer-related circulating and tumor-associated neutrophils - subtypes, sources and function. *FEBS J* **285**, 4316-4342 (2018).

149. Condamine, T. *et al.* Lectin-type oxidized LDL receptor-1 distinguishes population of human polymorphonuclear myeloid-derived suppressor cells in cancer patients. *Sci Immunol* **1** (2016).

150. Rosales, C. Neutrophil: A Cell with Many Roles in Inflammation or Several Cell Types? *Front Physiol* **9**, 113 (2018).

151. Fridlender, Z.G. *et al.* Polarization of tumor-associated neutrophil phenotype by TGF-beta: "N1" versus "N2" TAN. *Cancer Cell* **16**, 183-194 (2009).

152. Singhal, S. *et al.* Origin and Role of a Subset of Tumor-Associated Neutrophils with Antigen-Presenting Cell Features in Early-Stage Human Lung Cancer. *Cancer Cell* **30**, 120-135 (2016).

153. Wu, P. *et al.* gammadeltaT17 cells promote the accumulation and expansion of myeloid-derived suppressor cells in human colorectal cancer. *Immunity* **40**, 785-800 (2014).

154. Zilionis, R. *et al.* Single-Cell Transcriptomics of Human and Mouse Lung Cancers Reveals Conserved Myeloid Populations across Individuals and Species. *Immunity* **50**, 1317-1334 e1310 (2019).

155. Shaul, M.E. & Fridlender, Z.G. Tumour-associated neutrophils in patients with cancer. *Nat Rev Clin Oncol* **16**, 601-620 (2019).

156. Schmidt, H. *et al.* Elevated neutrophil and monocyte counts in peripheral blood are associated with poor survival in patients with metastatic melanoma: a prognostic model. *Br J Cancer* **93**, 273-278 (2005).

157. Peng, B., Wang, Y.H., Liu, Y.M. & Ma, L.X. Prognostic significance of the neutrophil to lymphocyte ratio in patients with non-small cell lung cancer: a systemic review and meta-analysis. *Int J Clin Exp Med* **8**, 3098-3106 (2015).

158. Krenn-Pilko, S. *et al.* The elevated preoperative platelet-to-lymphocyte ratio predicts poor prognosis in breast cancer patients. *Br J Cancer* **110**, 2524-2530 (2014).

159. Grenader, T. *et al.* Derived neutrophil lymphocyte ratio is predictive of survival from intermittent therapy in advanced colorectal cancer: a post hoc analysis of the MRC COIN study. *Br J Cancer* **114**, 612-615 (2016).

160. Takakura, K. *et al.* Comprehensive assessment of the prognosis of pancreatic cancer: peripheral blood neutrophil-lymphocyte ratio and immunohistochemical analyses of the tumour site. *Scand J Gastroenterol* **51**, 610-617 (2016).

161. Reid, M.D. *et al.* Tumor-infiltrating neutrophils in pancreatic neoplasia. *Mod Pathol* **24**, 1612-1619 (2011).

162. Ino, Y. *et al.* Immune cell infiltration as an indicator of the immune microenvironment of pancreatic cancer. *Br J Cancer* **108**, 914-923 (2013).

163. Eruslanov, E.B., Singhal, S. & Albelda, S.M. Mouse versus Human Neutrophils in Cancer: A Major Knowledge Gap. *Trends Cancer* **3**, 149-160 (2017).

164. Houghton, A.M. *et al.* Neutrophil elastase-mediated degradation of IRS-1 accelerates lung tumor growth. *Nat Med* **16**, 219-223 (2010).

165. Nozawa, H., Chiu, C. & Hanahan, D. Infiltrating neutrophils mediate the initial angiogenic switch in a mouse model of multistage carcinogenesis. *Proc Natl Acad Sci U S A* **103**, 12493-12498 (2006).

166. McLoed, A.G. *et al.* Neutrophil-Derived IL-1beta Impairs the Efficacy of NF-kappaB Inhibitors against Lung Cancer. *Cell Rep* **16**, 120-132 (2016).

167. Engblom, C. *et al.* Osteoblasts remotely supply lung tumors with cancer-promoting SiglecF(high) neutrophils. *Science* **358** (2017).

168. Veglia, F. *et al.* Fatty acid transport protein 2 reprograms neutrophils in cancer. *Nature* **569**, 73-78 (2019).

169. Patel, S. *et al.* Unique pattern of neutrophil migration and function during tumor progression. *Nat Immunol* **19**, 1236-1247 (2018).

170. Coffelt, S.B. *et al.* IL-17-producing gammadelta T cells and neutrophils conspire to promote breast cancer metastasis. *Nature* **522**, 345-348 (2015).

171. Acharyya, S. *et al.* A CXCL1 paracrine network links cancer chemoresistance and metastasis. *Cell* **150**, 165-178 (2012).

172. Wculek, S.K. & Malanchi, I. Neutrophils support lung colonization of metastasis-initiating breast cancer cells. *Nature* **528**, 413-417 (2015).

173. Steele, C.W. *et al.* CXCR2 Inhibition Profoundly Suppresses Metastases and Augments Immunotherapy in Pancreatic Ductal Adenocarcinoma. *Cancer Cell* **29**, 832-845 (2016).

174. El Rayes, T. *et al.* Lung inflammation promotes metastasis through neutrophil protease-mediated degradation of Tsp-1. *Proc Natl Acad Sci U S A* **112**, 16000-16005 (2015).

175. Faget, J. *et al.* Neutrophils and Snail Orchestrate the Establishment of a Pro-tumor Microenvironment in Lung Cancer. *Cell Rep* **21**, 3190-3204 (2017).

176. Szczerba, B.M. *et al.* Neutrophils escort circulating tumour cells to enable cell cycle progression. *Nature* **566**, 553-557 (2019).

177. Li, P. *et al.* Lung mesenchymal cells elicit lipid storage in neutrophils that fuel breast cancer lung metastasis. *Nat Immunol* **21**, 1444-1455 (2020).

178. Granot, Z. *et al.* Tumor entrained neutrophils inhibit seeding in the premetastatic lung. *Cancer Cell* **20**, 300-314 (2011).

179. Hagerling, C. *et al.* Immune effector monocyte-neutrophil cooperation induced by the primary tumor prevents metastatic progression of breast cancer. *Proc Natl Acad Sci U S A* **116**, 21704-21714 (2019).

180. Eruslanov, E.B. *et al.* Tumor-associated neutrophils stimulate T cell responses in early-stage human lung cancer. *J Clin Invest* **124**, 5466-5480 (2014).

181. Mittendorf, E.A. *et al.* Breast cancer cell uptake of the inflammatory mediator neutrophil elastase triggers an anticancer adaptive immune response. *Cancer Res* **72**, 3153-3162 (2012).

182. Governa, V. *et al.* The Interplay Between Neutrophils and CD8(+) T Cells Improves Survival in Human Colorectal Cancer. *Clin Cancer Res* **23**, 3847-3858 (2017).

183. Matlung, H.L. *et al.* Neutrophils Kill Antibody-Opsonized Cancer Cells by Trogoptosis. *Cell Rep* **23**, 3946-3959 e3946 (2018).

184. Cui, C. *et al.* Neutrophil elastase selectively kills cancer cells and attenuates tumorigenesis. *Cell* **184**, 3163-3177 e3121 (2021).

185. Blaisdell, A. *et al.* Neutrophils Oppose Uterine Epithelial Carcinogenesis via Debridement of Hypoxic Tumor Cells. *Cancer Cell* **28**, 785-799 (2015).

186. Finisguerra, V. *et al.* MET is required for the recruitment of anti-tumoural neutrophils. *Nature* **522**, 349-353 (2015).

187. Papayannopoulos, V. Neutrophil extracellular traps in immunity and disease. *Nat Rev Immunol* **18**, 134-147 (2018).

188. Takei, H., Araki, A., Watanabe, H., Ichinose, A. & Sendo, F. Rapid killing of human neutrophils by the potent activator phorbol 12-myristate 13-acetate (PMA) accompanied by changes different from typical apoptosis or necrosis. *J Leukoc Biol* **59**, 229-240 (1996).

189. Brinkmann, V. *et al.* Neutrophil extracellular traps kill bacteria. *Science* **303**, 1532-1535 (2004).

190. Yipp, B.G. *et al.* Infection-induced NETosis is a dynamic process involving neutrophil multitasking in vivo. *Nat Med* **18**, 1386-1393 (2012).

191. Pilsczek, F.H. *et al.* A novel mechanism of rapid nuclear neutrophil extracellular trap formation in response to Staphylococcus aureus. *J Immunol* **185**, 7413-7425 (2010).

192. Yipp, B.G. & Kubes, P. NETosis: how vital is it? *Blood* **122**, 2784-2794 (2013).

193. Van Avondt, K. & Hartl, D. Mechanisms and disease relevance of neutrophil extracellular trap formation. *Eur J Clin Invest* **48 Suppl 2**, e12919 (2018).

194. Ravindran, M., Khan, M.A. & Palaniyar, N. Neutrophil Extracellular Trap Formation: Physiology, Pathology, and Pharmacology. *Biomolecules* **9** (2019).

195. Papayannopoulos, V., Metzler, K.D., Hakkim, A. & Zychlinsky, A. Neutrophil elastase and myeloperoxidase regulate the formation of neutrophil extracellular traps. *J Cell Biol* **191**, 677-691 (2010).

196. Metzler, K.D., Goosmann, C., Lubojemska, A., Zychlinsky, A. & Papayannopoulos, V. A myeloperoxidase-containing complex regulates neutrophil elastase release and actin dynamics during NETosis. *Cell Rep* **8**, 883-896 (2014).

197. Lewis, H.D. *et al.* Inhibition of PAD4 activity is sufficient to disrupt mouse and human NET formation. *Nat Chem Biol* **11**, 189-191 (2015).

198. Hakkim, A. *et al.* Activation of the Raf-MEK-ERK pathway is required for neutrophil extracellular trap formation. *Nat Chem Biol* **7**, 75-77 (2011).

199. Douda, D.N., Yip, L., Khan, M.A., Grasemann, H. & Palaniyar, N. Akt is essential to induce NADPH-dependent NETosis and to switch the neutrophil death to apoptosis. *Blood* **123**, 597-600 (2014).

200. Sollberger, G., Tilley, D.O. & Zychlinsky, A. Neutrophil Extracellular Traps: The Biology of Chromatin Externalization. *Dev Cell* **44**, 542-553 (2018).

201. Metzler, K.D. *et al.* Myeloperoxidase is required for neutrophil extracellular trap formation: implications for innate immunity. *Blood* **117**, 953-959 (2011).

202. DeSouza-Vieira, T. *et al.* Neutrophil extracellular traps release induced by Leishmania: role of PI3Kgamma, ERK, PI3Ksigma, PKC, and [Ca2+]. *J Leukoc Biol* **100**, 801-810 (2016).

203. Leshner, M. *et al.* PAD4 mediated histone hypercitrullination induces heterochromatin decondensation and chromatin unfolding to form neutrophil extracellular trap-like structures. *Front Immunol* **3**, 307 (2012).

204. Li, P. *et al.* PAD4 is essential for antibacterial innate immunity mediated by neutrophil extracellular traps. *J Exp Med* **207**, 1853-1862 (2010).

205. Gosswein, S. *et al.* Citrullination Licenses Calpain to Decondense Nuclei in Neutrophil Extracellular Trap Formation. *Front Immunol* **10**, 2481 (2019).

206. Guiducci, E. *et al.* Candida albicans-Induced NETosis Is Independent of Peptidylarginine Deiminase 4. *Front Immunol* **9**, 1573 (2018).

207. Vorobjeva, N.V. & Pinegin, B.V. Neutrophil extracellular traps: mechanisms of formation and role in health and disease. *Biochemistry (Mosc)* **79**, 1286-1296 (2014).

208. Thiam, H.R., Wong, S.L., Wagner, D.D. & Waterman, C.M. Cellular Mechanisms of NETosis. *Annu Rev Cell Dev Biol* **36**, 191-218 (2020).

209. Li, Y. *et al.* Nuclear envelope rupture and NET formation is driven by PKCalpha-mediated lamin B disassembly. *EMBO Rep* **21**, e48779 (2020).

210. Sollberger, G. *et al.* Gasdermin D plays a vital role in the generation of neutrophil extracellular traps. *Sci Immunol* **3** (2018).

211. Kayagaki, N. *et al.* Caspase-11 cleaves gasdermin D for non-canonical inflammasome signalling. *Nature* **526**, 666-671 (2015).

212. Chen, K.W. *et al.* Noncanonical inflammasome signaling elicits gasdermin D-dependent neutrophil extracellular traps. *Sci Immunol* **3** (2018).

213. Neubert, E. *et al.* Chromatin swelling drives neutrophil extracellular trap release. *Nat Commun* **9**, 3767 (2018).

214. Amulic, B. *et al.* Cell-Cycle Proteins Control Production of Neutrophil Extracellular Traps. *Dev Cell* **43**, 449-462 e445 (2017).

215. Thiam, H.R. *et al.* NETosis proceeds by cytoskeleton and endomembrane disassembly and PAD4-mediated chromatin decondensation and nuclear envelope rupture. *Proc Natl Acad Sci U S A* **117**, 7326-7337 (2020).

216. Caielli, S. *et al.* Oxidized mitochondrial nucleoids released by neutrophils drive type I interferon production in human lupus. *J Exp Med* **213**, 697-713 (2016).

217. van der Linden, M., Westerlaken, G.H.A., van der Vlist, M., van Montfrans, J. & Meyaard, L. Differential Signalling and Kinetics of Neutrophil Extracellular Trap Release Revealed by Quantitative Live Imaging. *Sci Rep* **7**, 6529 (2017).

218. Park, J. *et al.* Cancer cells induce metastasis-supporting neutrophil extracellular DNA traps. *Sci Transl Med* **8**, 361ra138 (2016).

219. Rayes, R.F. *et al.* Neutrophil Extracellular Trap-Associated CEACAM1 as a Putative Therapeutic Target to Prevent Metastatic Progression of Colon Carcinoma. *J Immunol* **204**, 2285-2294 (2020).

220. Teijeira, A. *et al.* CXCR1 and CXCR2 Chemokine Receptor Agonists Produced by Tumors Induce Neutrophil Extracellular Traps that Interfere with Immune Cytotoxicity. *Immunity* **52**, 856-871 e858 (2020).

221. Albrengues, J. *et al.* Neutrophil extracellular traps produced during inflammation awaken dormant cancer cells in mice. *Science* **361** (2018).

222. Yang, L. *et al.* DNA of neutrophil extracellular traps promotes cancer metastasis via CCDC25. *Nature* **583**, 133-138 (2020).

223. Mauracher, L.M. *et al.* Citrullinated histone H3, a biomarker of neutrophil extracellular trap formation, predicts the risk of venous thromboembolism in cancer patients. *J Thromb Haemost* **16**, 508-518 (2018).

224. Collisson, E.A., Bailey, P., Chang, D.K. & Biankin, A.V. Molecular subtypes of pancreatic cancer. *Nat Rev Gastroenterol Hepatol* **16**, 207-220 (2019).

225. Garrido-Laguna, I. & Hidalgo, M. Pancreatic cancer: from state-of-the-art treatments to promising novel therapies. *Nat Rev Clin Oncol* **12**, 319-334 (2015).

226. Siegel, R.L., Miller, K.D. & Jemal, A. Cancer Statistics, 2017. *CA Cancer J Clin* **67**, 7-30 (2017).

227. Hezel, A.F., Kimmelman, A.C., Stanger, B.Z., Bardeesy, N. & Depinho, R.A. Genetics and biology of pancreatic ductal adenocarcinoma. *Genes Dev* **20**, 1218-1249 (2006).

228. Aguirre, A.J. *et al.* Real-time Genomic Characterization of Advanced Pancreatic Cancer to Enable Precision Medicine. *Cancer Discov* **8**, 1096-1111 (2018).

229. Qian, Z.R. *et al.* Association of Alterations in Main Driver Genes With Outcomes of Patients With Resected Pancreatic Ductal Adenocarcinoma. *JAMA Oncol* **4**, e173420 (2018).

230. Waddell, N. *et al.* Whole genomes redefine the mutational landscape of pancreatic cancer. *Nature* **518**, 495-501 (2015).

231. Chang, D.K., Grimmond, S.M. & Biankin, A.V. Pancreatic cancer genomics. *Curr Opin Genet Dev* **24**, 74-81 (2014).

232. Dreyer, S.B., Chang, D.K., Bailey, P. & Biankin, A.V. Pancreatic Cancer Genomes: Implications for Clinical Management and Therapeutic Development. *Clin Cancer Res* **23**, 1638-1646 (2017).

233. Notta, F. *et al.* A renewed model of pancreatic cancer evolution based on genomic rearrangement patterns. *Nature* **538**, 378-382 (2016).

234. Bailey, P. *et al.* Genomic analyses identify molecular subtypes of pancreatic cancer. *Nature* **531**, 47-52 (2016).

235. Torres, C. & Grippo, P.J. Pancreatic cancer subtypes: a roadmap for precision medicine. *Ann Med* **50**, 277-287 (2018).

236. Adamska, A., Domenichini, A. & Falasca, M. Pancreatic Ductal Adenocarcinoma: Current and Evolving Therapies. *Int J Mol Sci* **18** (2017).

237. Hammel, P. *et al.* Effect of Chemoradiotherapy vs Chemotherapy on Survival in Patients With Locally Advanced Pancreatic Cancer Controlled After 4 Months of Gemcitabine With or Without Erlotinib: The LAP07 Randomized Clinical Trial. *JAMA* **315**, 1844-1853 (2016).

238. Oettle, H. *et al.* Adjuvant chemotherapy with gemcitabine and long-term outcomes among patients with resected pancreatic cancer: the CONKO-001 randomized trial. *JAMA* **310**, 1473-1481 (2013).

239. Herman, J.M. *et al.* Analysis of fluorouracil-based adjuvant chemotherapy and radiation after pancreaticoduodenectomy for ductal adenocarcinoma of the pancreas: results of a large, prospectively collected database at the Johns Hopkins Hospital. *J Clin Oncol* **26**, 3503-3510 (2008).

240. Zeng, S. *et al.* Chemoresistance in Pancreatic Cancer. *Int J Mol Sci* **20** (2019).

241. Du, J., Gu, J. & Li, J. Mechanisms of drug resistance of pancreatic ductal adenocarcinoma at different levels. *Biosci Rep* **40** (2020).

242. Schumacher, T.N. & Schreiber, R.D. Neoantigens in cancer immunotherapy. *Science* **348**, 69-74 (2015).

243. Bailey, P. *et al.* Exploiting the neoantigen landscape for immunotherapy of pancreatic ductal adenocarcinoma. *Sci Rep* **6**, 35848 (2016).

244. Balachandran, V.P. *et al.* Identification of unique neoantigen qualities in long-term survivors of pancreatic cancer. *Nature* **551**, 512-516 (2017).

245. Chen, H. *et al.* Neoantigen-based immunotherapy in pancreatic ductal adenocarcinoma (PDAC). *Cancer Lett* **490**, 12-19 (2020).

246. Akce, M., Zaidi, M.Y., Waller, E.K., El-Rayes, B.F. & Lesinski, G.B. The Potential of CAR T Cell Therapy in Pancreatic Cancer. *Front Immunol* **9**, 2166 (2018).

247. Beatty, G.L. *et al.* Mesothelin-specific chimeric antigen receptor mRNA-engineered T cells induce anti-tumor activity in solid malignancies. *Cancer Immunol Res* **2**, 112-120 (2014).

248. Thistlethwaite, F.C. *et al.* The clinical efficacy of first-generation carcinoembryonic antigen (CEACAM5)-specific CAR T cells is limited by poor persistence and transient pre-conditioning-dependent respiratory toxicity. *Cancer Immunol Immunother* **66**, 1425-1436 (2017).

249. Varghese, A.M. Chimeric antigen receptor (CAR) T and other T cell strategies for pancreas adenocarcinoma. *Chin Clin Oncol* **6**, 66 (2017).

250. Kabacaoglu, D., Ciecielski, K.J., Ruess, D.A. & Algul, H. Immune Checkpoint Inhibition for Pancreatic Ductal Adenocarcinoma: Current Limitations and Future Options. *Front Immunol* **9**, 1878 (2018).

251. Pardoll, D.M. The blockade of immune checkpoints in cancer immunotherapy. *Nat Rev Cancer* **12**, 252-264 (2012).

252. Hodi, F.S. *et al.* Improved survival with ipilimumab in patients with metastatic melanoma. *N Engl J Med* **363**, 711-723 (2010).

253. Robert, C. *et al.* Pembrolizumab versus Ipilimumab in Advanced Melanoma. *N Engl J Med* **372**, 2521-2532 (2015).

254. Rizvi, N.A. *et al.* Activity and safety of nivolumab, an anti-PD-1 immune checkpoint inhibitor, for patients with advanced, refractory squamous non-small-cell lung cancer (CheckMate 063): a phase 2, single-arm trial. *Lancet Oncol* **16**, 257-265 (2015).

255. Skelton, R.A., Javed, A., Zheng, L. & He, J. Overcoming the resistance of pancreatic cancer to immune checkpoint inhibitors. *J Surg Oncol* **116**, 55-62 (2017).

256. Bian, J. & Almhanna, K. Pancreatic cancer and immune checkpoint inhibitors-still a long way to go. *Transl Gastroenterol Hepatol* **6**, 6 (2021).

257. Ho, W.J., Jaffee, E.M. & Zheng, L. The tumour microenvironment in pancreatic cancer - clinical challenges and opportunities. *Nat Rev Clin Oncol* **17**, 527-540 (2020).

258. Murakami, T. *et al.* Role of the tumor microenvironment in pancreatic cancer. *Ann Gastroenterol Surg* **3**, 130-137 (2019).

259. Vonlaufen, A. *et al.* Pancreatic stellate cells: partners in crime with pancreatic cancer cells. *Cancer Res* **68**, 2085-2093 (2008).

260. Provenzano, P.P. *et al.* Enzymatic targeting of the stroma ablates physical barriers to treatment of pancreatic ductal adenocarcinoma. *Cancer Cell* **21**, 418-429 (2012).

261. Okada, Y. *et al.* Nerve growth factor stimulates MMP-2 expression and activity and increases invasion by human pancreatic cancer cells. *Clin Exp Metastasis* **21**, 285-292 (2004).

262. Chen, X. & Song, E. Turning foes to friends: targeting cancer-associated fibroblasts. *Nat Rev Drug Discov* **18**, 99-115 (2019).

263. Gouirand, V. & Vasseur, S. Fountain of youth of pancreatic cancer cells: the extracellular matrix. *Cell Death Discov* **4**, 1 (2018).

264. Yang, J.S., Wang, C.C., Qiu, J.D., Ren, B. & You, L. Arginine metabolism: a potential target in pancreatic cancer therapy. *Chin Med J (Engl)* **134**, 28-37 (2020).

265. Karamitopoulou, E. Tumour microenvironment of pancreatic cancer: immune landscape is dictated by molecular and histopathological features. *Br J Cancer* **121**, 5-14 (2019).

266. Wartenberg, M. *et al.* Integrated Genomic and Immunophenotypic Classification of Pancreatic Cancer Reveals Three Distinct Subtypes with Prognostic/Predictive Significance. *Clin Cancer Res* **24**, 4444-4454 (2018).

267. Joshi, N.S. *et al.* Regulatory T Cells in Tumor-Associated Tertiary Lymphoid Structures Suppress Anti-tumor T Cell Responses. *Immunity* **43**, 579-590 (2015).

268. Liou, G.Y. *et al.* Mutant KRAS-induced expression of ICAM-1 in pancreatic acinar cells causes attraction of macrophages to expedite the formation of precancerous lesions. *Cancer Discov* **5**, 52-63 (2015).

269. Liou, G.Y. *et al.* Macrophage-secreted cytokines drive pancreatic acinar-to-ductal metaplasia through NF-kappaB and MMPs. *J Cell Biol* **202**, 563-577 (2013).

270. Liou, G.Y. *et al.* The Presence of Interleukin-13 at Pancreatic ADM/PanIN Lesions Alters Macrophage Populations and Mediates Pancreatic Tumorigenesis. *Cell Rep* **19**, 1322-1333 (2017).

271. Pylayeva-Gupta, Y., Lee, K.E., Hajdu, C.H., Miller, G. & Bar-Sagi, D. Oncogenic Kras-induced GM-CSF production promotes the development of pancreatic neoplasia. *Cancer Cell* **21**, 836-847 (2012).

272. Zhao, F. *et al.* Increase in frequency of myeloid-derived suppressor cells in mice with spontaneous pancreatic carcinoma. *Immunology* **128**, 141-149 (2009).

273. Sanford, D.E. *et al.* Inflammatory monocyte mobilization decreases patient survival in pancreatic cancer: a role for targeting the CCL2/CCR2 axis. *Clin Cancer Res* **19**, 3404-3415 (2013).

274. Jin, L., Kim, H.S. & Shi, J. Neutrophil in the Pancreatic Tumor Microenvironment. *Biomolecules* **11** (2021).

275. Chao, T., Furth, E.E. & Vonderheide, R.H. CXCR2-Dependent Accumulation of Tumor-Associated Neutrophils Regulates T-cell Immunity in Pancreatic Ductal Adenocarcinoma. *Cancer Immunol Res* **4**, 968-982 (2016).

276. Sano, M. *et al.* Blocking CXCLs-CXCR2 axis in tumor-stromal interactions contributes to survival in a mouse model of pancreatic ductal adenocarcinoma through reduced cell invasion/migration and a shift of immune-inflammatory microenvironment. *Oncogenesis* **8**, 8 (2019).

277. Nywening, T.M. *et al.* Targeting both tumour-associated CXCR2(+) neutrophils and CCR2(+) macrophages disrupts myeloid recruitment and improves chemotherapeutic responses in pancreatic ductal adenocarcinoma. *Gut* **67**, 1112-1123 (2018).

278. Stromnes, I.M. *et al.* Targeted depletion of an MDSC subset unmasks pancreatic ductal adenocarcinoma to adaptive immunity. *Gut* **63**, 1769-1781 (2014).

279. Das, S., Shapiro, B., Vucic, E.A., Vogt, S. & Bar-Sagi, D. Tumor Cell-Derived IL1beta Promotes Desmoplasia and Immune Suppression in Pancreatic Cancer. *Cancer Res* **80**, 1088-1101 (2020).

280. Choueiry, F. *et al.* CD200 promotes immunosuppression in the pancreatic tumor microenvironment. *J Immunother Cancer* **8** (2020).

281. Li, J. *et al.* Tumor Cell-Intrinsic USP22 Suppresses Antitumor Immunity in Pancreatic Cancer. *Cancer Immunol Res* **8**, 282-291 (2020).

282. Jin, W. *et al.* Neutrophil extracellular DNA traps promote pancreatic cancer cells migration and invasion by activating EGFR/ERK pathway. *J Cell Mol Med* **25**, 5443-5456 (2021).

283. Siret, C. *et al.* Deciphering the Crosstalk Between Myeloid-Derived Suppressor Cells and Regulatory T Cells in Pancreatic Ductal Adenocarcinoma. *Front Immunol* **10**, 3070 (2019).

284. Zhang, Y. *et al.* Interleukin-17-induced neutrophil extracellular traps mediate resistance to checkpoint blockade in pancreatic cancer. *J Exp Med* **217** (2020).

285. Kajioka, H. *et al.* Targeting neutrophil extracellular traps with thrombomodulin prevents pancreatic cancer metastasis. *Cancer Lett* **497**, 1-13 (2021).

286. Munir, H. *et al.* Stromal-driven and Amyloid beta-dependent induction of neutrophil extracellular traps modulates tumor growth. *Nat Commun* **12**, 683 (2021).

287. Shultz, L.D., Ishikawa, F. & Greiner, D.L. Humanized mice in translational biomedical research. *Nat Rev Immunol* **7**, 118-130 (2007).

288. Walsh, N.C. *et al.* Humanized Mouse Models of Clinical Disease. *Annu Rev Pathol* **12**, 187-215 (2017).

289. Bryder, D., Rossi, D.J. & Weissman, I.L. Hematopoietic stem cells: the paradigmatic tissue-specific stem cell. *Am J Pathol* **169**, 338-346 (2006).

290. De La Rochere, P. *et al.* Humanized Mice for the Study of Immuno-Oncology. *Trends Immunol* **39**, 748-763 (2018).

291. Shultz, L.D., Brehm, M.A., Garcia-Martinez, J.V. & Greiner, D.L. Humanized mice for immune system investigation: progress, promise and challenges. *Nat Rev Immunol* **12**, 786-798 (2012).

292. Bosma, G.C., Custer, R.P. & Bosma, M.J. A severe combined immunodeficiency mutation in the mouse. *Nature* **301**, 527-530 (1983).

293. Mombaerts, P. *et al.* RAG-1-deficient mice have no mature B and T lymphocytes. *Cell* **68**, 869-877 (1992).

294. Shinkai, Y. *et al.* RAG-2-deficient mice lack mature lymphocytes owing to inability to initiate V(D)J rearrangement. *Cell* **68**, 855-867 (1992).

295. Ito, M. *et al.* NOD/SCID/gamma(c)(null) mouse: an excellent recipient mouse model for engraftment of human cells. *Blood* **100**, 3175-3182 (2002).

296. Drake, A.C., Chen, Q. & Chen, J. Engineering humanized mice for improved hematopoietic reconstitution. *Cell Mol Immunol* **9**, 215-224 (2012).

297. Chen, Q., Khoury, M. & Chen, J. Expression of human cytokines dramatically improves reconstitution of specific human-blood lineage cells in humanized mice. *Proc Natl Acad Sci U S A* **106**, 21783-21788 (2009).

298. Billerbeck, E. *et al.* Development of human CD4+FoxP3+ regulatory T cells in human stem cell factor-, granulocyte-macrophage colony-stimulating factor-, and interleukin-3-expressing NOD-SCID IL2Rgamma(null) humanized mice. *Blood* **117**, 3076-3086 (2011).

299. Rathinam, C. *et al.* Efficient differentiation and function of human macrophages in humanized CSF-1 mice. *Blood* **118**, 3119-3128 (2011).

300. Tian, H., Lyu, Y., Yang, Y.G. & Hu, Z. Humanized Rodent Models for Cancer Research. *Front Oncol* **10**, 1696 (2020).

301. Gao, H. *et al.* High-throughput screening using patient-derived tumor xenografts to predict clinical trial drug response. *Nat Med* **21**, 1318-1325 (2015).

302. Zitvogel, L., Pitt, J.M., Daillere, R., Smyth, M.J. & Kroemer, G. Mouse models in oncoimmunology. *Nat Rev Cancer* **16**, 759-773 (2016).

303. Gupta, S., Chan, D.W., Zaal, K.J. & Kaplan, M.J. A High-Throughput Real-Time Imaging Technique To Quantify NETosis and Distinguish Mechanisms of Cell Death in Human Neutrophils. *J Immunol* **200**, 869-879 (2018).

304. Veras, F.P. *et al.* SARS-CoV-2-triggered neutrophil extracellular traps mediate COVID-19 pathology. *J Exp Med* **217** (2020).

305. Sandri, S. *et al.* Feasibility of Telomerase-Specific Adoptive T-cell Therapy for B-cell Chronic Lymphocytic Leukemia and Solid Malignancies. *Cancer Res* **76**, 2540-2551 (2016).

306. Liu, W.N. *et al.* Establishment and Characterization of Humanized Mouse NPC-PDX Model for Testing Immunotherapy. *Cancers (Basel)* **12** (2020).

307. Sengupta, A. & Weljie, A.M. NMR Spectroscopy-Based Metabolic Profiling of Biospecimens. *Curr Protoc Protein Sci* **98**, e98 (2019).

308. Ljusberg, J. *et al.* Proteolytic excision of a repressive loop domain in tartrate-resistant acid phosphatase by cathepsin K in osteoclasts. *J Biol Chem* **280**, 28370-28381 (2005).

309. Greenfield, N.J. Using circular dichroism spectra to estimate protein secondary structure. *Nat Protoc* **1**, 2876-2890 (2006).

310. Kenny, E.F. *et al.* Diverse stimuli engage different neutrophil extracellular trap pathways. *Elife* **6** (2017).

311. de Andrea, C.E. *et al.* Heterogenous presence of neutrophil extracellular traps in human solid tumours is partially dependent on IL-8. *J Pathol* **255**, 190-201 (2021).

312. Teijeira, A. *et al.* IL8, Neutrophils, and NETs in a Collusion against Cancer Immunity and Immunotherapy. *Clin Cancer Res* **27**, 2383-2393 (2021).

313. Borek, B., Gajda, T., Golebiowski, A. & Blaszczyk, R. Boronic acid-based arginase inhibitors in cancer immunotherapy. *Bioorg Med Chem* **28**, 115658 (2020).

314. Rojas, L.A. & Balachandran, V.P. Scaling the immune incline in PDAC. *Nat Rev Gastroenterol Hepatol* **18**, 453-454 (2021).

315. Schalper, K.A. *et al.* Elevated serum interleukin-8 is associated with enhanced intratumor neutrophils and reduced clinical benefit of immune-checkpoint inhibitors. *Nat Med* **26**, 688-692 (2020).

316. Sharma, P., Hu-Lieskovan, S., Wargo, J.A. & Ribas, A. Primary, Adaptive, and Acquired Resistance to Cancer Immunotherapy. *Cell* **168**, 707-723 (2017).

317. Topalian, S.L., Drake, C.G. & Pardoll, D.M. Immune checkpoint blockade: a common denominator approach to cancer therapy. *Cancer Cell* **27**, 450-461 (2015).

318. Ribas, A. *et al.* Association of Pembrolizumab With Tumor Response and Survival Among Patients With Advanced Melanoma. *JAMA* **315**, 1600-1609 (2016).

319. Schadendorf, D. *et al.* Pooled Analysis of Long-Term Survival Data From Phase II and Phase III Trials of Ipilimumab in Unresectable or Metastatic Melanoma. *J Clin Oncol* **33**, 1889-1894 (2015).

320. Jacquelot, N. *et al.* Predictors of responses to immune checkpoint blockade in advanced melanoma. *Nat Commun* **8**, 592 (2017).

321. Le, D.T. *et al.* Mismatch repair deficiency predicts response of solid tumors to PD-1 blockade. *Science* **357**, 409-413 (2017).

322. Trovato, R. *et al.* Immunosuppression by monocytic myeloid-derived suppressor cells in patients with pancreatic ductal carcinoma is orchestrated by STAT3. *J Immunother Cancer* **7**, 255 (2019).

323. Sandri, S. *et al.* Effective control of acute myeloid leukaemia and acute lymphoblastic leukaemia progression by telomerase specific adoptive T-cell therapy. *Oncotarget* **8**, 86987-87001 (2017).

324. Bagnara, D. *et al.* A novel adoptive transfer model of chronic lymphocytic leukemia suggests a key role for T lymphocytes in the disease. *Blood* **117**, 5463-5472 (2011).

325. Glodde, N. *et al.* Reactive Neutrophil Responses Dependent on the Receptor Tyrosine Kinase c-MET Limit Cancer Immunotherapy. *Immunity* **47**, 789-802 e789 (2017).

326. Zacchigna, S., Zentilin, L. & Giacca, M. Adeno-associated virus vectors as therapeutic and investigational tools in the cardiovascular system. *Circ Res* **114**, 1827-1846 (2014).

327. Tumeh, P.C. *et al.* PD-1 blockade induces responses by inhibiting adaptive immune resistance. *Nature* **515**, 568-571 (2014).

328. Ji, R.R. *et al.* An immune-active tumor microenvironment favors clinical response to ipilimumab. *Cancer Immunol Immunother* **61**, 1019-1031 (2012).

329. Broadfield, L.A., Pane, A.A., Talebi, A., Swinnen, J.V. & Fendt, S.M. Lipid metabolism in cancer: New perspectives and emerging mechanisms. *Dev Cell* **56**, 1363-1393 (2021).

330. Jennings, M.R., Munn, D. & Blazeck, J. Immunosuppressive metabolites in tumoral immune evasion: redundancies, clinical efforts, and pathways forward. *J Immunother Cancer* **9** (2021).

331. Chang, C.H. *et al.* Metabolic Competition in the Tumor Microenvironment Is a Driver of Cancer Progression. *Cell* **162**, 1229-1241 (2015).

332. Canale, F.P. *et al.* Metabolic modulation of tumours with engineered bacteria for immunotherapy. *Nature* **598**, 662-666 (2021).

333. Masucci, M.T., Minopoli, M., Del Vecchio, S. & Carriero, M.V. The Emerging Role of Neutrophil Extracellular Traps (NETs) in Tumor Progression and Metastasis. *Front Immunol* **11**, 1749 (2020).

334. Mortier, A. *et al.* Biological activity of CXCL8 forms generated by alternative cleavage of the signal peptide or by aminopeptidase-mediated truncation. *PLoS One* **6**, e23913 (2011).

335. Uribe-Querol, E. & Rosales, C. Neutrophils in Cancer: Two Sides of the Same Coin. *J Immunol Res* **2015**, 983698 (2015).

Aknowledgements

This thesis could not have been completed without the assistance and contribution of numerous individuals, that I would like to thank in the following pragraphs.

First, I would like to express my gratitude and sincere thanks to my tutor Prof. Vincenzo Bronte, who gave me the opportunity to grow as a scientist by working in his lab. In addition, special thanks go to all the members of the lab. I also thank my fellow lab mates, Rosalinda, Francesca, Chiara, Annalisa, Cristina and Sara that put up with me and supported me for four years rendering my days in and out of the lab beautiful. I would also like to thank Cristina Anselmi for her support and careness.

Most importantly, I would like to express my gratitude to the direct supervisor of my thesis, Stefania Canè, the best mentor I could have asked for. It would be impossible to conclude this thesis without her help and her guidance. I would like also to thank her for the numerous life lessons that she gave me even without knowing it, for sharing with me not only her passion and love for research but also her never-ending knowledge, in and out of the laboratory life. Her presence in difficult moments and her continuous belief in me gave me the strength to finish successfully my PhD thesis. I will forever treasure our collaboration.

Finally, I would like to acknowledge with gratitude the support and love of my parents and brother. Thank you for always loving and believing in me and for being there for me when I needed you without ever blocking my career or doubting my decisions. Special thanks go to my lovely friends Maria, Lena, Roza, Anneta, Maria, Lydia and Marina for always being close even though we are miles apart. Finally yet importantly, I would like to thank 'i miei amici passeggeri', Claudia, Jay, Enrico, Silvia e Niccolo for making me feel like home.